SEGMENTAL DYNAMICS OF INDIVIDUAL SPECIES IN A MISCIBLE POLYMER BLEND

Thesis by

Geun-Chang Chung

In Partial Fulfillment of the Requirements

for the Degree of

Doctor of Philosophy

California Institute of Technology

Pasadena, California

1995

(Defended June, 1994)

To my wife Sujung

with my deepest love,

for her support and encouragement.

Acknowledgments

Special thanks are due to my adviser Julia A. Kornfield, who introduced me to interesting research areas of polymer physics and provided many critical discussions in the course of this research. I appreciate that I could learn a lot from her thorough reasoning and pursuit of perfection. I would also like to thank her for her forgiveness and patience.

Much of the experimental difficulty came from instrumental problems, and I owe a special debt of gratitude to Tom Dunn who has spent so much time carefully checking all the electronic components to fix the spectrometer. I also appreciate Dr. Dieter Schaefer for his helpful guides in carrying out the experiments.

I was lucky that I could have so much help, direct or indirect, from members of my research group. I'd like to especially thank Kannan and Vinay for many useful discussions and suggestions.

During the past five years, the steady and slow experiments were often quite difficult for me to bear alone. I'd like to thank my Korean friends, Heewon, Jayhyung, and Namkyoo, and many others who refreshed my entangled mind with diverse areas of interest.

Last but not least, I am deeply grateful to my wife, Sujung, and my parents for their continuous encouragement and loving support.

Abstract

The segmental motion of each species in polyisoprene/poly(vinylethylene) (PI/PVE) miscible blends is studied at three different compositions using two-dimensional deuteron exchange NMR. The individual species exhibit widely different mean mobilities and broad mobility distributions near the glass transition of each blend. As PVE content increases, both the difference in mean mobilities between the two species and the width of mobility distribution for both components increase. Such enhancement of these two types of dynamic heterogeneity with PVE content appears to produce the anomalous broadening of the glass transition. The mean reorientational correlation times of each component can differ by two orders of magnitude under identical conditions. The mean correlation times and the monomeric friction coefficients can be described by a common temperature dependence, which differs for individual species. This difference can be described in terms of distinct effective glass transition temperatures, T_g^*, for the two species. The separation between the two effective glass transition temperatures increases with PVE content, consistent with more pronounced thermorheological complexity of blends rich in PVE. The individual T_g^*'s also exhibit different compositional dependence from that of the calorimetric T_g of blend. This behavior can give rise to the complex compositional dependence of individual mobilities, apparent when mobilities are compared at the same $T - T_g$, with respect to the calorimetric T_g of blend. Origins of these two types of dynamic heterogeneity are examined further by using a simple model that takes into account effect of random

compositional variations. Although compositional variations can give rise to the observed width of mobility distribution and its compositional dependence, the observed difference in mean mobilities cannot be explained at the same time. This suggests that the observed dynamic heterogeneities can be explained only by including two distinct contributions: local compositional variations in the blend and intrinsic difference in chain mobilities. Distinct dynamic constraints between the two species can arise from their structural differences. In light of phenomenological models of cooperative local dynamics, distinct mobilities can arise from the difference in critical size of free volume or in cooperativity.

Contents

List of Figures

Chapter 1

Introduction

Polymer blends have attracted great practical interest because a range of useful properties can be obtained without developing new polymers and synthetic processes. Blending can be used to improve virtually all properties of technological importance, the most important ones being mechanical properties, transport properties, stability and cost. The glass transition temperature and width of the glass transition can be altered to control applicable temperature ranges. Material processing can be facilitated by the modification of flow properties through blending. Improved thermal and mechanical stability is essential for the production of technologically useful biodegradable polymer material at a reasonable cost. One important goal is to rationally tailor the blend properties based on the known properties of constituent polymers. Since homogeneous blends give better control of material properties and also exhibit better mechanical properties, miscible blends or compatibilized blends are more favored technologically than phase-separated blends.

Miscible polymer blends are of particular interest from a scientific point of view because they can serve as ideal model systems to study the molecular motions of individual species that control mechanical and transport properties of both compatible and phase-separated blends. In addition, the study of miscible blends leads to a deeper understanding of the role of intrinsic dynamic properties and intermolecular interactions in determining the dynamics of polymers. Specifically, in miscible blends, the intramolecular constraints are constant, fixed by the chemical structure of the components independently of the blend composition, whereas the intermolecular interactions depend on the blend composition. In this study, we focus on the individual chain dynamics and their dependence on temperature and composition.

1.1 Historical perspectives

When two different polymers are intimately mixed together, the dynamics of each species are strongly influenced by neighboring chains, and hence the blend properties as a whole become intermediate between those of the two constituent homopolymers. The changes in their dynamics are often so substantial that distinctions between individual species can hardly be observed in miscible blends. Specifically, miscible blends undergo one broad glass transition at an intermediate temperature ranges between the glass transition temperatures, T_g's, of the two homopolymers. The frictional resistance imposed by the surrounding chains appears essentially identical for each species, perhaps because the average composition surrounding each type of chain is nearly the same. The possibilities that individual components exhibit quite distinct

motions even in blends have been considered to be insignificant, simply because such features have not been observed until very recently.

One of the most useful and most studied miscible blends is the blend of poly(2,6-dimethyl-phenylene oxide) (PPO) (T_g=219 °C) with polystyrene (PS) (T_g=101 °C), which constitute the Noryl series of commercial resins from General Electric Co. A number of studies at various blend ratios have been performed on the physical properties of this blend, which include the mechanical, calorimetric, dielectric, and pressure-volume-temperature (PVT) properties [1, 2, 3]. Miscibility of this blend has been inferred from a single, albeit broad, glass transition, even though the glass transition temperatures of the two pure components differ by more than 100 K. The blend also exhibits a simple viscoelastic response, intermediate between those of two constituent species [2]. For example, the blend exhibits a single terminal relaxation process and its temperature dependence appears to follow time-temperature superposition. The monomeric friction coefficient of the blend (common to both components) also appears to be independent of composition when compared at iso-free volume temperatures. Compositional dependence of the glass transition temperature and the plateau modulus is explained in terms of a simple mixing rule with pure component properties. Consequently, it has been believed that the macroscopic viscoelastic properties of miscible blends have essentially the same features common in most homopolymers such as a single glass transition, thermorheological simplicity and a single friction factor for the blend, which exhibit simple compositional dependence. Any deviation from this simplicity has been ascribed to incomplete miscibility.

In order to describe the effect of blending on the glass transition temperature, various phenomenological models are proposed to predict the compositional dependence of the blend T_g [4, 5, 6]. Such relations often require a number of fitting parameters. Furthermore, broadening of the temperature range over which the glass transition occurs is neglected, or simply ascribed to compositional variations inherent in blends. The viscoelastic behavior of blends have been described in terms of single-chain relaxation behavior, where the virtual single chain properties are usually intermediate between those of two constituent homopolymers. The theories that predict the viscoelastic responses based on molecular properties of the constituent polymers remain to be established. A primitive mixing rule for the rubbery plateau modulus G_N^0, or the entanglement molecular weight $M_e = \rho RT/G_N^0$ of miscible blends, is suggested recently and needs to be tested further experimentally [7]. Blending significantly alters the monomeric friction coefficient that dominates the temperature dependence of chain relaxation and hence the viscoelastic responses. Appropriate mixing rules for the monomeric friction coefficient has not been developed, perhaps due to the difficulty of understanding the microscopic origin of the monomeric friction coefficient, even in homopolymer melts.

Numerous rheological experiments have been performed to establish a firm basis for the theories that can predict the viscoelastic response of blends based on the known properties of the two components. The broad glass transition behavior has also been examined more carefully by studying molecular motions underlying the glass transition. As a result, genuine complexity of miscible blends has been revealed gradually

over the past decade. Many new discoveries of complex viscoelastic response of blends have been possible through the advanced synthesis of monodisperse polymers and development in experimental methods. Specifically, some broadening of the terminal relaxation process due to chain length variation has been largely suppressed, through which the chain relaxation of individual species could be better resolved [13, 9]. The dynamic response from a specific component can even be studied using a selectively labeled polymer. Experimentally accessible ranges of frequency and temperature have been expanded and a number of new spectroscopic techniques are applied to study dynamic responses of a specific component.

In summary, a number of features in the macroscopic viscoelastic responses have been observed recently, which differ qualitatively from those of homopolymers. The most dramatic one is the failure of time temperature superposition, a principle that is generally valid in simple homopolymers. There is increasing evidence that viscoelastic response can be explained better in terms of two separate monomeric friction coefficients, ζ_0, for each species. The monomeric friction coefficients appear to exhibit non-monotonic compositional dependence when viewed at fixed $T - T_{g,blend}$, unlike the simple linear mixing rule that predicts a monotonic variation in ζ_0. Related to the broad glass transition of blends, distinct segmental mobilities are observed above the glass transition, which are reminiscent of the two distinct ζ_0's for the two components.

1.2 Current issues and objectives

1.2.1 Macroscopic chain dynamics

The dynamics of a short polymer chain (relative to the entanglement molecular weight, M_e) can be modeled successfully by considering a string of beads connected by springs. In the Rouse model, motion of the beads are governed by the elastic spring force, random Brownian force from neighboring molecules and a frictional drag that is proportional to the velocity of the bead. The proportionality constant is called the monomeric friction coefficient and is typically denoted as ζ_0. When a polymer has molecular weight larger than M_e, the motion of chain becomes more complex. Due to the topological constraint exerted by neighboring chains that hinder lateral displacement beyond certain ranges, the average trajectory of the chain is confined to a virtual tube. The curvilinear diffusion of a chain within the virtual tube is assumed to be consistent with the Rouse dynamics, and is also governed by the monomeric friction coefficient. The time that it takes for a chain to pass completely through the confining tube is called the disengagement time, $\tau_d = \tau_0 N^a$, where τ_0 is a microscopic time scale, N is the number of beads and the exponent a is 3 from the reptation model and 3.4 empirically. Highly entangled polymer melts behave like viscous liquids under perturbations that are slow compared to the disengagement time; whereas they behave like a rubber with constant plateau modulus, G_N^0, for slightly faster perturbation. This change in the flow behavior observed when the mechanical response is probed at the threshold frequency, $\omega_c = 1/\tau_d$, is called the terminal transition.

It has recently been suggested from many diffusion [8] and dynamic mechanical

measurements [9] that chain dynamics in miscible blends can be explained by reptation process. The molecular weight dependence of the terminal relaxation time, τ_d, and the center of mass diffusivity of a labeled chain have been observed to be in accord with reptation behavior. However, viscoelastic properties of miscible blends are controlled by two types of chemically distinct chains, and hence a number of important questions need to be considered before the reptation model can be successfully extended to miscible blends.

A. Distinct chain dynamics of individual species

First, the two species can have distinct relaxation process for a number of possible reasons. Most obvious difference can arise when the chain lengths of the two species differ significantly. For homopolymers with bimodal molecular weight distributions [10] and for blends with different molecular weights [9], two resolved terminal relaxations have been observed. Similar effect is expected if the entanglement molecular weight can differ significantly. However, the entanglement effect comes from the un-crossibility of surrounding chains and hence two species should have similar entanglement molecular weight, because of the same average compositions felt by the two species. The entanglement molecular weight for each type of chain in the blend can be determined by resolving the contribution of two species on the plateau modulus. From recent rheo-optical measurements, it has been observed that the entanglement molecular weight is quite similar for each species [11, 12].

The relaxation behavior of the two species can exhibit dramatic differences, when two species have different monomeric friction coefficients. The distinct monomeric

friction factors for each species have been inferred from recent dynamic mechanical and tracer diffusion measurements on a number of miscible blends [13, 9, 8]. Specifically, when the terminal relaxation of miscible blends are examined carefully as a function of temperature, changes in the terminal relaxation spectrum are observed. The changes are most dramatic for blends with significantly different molecular weights, in which two terminal relaxation times shift differently with temperature. The dynamics of two species in the blends have also been studied separately by tracer diffusion measurements. When the diffusion of a deuterium labeled chain through the blend matrix is studied for both species, the observed tracer diffusivities normalized by the individual chain length differ significantly. In the context of the reptation model, the failure of time-temperature superposition and the different tracer diffusivities can be explained in terms of the different monomeric friction coefficient for individual species.

In fact, different monomeric friction for each component has been modeled by a simple linear mixing rule [14],

$$\zeta_A(\phi) = \phi\,\zeta_{AA} + (1-\phi)\,\zeta_{AB}, \tag{1.1}$$

$$\zeta_B(\phi) = (1-\phi)\,\zeta_{BA} + \phi\,\zeta_{BB}, \tag{1.2}$$

where $\zeta_{AA}, \zeta_{AB}, \zeta_{BA}$, and ζ_{BB} are pair-wise friction, and ζ_{AB} and ζ_{BA} are assumed to be the same. However, measured monomeric friction coefficients showed a completely different compositional dependence, when comparison is made at an "iso-free-volume" condition at which all ζ_{ij}'s with i and j indexing A or B are assumed to be independent of temperature and composition. The iso-free-volume condition is often approx-

imately achieved at temperatures with constant $T - T_g(\phi)$. In such condition, the ratio of two ζ_i's showed a distinct extremum at an intermediate composition, which cannot be described by a simple linear mixing rule. To develop a better mixing rule for the monomeric friction coefficients, the temperature and composition dependence of the individual monomeric friction coefficients need to be studied quantitatively.

B. Compositional variations

Second, local compositional variations inherent in miscible blends can affect the chain relaxation dynamics. Relative to blends that have attractive interactions, the extent of compositional variation is expected to be more pronounced for blends with very weak enthalpic interactions, because equilibrium compositional fluctuations decay only by very weak entropic driving force. In such systems, monomeric friction coefficient that governs the chain relaxation dynamics is some average of the locally heterogeneous friction coefficients. Information regarding the way that locally heterogeneous friction affects the average friction coefficient is completely lacking, even though it is important in describing the viscoelastic properties of many compatible blends that possess similar or even stronger compositional heterogeneities.

1.2.2 Local segmental dynamics

Amorphous polymer materials exhibit elastic, glassy response when external perturbation is faster than a certain microscopic time-scale. Below that threshold frequency, this glassy response decays rapidly and the material behaves like a viscous fluid for small molecular weight (unentangled) polymers, or becomes rubbery for well entan-

gled polymers. This transition is called the dynamic glass transition, softening transition, glass-to-liquid or glass-to-rubber transition. The threshold frequency is believed to be related to the rate of reorientation of back-bone segments. Since this segmental reorientation process gives rise to the primary peak in the molecular relaxation spectrum, this is also called the α transition. As temperature decreases, the threshold frequency decreases very strongly, and the segmental motion eventually becomes slower than the typical observation time-scale, 1 Hz. The glass transition can be defined as the state at which the segmental motion becomes slower than a typical observation time-scale. Perhaps the most important characteristic of this segmental motion is the cooperativity or dynamic coupling between many neighboring segments, which is a natural consequence of connectivity along the backbone and high packing density of a chain with its neighbors.

Temperature dependence of the segmental mobility in homopolymers can be described by the empirical relation proposed by Williams, Landel and Ferry (WLF equation),

$$\log \frac{\tau_0(T)}{\tau_0(T_g)} = \frac{-C_1^g(T - T_g)}{C_2^g + (T - T_g)}, \tag{1.3}$$

where τ_0 is the time scale of segmental motion, T_g is the glass transition temperature and (C_1^g, C_2^g) are parameters that depend on a specific polymer. The WLF equation can be explained successfully by a number of phenomenological models. Two different physical pictures are most commonly adopted in describing the segmental motion: the free volume model and the Adam-Gibbs model of cooperative rearrangement [15, 16]. In the simplest free volume model, the motion of a segment is allowed only when there

is enough empty space in its neighborhood. The average rate of segmental motion then is related to the amount of free-volume in the polymer,

$$\begin{aligned} \ln(\tau_0) &= \ln A + B(V - V_f)/V_f \\ &= \ln A + B(1/f - 1). \end{aligned} \tag{1.4}$$

The total and the free volume are denoted by V and V_f, the constant B depends on material property and f is the fractional free volume, which has linear temperature dependence,

$$f = f_g + (T - T_g)\,\alpha_f, \tag{1.5}$$

where α_f is the thermal expansion coefficient of the free volume and f_g is the fractional free volume at the glass transition. On the other hand, the Adam-Gibbs model postulates that the transition probability of segmental rearrangement, W, is given by,

$$\ln W(T) = \ln A - \frac{z^* \Delta\mu}{k_B T}, \tag{1.6}$$

where $z^*(T)$ is the smallest number of cooperatively rearranging units, $\Delta\mu$ is the energy barrier per unit segment and k_B is the Boltzman constant. The WLF temperature dependence results from the strong temperature dependence of the cooperativity, $z^*(T)$.

In contrast to homopolymers, miscible blends consist of two different types of polymers whose glass transition temperatures can be widely separated. This raises a number of interesting questions to be addressed: To what extent is the intrinsic dynamic difference between the two species preserved in the broad glass transition of blends? How does the cooperativity affect the segmental motion and how does

the temperature dependence of motion change by blending? What is the effect of equilibrium compositional variation on the broadening of glass transition region and the segmental relaxation spectrum? Recently, a number of experiments have been conducted to probe the segmental dynamics of individual species.

In a ^{13}C linewidth measurement under magic angle spinning/dipolar decoupling (MAS/DD) condition, maximum line broadening is observed when the frequency of segmental motion is comparable to the spinning frequency controlled to $\sim$ 4 kHz. The maximum line-broadening for individual species in a blend are observed at two different temperatures separated by 15 K [17]. Similar behavior is also observed from ^{13}C NMR relaxation time measurement [18]. Furthermore, separation between the temperatures, at which line broadening is maximized, increases with fraction of the high T_g component [18]. Although the connection between the local segmental mobility and the monomeric friction coefficient is not clear, the distinct segmental mobilities are reminiscent of the difference in monomeric friction coefficients. Thus, it is plausible that the temperature and compositional dependence of monomeric friction coefficient can be related to the cooperative segmental dynamics.

However, the difference in segmental mobilities can also be attributed to local compositional variations, since different segmental mobilities are expected in regions of different local compositions. In miscible blends or block copolymers, this spatial heterogeneity has been studied using NMR by probing the spin diffusion from relatively mobile segments to less mobile segments [19]. Such spin-diffusion measurement performed on PS/PMMA blends suggests that the difference in segmental mobilities

is strongly correlated with the nanometer scale compositional heterogeneity [19]. Furthermore, this local compositional variation can give rise to an anomalously broad glass transition, observed in miscible blends. However, the extent of compositional heterogeneity and its effect on segmental motion and consequently on the broad glass transition behavior has not been understood clearly.

1.2.3 Objectives

Our objective in this work is to provide quantitative experimental measurements on segmental dynamics of the individual components in a miscible polymer blend. The segmental motion of interest is correlated with the glass transition [20]. Therefore, the results pertain directly to understanding the compositional dependence of the dynamics underlying the broad glass transition. The rate of segmental motion is examined as a function of temperature and composition. By characterizing the average segmental mobility and the width of mobility distribution simultaneously for each species, we can deepen our insight regarding the effect of intrinsic dynamic difference and compositional heterogeneity on the cooperative segmental dynamics.

The observed dynamics are also related to the longer length scale dynamics manifested in the viscoelastic and diffusion behavior at temperatures much above T_g. Thus, knowledge of the segmental mobilities of each species also represents a first step toward understanding the failure of time-temperature superposition and the non-monotonic compositional dependence of monomeric friction coefficients. However, the exact nature of the latter relation requires further knowledge of the way that the heterogeneity in local segmental motion propagates out to the larger molecular scale,

beyond a Rouse segment in the blend. To determine the relationship between local segmental motions and the larger length scale chain dynamics that control melt rheology, this study is coordinated with a rheo-optical investigation of the contribution of each species to macroscopic blend viscoelasticity [12].

To quantitatively characterize the dynamics of each species in a blend, we use both selective isotopic labeling and an appropriate spectroscopic technique. Specifically, the dynamics of each component are resolved clearly by selective deuterium labeling. The rate and the distribution of segmental reorientation is quantitatively determined using 2D ^{2}H NMR. This experimental approach gives several distinct advantages over many previous studies: 1) the dynamics of both components are studied selectively, 2) the rate of segmental reorientation of the backbone is quantitatively determined, 3) the width of the segmental mobilities distribution is also estimated for each species. Furthermore, we focus on a blend where enthalpic interaction is negligible, in which the equilibrium compositional variation can be modeled by random statistics.

1.3 Outline of the thesis

In this thesis, effects of blending on the segmental dynamics of individual species are discussed in relation to the observed macroscopic properties. In chapter 2, solid state ^{2}H NMR methods will be briefly discussed. The sensitivity of the method to segmental reorientation dynamics are emphasized. In chapter 3, segmental dynamics characterized by DSC and ^{2}H NMR methods are presented. The distinct mobilities of each species in the blend are demonstrated, and their dependence on composition

and temperature are elaborated. In chapter 4, we discuss the implications of our experimental results, in relation to the anomalously broad glass transition and thermorheological complexity. Our results are compared with the rheo-optical studies of the larger length scale chain dynamics to understand the effect of microscopically heterogeneous dynamics on the average friction coefficient. Possible origins of the broad glass transition and thermorheological complexity is discussed in terms of a simple physical picture of cooperative local segmental dynamics.

Chapter 2

Solid state ^{2}H NMR spectroscopy

The segmental motion of deuterium labeled polymers is probed using ^{2}H NMR. The sensitivity of this method on segmental reorientation process arises from the orientation dependence of deuteron magnetic resonance frequency. In particular, 2D ^{2}H exchange NMR method can be used to study the type and the rate of segmental reorientation processes in polymers. In this section, principles of 1D and 2D ^{2}H NMR methods are discussed briefly. The effect of segmental motion on the NMR spectra is emphasized.

2.1 Orientation dependence of ^{2}H NMR spectrum

The deuteron, ^{2}H, is a spin $I = 1$ nucleus and its three spin states, denoted as spin +1, 0, and -1, split into three discrete energy levels in the presence of a magnetic field. For a ^{2}H located in a strong magnetic field along the z-axis, the nuclear spin Hamiltonian is dominated by the interaction of nuclear magnetic dipole moment with

the magnetic field (Zeeman interaction), and is given by,

$$H_z = -\boldsymbol{\mu}\cdot\boldsymbol{B} = -\gamma\hbar\boldsymbol{I}\cdot\boldsymbol{B} = -\gamma\hbar B \cdot I_z, \tag{2.1}$$

where H_z is the Zeeman Hamiltonian, $\boldsymbol{\mu} = \gamma\hbar\boldsymbol{I}$ is nuclear magnetic dipole moment, $\boldsymbol{B} = B\hat{e}_z$ is the magnetic field and $\boldsymbol{I} = I_z\hat{e}_z$ is the angular momentum. The coefficient γ is called the gyromagnetic ratio and $h = 2\pi\hbar$ is Planck's constant. The energy difference, ΔE, between the two adjacent levels is given by

$$\Delta E = \hbar\gamma B = \hbar\omega_0, \tag{2.2}$$

where $\omega_0 = \gamma B$ is called the Larmor frequency. For a deuteron in a magnetic field with strength $B = 4.7$ tesla (as in the 200 MHz spectrometer used in this work), the Larmor frequency is 30.72 MHz. Due to this energy difference, there exist a spin population difference between energy levels, which gives rise to an equilibrium magnetization along the direction of $\boldsymbol{B}$. The NMR experiment consists of causing transitions between these energy levels by applying oscillating magnetic fields at the magnetic resonance frequency, which can be visualized as the rotation of the average magnetization away from its equilibrium orientation along $\boldsymbol{B}$.

In addition to the interaction between the NMR magnetic field and the nuclear spin magnetic dipole moment (Zeeman interaction), the deuteron spin energy levels are altered by the interaction of the local electric field gradient with the ^{2}H electric quadrupole moment arising from a nonspherical charge distribution at the nucleus. Since this interaction is much stronger than other magnetic interactions such as the dipole interactions between nuclei and chemical-shift anisotropy, the dominant perturbation to the Zeeman interaction is given by this quadrupolar interaction. For

deuterons in C-^{2}H bonds, the electric field gradient can be approximated to be axially symmetric, for which the spin Hamiltonian is given by

$$H/\hbar = -\omega_0 I_z + \frac{\delta}{2}(3I_{z'}^2 - I^2), \tag{2.3}$$

where z' is the direction of the electric field gradient and differ from z in general. The δ specifies the strength of the nuclear electric quadrupole interaction, which is typically 125 kHz for a static C-^{2}H bond in amorphous polymers.

This perturbation due to the electric quadrupole interaction gives rise to orientation dependent changes in energy levels (**Figure (2.1)**). The magnetic resonance frequencies shift symmetrically from the Larmor frequency and is given by

$$\omega^{\pm}(\theta) = \omega_0 \pm \omega_Q = \omega_0 \pm \frac{\delta}{2}\,[3\cos^2(\theta) - 1)], \tag{2.4}$$

where the two resonance frequencies ω^+ and ω^- correspond to the two possible transitions between the adjacent energy levels and θ is an orientation angle of a C-^{2}H bond with respect to the static magnetic field of NMR spectrometer (*i.e.*, angle between z and z') [21]. In a frame of reference that rotates at the Larmor frequency, the net precession of the magnetization can be described only by the second term, $\Delta\omega^{\pm}(\theta) = \pm\frac{\delta}{2}\,[3\cos^2(\theta) - 1)]$. For a chemical group undergoing a fast symmetric motion with small correlation time of molecular motion ($\tau_c < 10^{-7}$s), the orientation dependence of ω_Q is modified by the motion. For example, the C-^{2}H bonds of a methyl group performs very fast symmetric motion around its three-fold symmetry axis even below the glass transition temperature, and hence δ is substituted by an effective quadrupole interaction strength, $\overline{\delta} \simeq \delta/3$, and the relevant orientation angle θ becomes that of the symmetry axis.

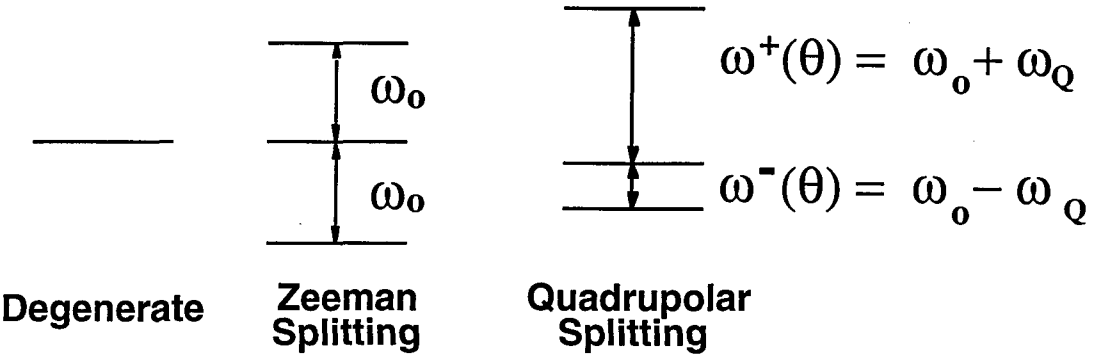

Figure 2.1: Energy level of a ^{2}H under Zeeman and quadrupolar interaction. Two resonance frequencies, $\omega^+(\theta)$ and $\omega^-(\theta)$, are associated with a C-^{2}H bond oriented at an angle θ with respect to the NMR magnetic field $\boldsymbol{B}$.

The orientation dependence of deuteron magnetic resonance frequency makes ^{2}H NMR a very valuable tool to study molecular orientation distributions and reorientation dynamics of many different systems, including liquid crystalline molecules, membrane lipids, and polymers. For example, the orientation distribution $P(\theta)$ of some molecules can be inferred from the distribution of NMR spectral intensity as a function of magnetic resonance frequency, $S(\omega)$. Although some polymers can obtain partial orientational order, most polymers as a whole have isotropic orientation distribution, either because of intrinsically disordered structure or because of many randomly oriented domains. In such systems, the orientation distribution $P(\theta)$ becomes

$$P(\theta) = \frac{1}{2}\sin(\theta). \tag{2.5}$$

The mapping of this orientation distribution to the distribution of spectral intensities

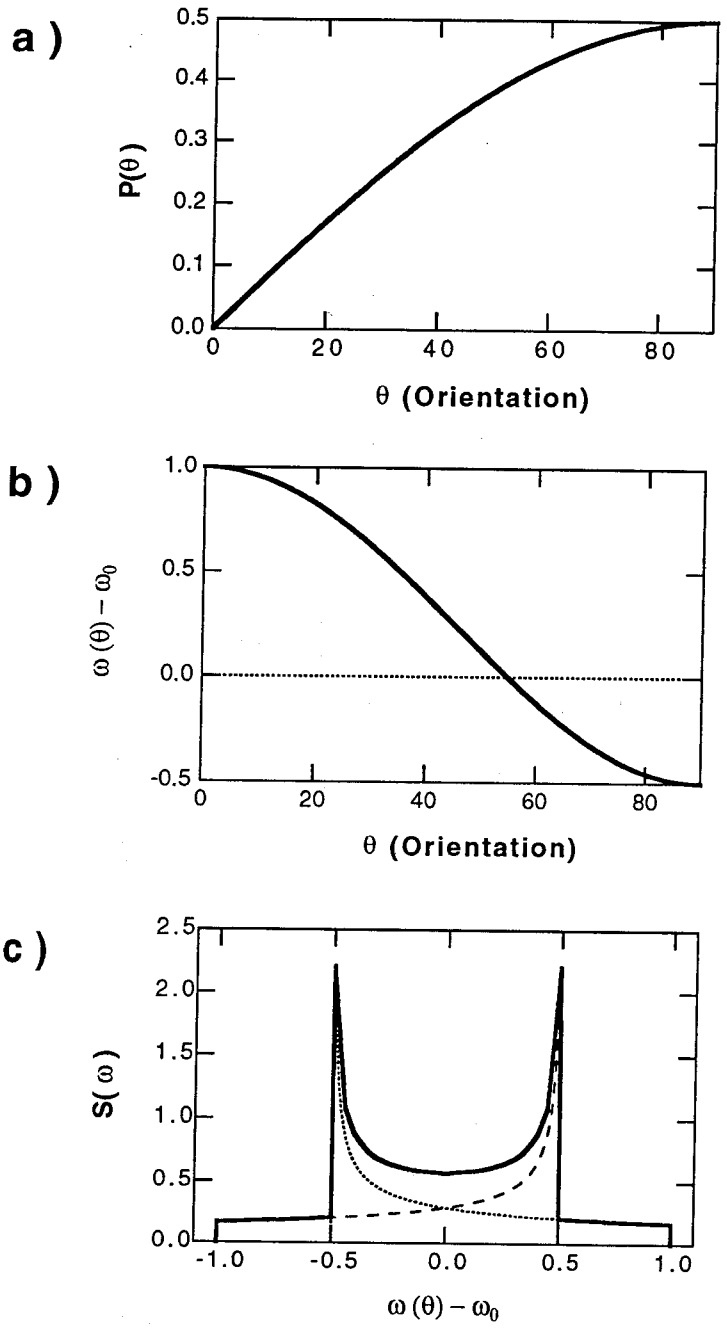

Figure 2.2: One-dimensional ^{2}H spectrum for isotropic solid: Pake pattern.

is illustrated in **Figure 2.2**, and the resulting spectrum is called the Pake pattern. The Pake pattern has a symmetric distribution of spectral intensities, because two resonance frequency lines are associated with each C-^{2}H bond.

Information regarding the reorientation dynamics can be obtained when the changes in orientation angles during a fixed time period can be determined. The changes in orientation with time can be specified as the joint probability density of orientations, $P(\theta_1, \theta_2; t_m)$, where θ_1 and θ_2 are orientations at time $t = 0$ and at $t = t_m$. Analogous to 1D spectrum, this joint probability density $P(\theta_1, \theta_2; t_m)$ can be obtained by analyzing the spectral intensities, $S(\omega_1, \omega_2; t_m)$, where the resonance frequency before (ω_1) and after (ω_2) a controlled time period, t_m, are dictated by the orientations θ_1 and θ_2. Specifically, spectral intensity at ($\omega_1(\theta_1)$, $\omega_2(\theta_2)$) is directly proportional to the number of C-^{2}H bonds that have orientation θ_2 at t_m starting from an orientation θ_1 at $t = 0$.

2.2 1D ^{2}H NMR experiment

In most contemporary NMR experiments, short pulses of oscillating magnetic field are used to rotate the equilibrium magnetization. When the equilibrium magnetization along the z-axis is rotated to the x-y plane, the magnetization precesses with its resonance frequency under the torque exerted by the magnetic field. The precession of the transverse magnetization induces an oscillating current at its resonance frequency, and this signal is acquired in the time domain. The spectral information is obtained by Fourier transforming the signal. Since the spectral intensity for static solid is spread

over a very broad frequency range (e.g. for deuterons with $\delta \simeq 125$kHz, spectral width $\simeq 250$kHz), corresponding time-domain signal has component that decays very rapidly. Therefore, two experimental requirements should be satisfied, in order to obtain complete spectral information.

First of all, magnetizations having a wide range of resonance frequencies need to be excited to the same degree. Since the excitation band of a pulse falls down very rapidly for $\omega > 1/t_p$ where t_p is the pulse width, t_p must be much smaller than 8μs to excite the whole band spread over ± 125 kHz. Same band width is also required for the receiver electronics as well. Secondly, the decay of signal is so rapid that fraction of initial oscillation is lost during the time it takes for the receiver electronics to settle down after the application of the resonant pulse (receiver dead time, typically 10μs). This loss of time domain signal gives rise to significant spectral distortions that cannot be compensated simply by phase correction. The solid echo pulse sequence can be used to delay the beginning of the time-domain signal, so that the complete time-domain signal can be obtained after the receiver dead time [22]. The solid echo pulse sequence is schematically shown in **Figure 2.3a**. The time-domain signal from the solid echo, $f(t)$, is given by the ensemble average of the oscillatory signals over all magnetizations, and is given by

$$f(t) = \langle \cos(\omega_a \cdot t) \rangle = \int \cos(\omega_a \cdot t) P(\omega_a)\, d\omega_a, \tag{2.6}$$

where $\langle \cdot \rangle$ represents ensemble average over all resonance frequencies, and $P(\omega_a)$ is the probability density that a certain magnetization has resonance frequency ω_a. Fourier transform of the signal, $\widehat{f(t)}$, results in the spectral density of magnetic resonance,

$S(\omega)$, which is essentially identical to $P(\omega)$,

$$\begin{aligned} S(\omega) = \widehat{f(t)} &\equiv \int f(t)\, e^{i\omega t}\, dt \\ &= \int [\int \cos(\omega_a \cdot t)\, e^{i\omega t}\, dt]\, P(\omega_a)\, d\omega_a \\ &= \frac{1}{2}\int [\delta(\omega_a + \omega) + \delta(\omega_a - \omega)] P(\omega_a) d\omega_a \\ &= \frac{1}{2}[P(-\omega) + P(\omega)]. \end{aligned} \tag{2.7}$$

Further, using the direct relationship between θ and ω, the orientation distribution of C-^{2}H bonds can be directly inferred from the 1D NMR spectrum, $S(\omega)$, obtained by solid echo experiment.

The above relationship between the solid echo spectrum and the orientation distribution is valid only when the orientation distribution is frozen on the time-scale of the NMR experiment. In the presence of molecular motion, the shape and the absolute signal intensity of the solid echo spectra changes depending on the type and the rate of motion. The most prominent lineshape changes occur when the correlation time of molecular motion, τ_c, is in the "intermediate dynamic regime," *i.e.*, on the order of the inverse spectral width ($10^{-6} \leq \tau_c \leq 10^{-4}$ for ^{2}H) [22]. The changes in the solid echo lineshape also accompany a significant reduction in spectral intensity. This reduction in spectral intensity and the changes in the lineshape can be partially explained by the molecular motion occurring during the solid echo duration, Δ (**Figure 2.3a**). Such motion changes the magnetic resonance frequency during the solid echo, and hence results in incomplete echo formation. Since the components that do not refocus properly tend to cause destructive interference with the properly refocussed magnetizations, the solid echo spectrum has both reduced intensity and

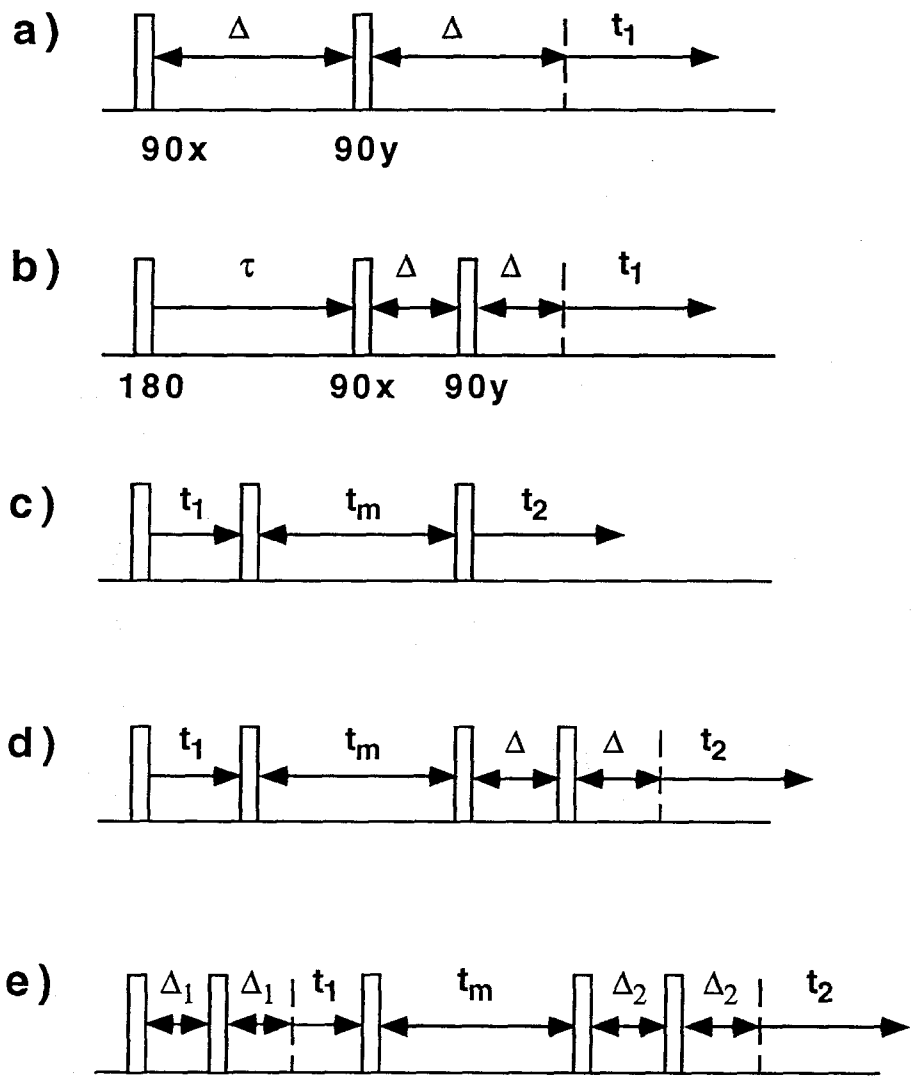

Figure 2.3: Solid state ^{2}H NMR pulse sequences. (a) standard solid echo, (b) inversion recovery T_1, (c) Jeener-Broekaert three pulse 2D exchange, (d) four pulse 2D exchange, and (e) five pulse 2D exchange.

distorted lineshape.

The reduction of solid echo intensity can also arise from the effective T_2 relaxation process, which describes the decay of magnetization in x-y plane. This process arises from the loss of coherence among the individual nuclear spins that form a net magnetization, and can be visualized as the irreversible decrease of transverse magnetization with time. Since the effective T_2 relaxation time can be as short as 10's of microseconds, this process can reduce the amplitude of magnetization significantly over the duration of solid echo experiment, in which Δ is typically 30μs. The T_2 relaxation time can be obtained using the solid echo pulse sequence by measuring the echo amplitude as a function of Δ. As Δ increases, a greater fraction of magnetization loses its coherence in an approximately exponentially manner over a wide temperature range above the glass transition. The changes in T_2 relaxation time with the rate of motion is coupled with the loss of spectral intensity occurring in the intermediate dynamic regime discussed above.[1] In particular, the reduction in intensity due to the effective T_2 relaxation is maximized when $\tau_c \simeq 2/\delta$, for which the T_2 relaxation time is minimized [23, 22].

The presence of fast dynamic processes occurring at frequencies comparable to the Larmor frequency ($\tau_c \simeq 4 \times 10^{-7}$s for 4.7 T magnet) can effectively provide means to bring excited magnetization back to equilibrium. This process is often called the T_1 relaxation process, and this can be experimentally probed using the

[1]Since the T_2 measurement is based on the solid echo experiment, the measured echo amplitude is reduced not only due to the effective T_2 relaxation, but also due to an incomplete refocussing close to the intermediate dynamic regime. Therefore, effect of T_2 relaxation process cannot be completely separated from the effect of incomplete refocussing.

"Inversion Recovery" pulse sequence shown in **Figure 2.3b**. At high temperatures, the inversion recovery experiments yields a well defined relaxation time via

$$I(\tau) = I_0\,(1 - 2\,\exp\,(-2\tau/T_1)), \tag{2.8}$$

where $I(\tau)$ is the signal intensity obtained for a given τ, I_0 is the intensity for $\tau \rightarrow 0$ or ∞, and τ is as defined in the figure. As temperature decreases to the glass transition, back-bone reorientation becomes very slow ($\tau_c \sim 1$ s) and the relaxation time increases rapidly. In this regime, the T_1 relaxation process becomes strongly non-exponential, and the relaxation time is not well-defined any more. The relaxation can often be fitted by multiple exponential relaxations, but no successful correlation with the underlying dynamics can be made. The need of multiple exponential relaxation is often attributed to heterogeneity that is frozen on the time-scale of the T_1 relaxation process.

These 1D solid state ^{2}H NMR experiments can yield not only the static orientation distribution but also valuable information on segmental dynamics. For example, the solid echo intensity and the T_2 relaxation time exhibit strong dependence on temperature and hence on the rate of motion. Furthermore, the change in solid echo intensity as a function of mean correlation time, $\langle\tau_c\rangle$, yields valuable information regarding the distribution of correlation times. The broader the distribution of correlation times, the higher the intensity in the intermediate dynamic regime, since more of the C-^{2}H bonds reorient at a rate outside the intermediate dynamic regime. This can be used to qualitatively describe the change in correlation time distribution with blending. The T_1 relaxation times can also be used to understand fast segmental dynamics

occurring at the reciprocal of the Larmor frequency. However, quantitative results on segmental dynamics can hardly be obtained by using these measurements alone. These disadvantages can be overcome by coordinating the 1D NMR experiments with 2D exchange NMR method. In the next section, advantages of 2D ^{2}H exchange NMR method are discussed, with particular emphasis on the direct relationship between the experimental spectra and the underlying segmental dynamics.

2.3 Principles of 2D ^{2}H exchange NMR

The segmental reorientation dynamics of polymers near the glass transition can be quantitatively studied using 2D ^{2}H exchange NMR [24, 25]. The essence of this method is that the type and the rate of segmental reorientation can be determined by analyzing the correlation of deuteron resonance frequency before and after the mixing time, t_m [24, 25]. Analogous to the direct relationship between the 1D NMR spectrum, $S(\omega)$, and the distribution of resonance frequencies, $P(\omega)$, the 2D NMR spectrum, $S(\omega_1, \omega_2; t_m)$, is essentially identical to the joint probability density, $P(\omega_1, \omega_2; t_m)$, which contains a complete information of the reorientation dynamics. Similar to equation 2.7 in the previous section,

$$S(\omega_1, \omega_2; t_m) = \frac{1}{2}[P(-\omega_1, -\omega_2; t_m) + P(\omega_1, \omega_2; t_m)]. \tag{2.9}$$

Working backward, we can easily see that the time domain signal needed to yield this correlated spectral information is

$$f(t_1, t_2) = \frac{1}{2}\langle[e^{i\omega_a t_1} \cdot e^{i\omega_b t_2} + e^{-i\omega_a t_1} \cdot e^{-i\omega_b t_2}]\rangle$$

$$= \langle \cos(\omega_a t_1) \cdot \cos(\omega_b t_2) \rangle - \langle \sin(\omega_a t_1) \cdot \sin(\omega_b t_2) \rangle, \qquad (2.10)$$

where $f(t_1, t_2)$ is time-domain 2D NMR signal, ω_a and ω_b are magnetic resonance frequencies before and after t_m.

The 2D exchange NMR experiment can be used to generate this time-domain data, as schematically illustrated in **Figure 2.4** for a five pulse 2D exchange NMR experiment. This five pulse experiment has same basic features as the simpler three pulse sequence shown in **Figure 2.3c**. Following each of the three basic pulses, three characteristic events take place; evolution of initial magnetization during t_1, mixing between different orientations over t_m, and detection of signal as a function of t_2. During the first evolution period, a transverse magnetization is prepared and its amplitude evolves sinusoidally with $\omega_1 \cdot t_1$ as dictated by the initial orientation of the C-^{2}H bond, θ_1. Instead of acquiring the initial oscillatory modulation and generating an NMR spectrum by Fourier transforming with respect to t_1, the state of the magnetization is stored by the pulse just after t_1. Reorientation may take place during the mixing time, t_m. The time-domain signal is recorded during the detection period as a function of time, t_2. The initial amplitude of the signal oscillates with $\omega_1 \cdot t_1$, as prepared at the end of t_1. As a function of t_2, the signal oscillates with $\omega_2 \cdot t_2$ as dictated by the final orientation, θ_2. By repeating the experiment with an incremented value of t_1, the complete 2D data can be obtained, $f(t_1, t_2; t_m)$, which after two subsequent Fourier transforms yield a 2D spectrum, $S(\omega_1, \omega_2; t_m)$. It should be emphasized that by performing the 2D exchange NMR experiment as a function of t_m, the type and the rate of segmental reorientation process can be determined

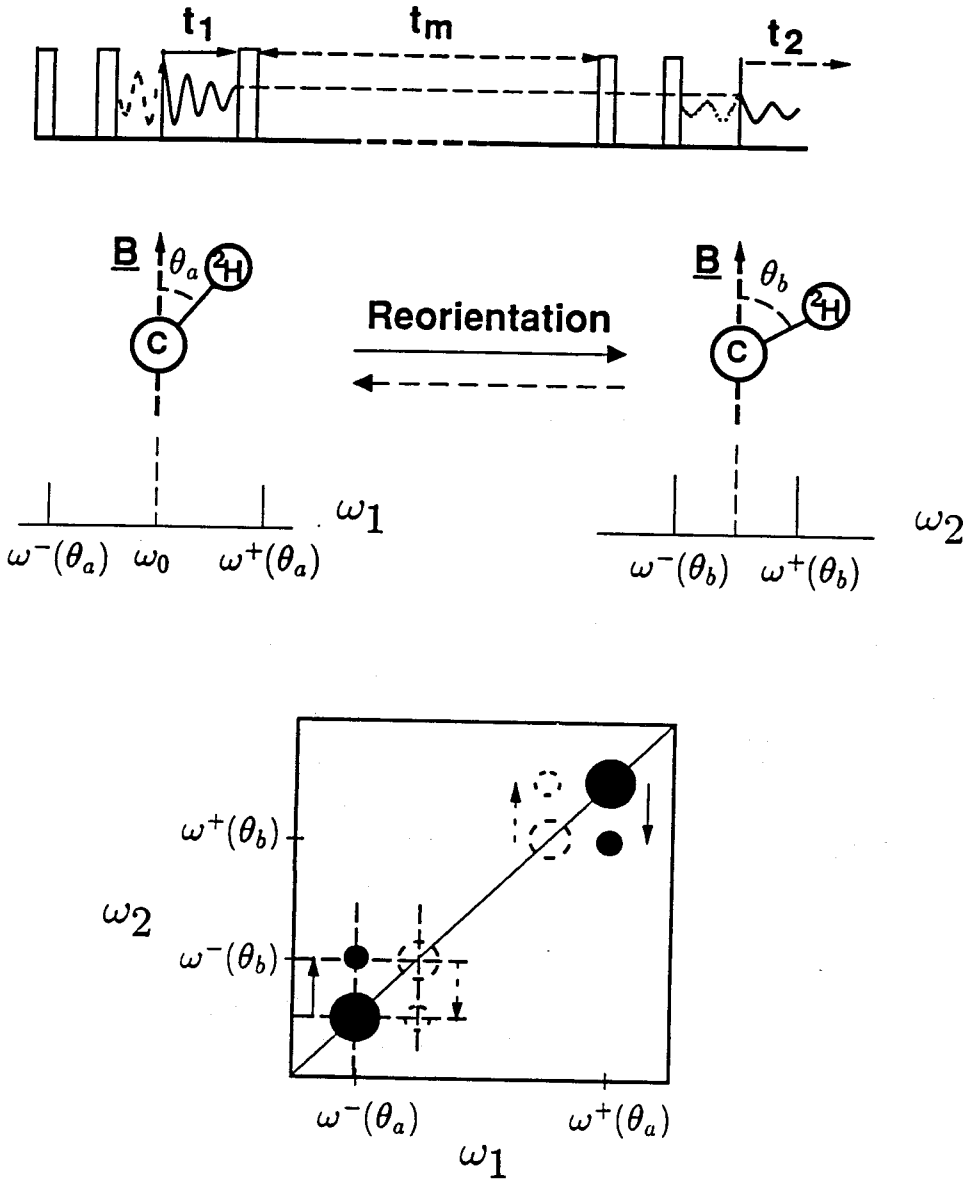

Figure 2.4: Two-dimensional exchange NMR and reorientational motion. From the top: five pulse sequence corresponding to Figure 2.3e (also see Figure 2.3 for three and four pulse sequences), reorientation and corresponding changes in the resonance frequency, 2D exchange spectrum for a reorientation between two fixed orientations.

directly.

The contribution due to just two orientations are shown in the schematic diagram. When the range of times t_1 and t_2 is short ($\sim 2 \times 10^{-4}$s) compared to the correlation time, τ_c, for reorientation of C-^{2}H bonds, we can neglect reorientation during t_1 and t_2 [26, 27, 28]. This is typically the case in amorphous polymers near T_g, ($\tau_c \geq 10^{-3}$s). The mixing time t_m is held fixed for each 2D spectrum. If t_m is short compared to τ_c, very few C-^{2}H bonds undergo reorientation during t_m. Therefore, the spectrum will be confined to the diagonal; the initial and final resonance frequencies $\omega^{\pm}(\theta_i), \omega^{\pm}(\theta_f)$ of each ^{2}H are the same since $\theta_i = \theta_f$. If t_m is on the order of τ_c or longer, a significant fraction of C-^{2}H bonds undergo reorientation during t_m. Deuterons on a C-^{2}H bond that is initially oriented at $\theta_i = \theta_a$, but has final orientation $\theta_f = \theta_b$ contribute to off-diagonal intensity at positions $(\omega_1, \omega_2) = (\omega^{\pm}(\theta_a), \omega^{\pm}(\theta_b))$, as shown in **Figure 2.4.** By microscopic reversibility, as many bonds reorient from $\theta_b \Rightarrow \theta_a$ as from $\theta_a \Rightarrow \theta_b$. Thus, the spectrum is symmetric about the diagonal. The profile of the off-diagonal intensity shows both the type and the extent of reorientation during a particular mixing time [24, 29]. As we increase the mixing time, the spectra reveal reorientation of progressively slower fractions of the correlation time distribution that contribute dominantly to the rigid diagonal intensity at small t_m. Therefore, the evolution of the two-dimensional spectrum over a range of t_m reveals the distribution of motional rates as well as the mean.

Four or five pulse 2D exchange NMR sequences are used for ^{2}H NMR (see **Figure 2.3d, e**) in practice, in order to circumvent the receiver dead time problem, as

well as to obtain both parts of the signal in eqn. 2.10, $\langle \cos(\omega_a t_1) \cdot \cos(\omega_b t_2) \rangle$ and $\langle \sin(\omega_a t_1) \cdot \sin(\omega_b t_2) \rangle$ separately. This four pulse sequence has been used extensively for the past eight years to study dynamics of numerous polymer systems including many amorphous polymers, semicrystalline polymers, and liquid-crystalline polymers. One practical disadvantage of the four pulse sequence is that the value of t_1 cannot be started at 0. For many spectrometers, the shortest possible t_1 is about 1μs, and this can give rise to a serious distortion of 2D spectrum. In order to eliminate this distortion, the data obtained by the four pulse method is extrapolated to $t_1 = 0$[25]. In the five pulse sequence, the magnetization is prepared for evolution by utilizing a two pulse echo similar to the quadrupole echo detection sequence. Then, the evolution of magnetization can be started at $t_1 = 0$, without any practical difficulty. In this work, all 2D spectra have been obtained using this five pulse sequence.

Two practical considerations can indicate the range of temperatures in which 2D ^{2}H exchange NMR is applicable. First, it is often not practical to perform 2D NMR experiments much below the glass transition. Below the glass transition, mean correlation time increases very strongly and becomes so large ($\tau_{c_0} >> 1$s) that significant exchange pattern can only be observed for $t_m > 1$s. However, the T_1 relaxation time, which is a half life-time of the magnetization, does not increase as rapidly as τ_{c_0}. The magnetic resonance information stored before the mixing time is almost completely lost for the t_m during which appreciable reorientation can take place. Consequently, the quantitative information regarding the segmental reorientation cannot be obtained reliably much below the glass transition. Second, two-dimensional exchange

NMR spectrum, $S(\omega_1, \omega_2; t_m)$, is directly related to the joint orientation density, $P(\theta_1, \theta_2; t_m)$, when the reorientation over the evolution and the detection period is negligible. Since t_1 and t_2 are relatively short ($\sim 2 \times 10^{-4}$s), the above condition is satisfied for polymers near T_g ($\tau_c \geq 10^{-3}$s). However, when the reorientation is much faster, or is characterized by a very broad distribution of motional rates (3 to 5 decades), reorientation during the evolution and detection period cannot be neglected. Although it has been shown recently that the 2D spectrum can be used to extract dynamic information through elaborate line-shape fitting [28], the 2D exchange spectrum loses its special meaning as a direct probe of reorientational dynamics.

2.4 ^{2}H NMR experiment and analysis

All 2D spectra are recorded using a Bruker MSL 200 spectrometer, equipped with a VT1000 temperature controller unit. A slightly modified Bruker broadband wideline probe with a 7.5 mm coil is used. The 90° pulse length is typically 3.0 μs, and a digitization rate of 3.2 μs is used to capture the complete range of the spectra both along the ω_1 and ω_2 dimensions. The repetition time is varied from 300 to 800ms to obtain sufficiently relaxed spectra. Reasonable signal to noise is achieved with 128 scans at the smallest mixing time and up to 1600 at the largest mixing time. The typical data size is 256 complex points along t_2 and 60 points along t_1. Echo durations for the five pulse sequences are 3μs and 30μs for the evolution and detection periods, respectively. At each temperature, spectra are taken at three or more mixing times to probe the evolution of the reorientation distribution with time.

The mixing time is varied from 0.5 ms to 400 ms, spanning almost three decades in time. At an identical condition, the 2D NMR experiment is performed twice to obtain each part of the complete time domain data (eqn. 2.10), $\langle \cos(\omega_a t_1) \cdot \cos(\omega_b t_2) \rangle$ and $\langle \sin(\omega_a t_1) \cdot \sin(\omega_b t_2) \rangle$.

The time domain data are then Fourier transformed twice along t_2 and t_1 to obtain the 2D spectrum. When the variable times, t_1 and t_2, do not start exactly at the beginning of echo, significant spectral distortion arises, which cannot be corrected by routine phase corrections in the frequency domain. Using a five pulse sequence, the acquisition of time domain data can be started before the beginning of the echo both along the t_1 and t_2 directions, which can be interpolated to the beginning of echo, *i.e.*, $t_1 = 0$ and $t_2 = 0$, to eliminate such lineshape distortions. The interpolated data set is first Fourier transformed along t_2, which is then Fourier transformed along t_1 after baseline correction to remove any non-zero constant component. The Fourier transform is performed for the two separate data sets, $\langle \cos(\omega_a t_1) \cdot \cos(\omega_b t_2) \rangle$ and $\langle \sin(\omega_a t_1) \cdot \sin(\omega_b t_2) \rangle$, and a complete 2D spectrum is obtained by subtracting them (eqn. 2.10) [25]. Since the T_1 relaxation times differ for the $\langle \cos(\omega_a t_1) \cdot \cos(\omega_b t_2) \rangle$ and $\langle \sin(\omega_a t_1) \cdot \sin(\omega_b t_2) \rangle$ parts, it is often necessary to apply a weighting factor for one of the spectra.

The shapes of the present spectra indicate that the C-^{2}H bond reorientation dynamics can be modeled as isotropic rotational diffusion, as has been observed in other amorphous polymers [26, 28, 31, 20]. Therefore, we fit the experimental spectra by calculating the 2D spectra that would arise from isotropic rotational diffusion. The

2D spectra are simulated by first solving the rotational diffusion problem,

$$\frac{\partial}{\partial t_m} P(\theta_1, \theta_2; t_m) = \Delta_{\theta_2} P(\theta_1, \theta_2; t_m), \tag{2.11}$$

where

$$\Delta_{\theta_2} = D \frac{1}{\sin(\theta_2)} \frac{\partial}{\partial \theta_2} (\sin(\theta_2) \frac{\partial}{\partial \theta_2}), \tag{2.12}$$

with an isotropic initial orientation distribution,

$$P(\theta_1, \theta_2; 0) = \frac{1}{2} \sin(\theta_1) \delta(\theta_1 - \theta_2). \tag{2.13}$$

The 2D spectrum is then constructed by mapping $P(\theta_1, \theta_2; t_m)$ onto $S(\omega_1, \omega_2; t_m)$ using eqn. 2.4, which can be formally written as

$$\begin{aligned} S(\omega_1, \omega_2; t_m) &= \int d\theta_1 \int d\theta_2 \, \delta[\omega^{\pm}(\theta_1) - \omega_1] \\ &\quad \times \delta[\omega^{\pm}(\theta_2) - \omega_2] P(\theta_1, \theta_2; t_m). \end{aligned} \tag{2.14}$$

The correlation time for this process is inversely related to the effective rotational diffusivity D by $\tau_c = \frac{1}{6D}$[27].

The evolution of the 2D spectra with t_m can be roughly described by a single correlation time, τ_c. The quantitative agreement, however, improves significantly by introducing a distribution of correlation times. The simple log-Gaussian distribution of correlation times is found to fit the experimental spectra successfully:

$$P(\ln \tau_c) = \frac{\exp[-(\ln \tau_c - \ln \tau_{c0})^2 / 2\sigma_{ln}^2]}{\sqrt{2\pi\sigma_{ln}^2}}, \tag{2.15}$$

where $\tau_{c0} = \exp\langle \ln \tau_c \rangle$ is the log-mean correlation time and σ_{ln} is the log-mean standard deviation [28]. The width of the correlation time distribution in decades is $\sigma = \sigma_{ln}/ln(10)$.

The procedure we use to determine τ_{c_0} and σ begins by finding the value of τ_{c_0} that produces the best fit for all t_m with 2σ constrained to be small, typically one decade. If this fit shows systematic deviations that indicate the presence of significantly faster and slower processes, the width of the distribution is increased by a half decade, and τ_{c_0} is optimized again. This is repeated until the fit can no longer be improved by increasing 2σ. Since the range of t_m only spans up to three decades, it is not possible to accurately determine 2σ when it exceeds three. Nevertheless, the fit is quite sensitive to τ_{c_0}, so uncertainties in this parameter are relatively small (less than a factor of two).

Chapter 3

Segmental dynamics of individual species in PI/PVE blends

We study segmental dynamics of individual components in miscible polymer blends of polyisoprene(PI) and polyvinylethylene (PVE). The changes in glass transition behavior with blending are examined using the differential scanning calorimetry measurement. Dynamics of individual species underlying the glass transition are characterized using ^{2}H NMR. To selectively probe the motion of individual components in the blend, we use blends with a deuterium labeled component. Reorientation of the deuterium labeled species are studied selectively using a combination of 1D and 2D solid-state deuteron NMR methods. In particular, the mean and width of the reorientational correlation time distribution are quantitatively determined near the glass transition by two-dimensional deuteron exchange NMR (2D ^{2}H NMR). The segmental reorientation dynamics at and above the glass transition are examined for both homopolymers, and are contrasted with those observed within the blends.

3.1 Sample preparation and characterization

In this work, blends of polyvinylethylene (PVE) (also known as 1,2-polybutadiene) and 1,4-polyisoprene (PI) are used as model systems. This pair is ideal for our study since it has been shown to be miscible in all proportions, yet has very weak enthalpic interactions. Recent SANS experiments have shown that PI/PVE blends can be described by an interaction parameter, χ, that is small but negative at all accessible temperatures [32]. This indication that the blend is completely miscible without specific interaction is consistent with numerous other studies [33, 34, 35, 36]. For example, DSC traces of PI/PVE blends and block-copolymers of the same overall composition are nearly identical. This suggests that the broad glass transition in this blend is not due to concentration fluctuations associated with incipient phase separation, since such fluctuations would be much smaller in the block copolymers [37].

Four polymers are used in these experiments: hydrogenous and deutero 1,4-polyisoprene (PI, dPI), and hydrogenous and deutero polyvinylethylene (PVE, dPVE). All polymers are synthesized by anionic polymerization and have narrow molecular weight distributions. The glass transition temperature of each species and their miscibility are known to depend strongly on the microstructure of PI and PVE [17, 35, 38]. The microstructure of PI and PVE are determined using the ^{13}C NMR spectra that are obtained at room temperature from 15% (w/v) $CDCl_3$ solutions of PI and PVE using a GE QE-300 spectrometer. Molecular weight distributions of normal and deutero PI and PVE are determined with respect to poly(isoprene) standards by

gel-permeation chromatography (Waters ALC-GPC), operated at 60°C with reagent grade toluene. The ^{13}C NMR results indicate that microstructures of the matching pair of polymers are the same within experimental uncertainties (**Table 3.1**). The molecular weights of all polymers are large enough that the glass transition behavior and the local segmental dynamics studied here should not be sensitive to the small difference in molecular weight between normal and deutero-chains. Characterization results for these homopolymers are summarized in **Table 3.1**.

Table 3.1: PI and PVE characterization results

sample	M_n(kg/mol)	M_w/M_n	microstructure,(%)			T_g(K)
			cis-1,4	trans-1,4	3,4	
PI	108	1.07	78.5 ±0.5	16.0 ±1.0	6 ±1.0	210
dPI	110	1.45	78 ±1.5	15 ±1.5	7 ± 2	210
			1,2	1,4		
PVE	83	1.06	94 ±2	6 ±2		273
dPVE	69	1.36	93 ±2	7 ±2		271

For ^2H NMR measurements, we use deutero homopolymers and pairs of dPI/PVE and PI/dPVE blends with PI weight fractions of 25, 50, and 75%. The blends are prepared by mixing 3 wt % toluene solutions of each component and slowly casting on a Teflon surface. The cast solution is dried at room temperature first under a hood and further under vacuum for more than a week. The blend films are clear and free of bubbles, suggesting that the film is homogeneous and completely dried. No

anti-oxidant is added to the blends to avoid possible effects on the local dynamics and T_g. The blend samples are subsequently sealed off under air in NMR sample tubes and kept in the freezer to retard oxidation.

3.2 Calorimetric glass transition of PI/PVE blends

When the melt of a non-crystallizable polymer is cooled below a certain temperature, motion of polymer chains slows down very rapidly, and eventually the motion becomes completely frozen at the time-scale of observation. Along with the freezing of molecular motion, polymer loses its flexibility and becomes relatively hard polymer glass. The temperature at which polymer undergoes this change is known as the glass transition temperature, T_g, and serves as an important practical criterion that determines the applicable temperature ranges and processibility of a polymeric material. The T_g is also a useful reference temperature, with which the temperature dependence of the viscoelastic properties are described via WLF equation (eqn. 1.3). The freezing of molecular motion also accompanies an abrupt change in such properties as the thermal expansion coefficient and heat capacity. In practice, the T_g is most commonly determined by measuring one of these properties as a function of temperature with a certain rate of temperature scanning. The glass transition temperature varies with the experimental observation time scale (*e.g.*, temperature scanning rate) because the temperature at which the underlying molecular motion becomes effectively frozen compared to the observation time-scale changes. In other words, a certain rate of molecular motion or a structural relaxation time can be asso-

ciated with an experimentally determined T_g. For example, the macroscopic enthalpy relaxation time reaches $\sim$ 100s at the conventional onset temperature observed by differential scanning calorimetry (DSC) measurement with scanning rate of 10°/min.

In polymer blends, glass transition behavior is often used to discriminate phase separated blends, since the phase separated blends undergo multiple glass transitions including the ones near their pure component T_g. In contrast, a single broad glass transition is observed in most compatible blends, where not only the T_g but the width of T_g is also practically important. The significance of the broad glass transition has been appreciated so poorly that the width of T_g has never been studied carefully, even though the width shows very strong compositional dependence. Furthermore, the origin of the broad glass transition in compatible blends are not completely understood. In this work, the broad glass transition behavior is examined carefully first by calorimetric measurement, and then discussed in terms of the dynamics of individual species underlying the broad glass transition.

The glass transition of the pure PI and PVE homopolymers observed by differential scanning calorimetry (DSC) (**Figure 3.1**) are widely separated (PI at -62.5 °C) and (PVE at -2.5 °C). The DSC traces were recorded for the specimens (ca. 25 mg) between -80 and 20°C at a heating rate of 10°C/min using a Perkin Elmer System DSC-7. The width of glass transition under these conditions is about 5 K for both homopolymers. In PI/PVE blends, a single glass transition is occurring at an intermediate temperature. Although the width of glass transition is much broader in blends, heat capacity does not change near the T_g of two homopolymers, consistent

with the single phase behavior of these blends. Furthermore, the DSC traces observed for block copolymers of comparable compositions have almost identical width as that of blends [40]. This similarity suggests that this broadening of the DSC glass transition is not due to the incipient phase separation, because such phase inhomogeneity will be suppressed in the block copolymers.

The DSC traces for the deuterium labeled polymers and their blends are compared with those of normal polymers for pure PVE and for 50/50 blend (**Figure 3.1**). The pair of PVE show slightly different T_gs , probably due to a small difference in their microstructure [38, 39], while the pair of PI's have essentially the same T_g. The glass transition behavior of PI/dPVE blends are also affected by this small difference. More importantly, PI segment fraction of these blends differ slightly for a given PI weight fraction, because of the small differences in molecular weights of normal and deuterium labeled species. Specifically, 50 wt% dPI blend contains less PI segments than for 50 wt% normal PI blends, thus causing the onset of glass transition to shift slightly to higher temperature than that of the normal and dPVE labeled blends. For a given temperature, these effects decrease the mobility of dPI species in the blends with same wt%, while they have opposite effects on the mobility of dPVE species. Therefore, suppose the mobilities of both PI and PVE species are the same in PI/PVE blends, the mobility of dPI should be smaller than that of dPVE.

The DSC T_g is conventionally defined as the temperature at which the heat capacity change becomes half of the total ΔC_p at the glass transition. The T_g of PVE rich blends decreases rapidly with the addition of PI, but the change in T_g becomes

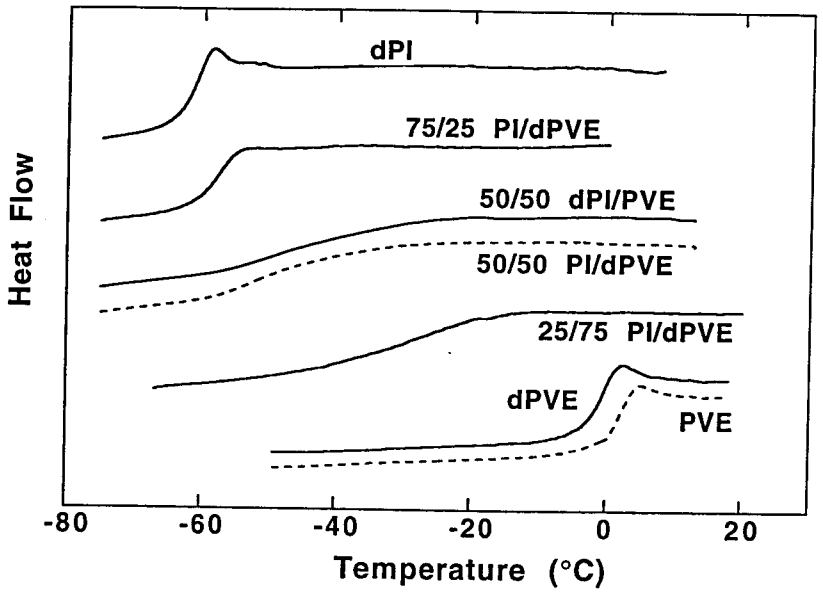

Figure 3.1: DSC traces for PI/PVE blends and homopolymers

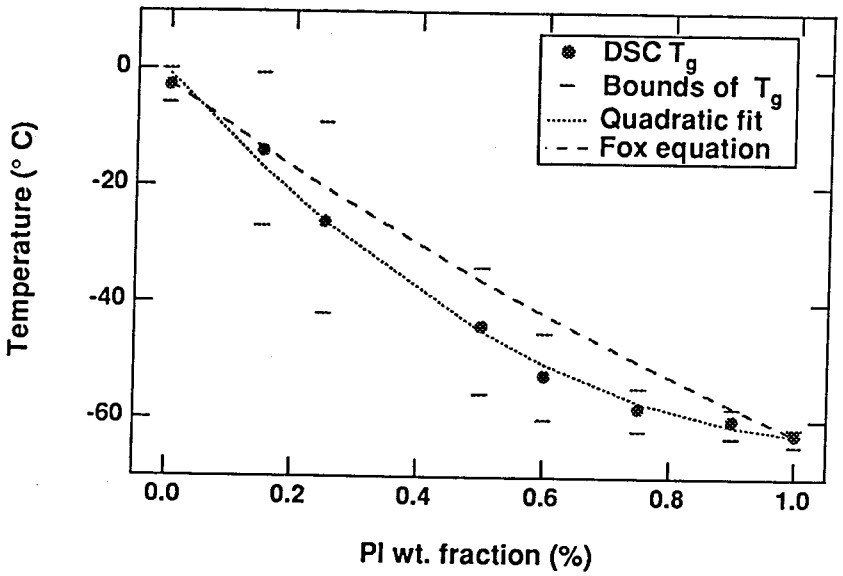

Figure 3.2: Compositional dependence of glass transition temperature. The bound of T_g is also included.

very gradual for PI fraction higher than 60% (**Figure 3.2**). The width of the glass transition also varies strongly with composition, exhibiting anomalous broadening for PI fractions less than ~50%. The bounds of the glass transition are defined graphically as the two intersections between the tangent line at the T_g and the upper and lower baselines. The width of the glass transition varies from 3 K for homopolymers and up to about 30 K for blends with PI fractions about $15 - 50\%$. The bounds of glass transition can also be defined as the temperatures at which the DSC traces start deviating from baselines below and above the T_g. This defines another measure of the broad glass transition that is always larger than the previous definition. The width of glass transition appears to be correlated with the sensitivity of the glass transition to a small change in composition (**Figure 3.2**). This behavior is in qualitative agreement with the conventional interpretation that the broad glass transition arises from compositional fluctuations, because a given compositional fluctuation affects the width of glass transition more strongly when the T_g changes sensitively with composition. The molecular origin for the strong compositional dependence of the width of glass transition is examined experimentally using ^{2}H NMR and in terms of a simple model of statistical composition variations in the next chapter.

3.3 Component dynamics in PI/PVE blends: ^{2}H NMR investigation

Segmental reorientation of two labeled species, dPI and dPVE, are quantitatively studied in pure states and in blends near the calorimetric glass transitions. The mean,

τ_{c_0}, and the width, σ, of the correlation time distribution are determined from the 2D ^{2}H NMR spectra. A mean correlation time at higher temperature than is accessible by 2D ^{2}H NMR is obtained using a 1D NMR approach that is sensitive to faster segmental motions. The mean correlation times of two homopolymers are compared with other relaxation times available from literature determined by other methods. The τ_{c_0} and σ of the individual species in blends are compared with each other and also with those of both homopolymers. The time-scale of segmental reorientation at the DSC T_g is estimated and this connection is used to describe the compositional dependence of the segmental dynamics underlying the broad glass transition.

3.3.1 Segmental dynamics of homopolymers: dPI and dPVE

Typical 2D ^{2}H exchange NMR spectra for the pure components dPVE and dPI are shown in **Figure 3.3, 3.4** at temperatures close to their calorimetric T_g's ($T_g + 2.7$ for dPI and $T_g + 1.2$ for dPVE). For each species, 2D spectra are obtained at four different mixing times, t_m, ranging from 10 ms to 200 or 250 ms. At small t_m, spectral intensity is confined near the diagonal (top row at t_m = 10ms**Figure 3.3, 3.4**): the initial and final resonance frequencies, $\omega(\theta_i)$ and $\omega(\theta_f)$, are the same because negligible reorientation has taken place during this small t_m (*i.e.*, $\theta_i \simeq \theta_f$). The spectral intensity along the diagonal shows the familiar Pake pattern for both species, in accord with the fact that both polymers are amorphous and hence the C-^{2}H bonds pendant to the backbone have an isotropic orientation distribution. The separation between the two peaks along the diagonal associated with the orientation $\theta = 90°$ corresponds to the effective strength of the quadrupolar coupling, δ or $\overline{\delta}$. The separation between

the peaks for dPI is smaller than for dPVE by about a factor of 3, due to rapid motion of the methyl rotor of dPI around its three fold symmetry axis ($\overline{\delta}_{methyl} \simeq \delta_{alkyl}/3$). Although dPI has more alkyl deuterons (5 per monomer) than methyl deuterons (3 per monomer), the signal from the alkyl deuteron is spread out through a much wider spectral window and hence has weaker spectral intensity than that of the narrow methyl deuterons. Since the methyl rotor is rigidly attached to the backbone, the motion of the symmetry axis for the methyl rotor would be identical as the C-^{2}H bonds on the backbone [31], and we'll focus on the narrow spectral window of methyl deuteron for dPI throughout this study.

As the mixing time increases, more C-^{2}H bonds undergo reorientation during t_m and this gives rise to off-diagonal intensity. Here, the profile of the off-diagonal intensity shows square ridges growing symmetrically along both frequency axis as t_m increases. As t_m becomes comparable to the mean correlation time of reorientation, the off-diagonal ridges meet at the antidiagonal cross region and form closed square enclosing the spectral plane between the diagonal peaks. Both dPI and dPVE spectra have the same qualitative shape except for the difference in spectral width. Additional differences come mainly from the experimental limitations. For example, the shoulder of the Pake pattern is truncated for dPVE spectra due to the limited spectral band of the receiver electronics. The small dip or peak present on off-diagonal region near $(\omega_1 = \pm\delta/2, \omega_2 = \mp\delta/2)$ arise when the sine and cosine sub-spectra are added to form the complete spectrum, since the height of the peaks of sine and cosine sub-spectra are often slightly different.

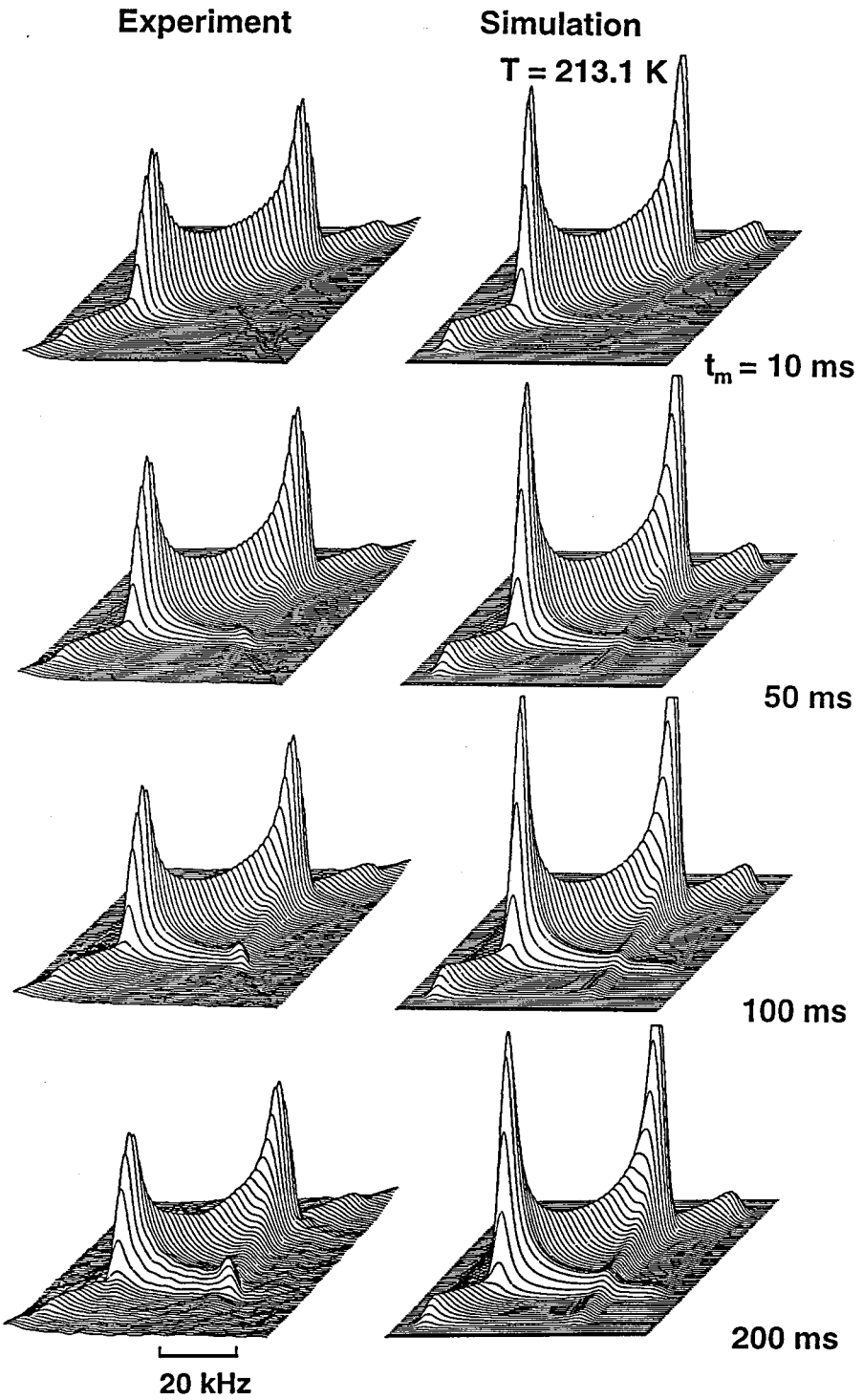

Figure 3.3: 2D NMR spectra of dPI homopolymer obtained close to T_g as a function of t_m.

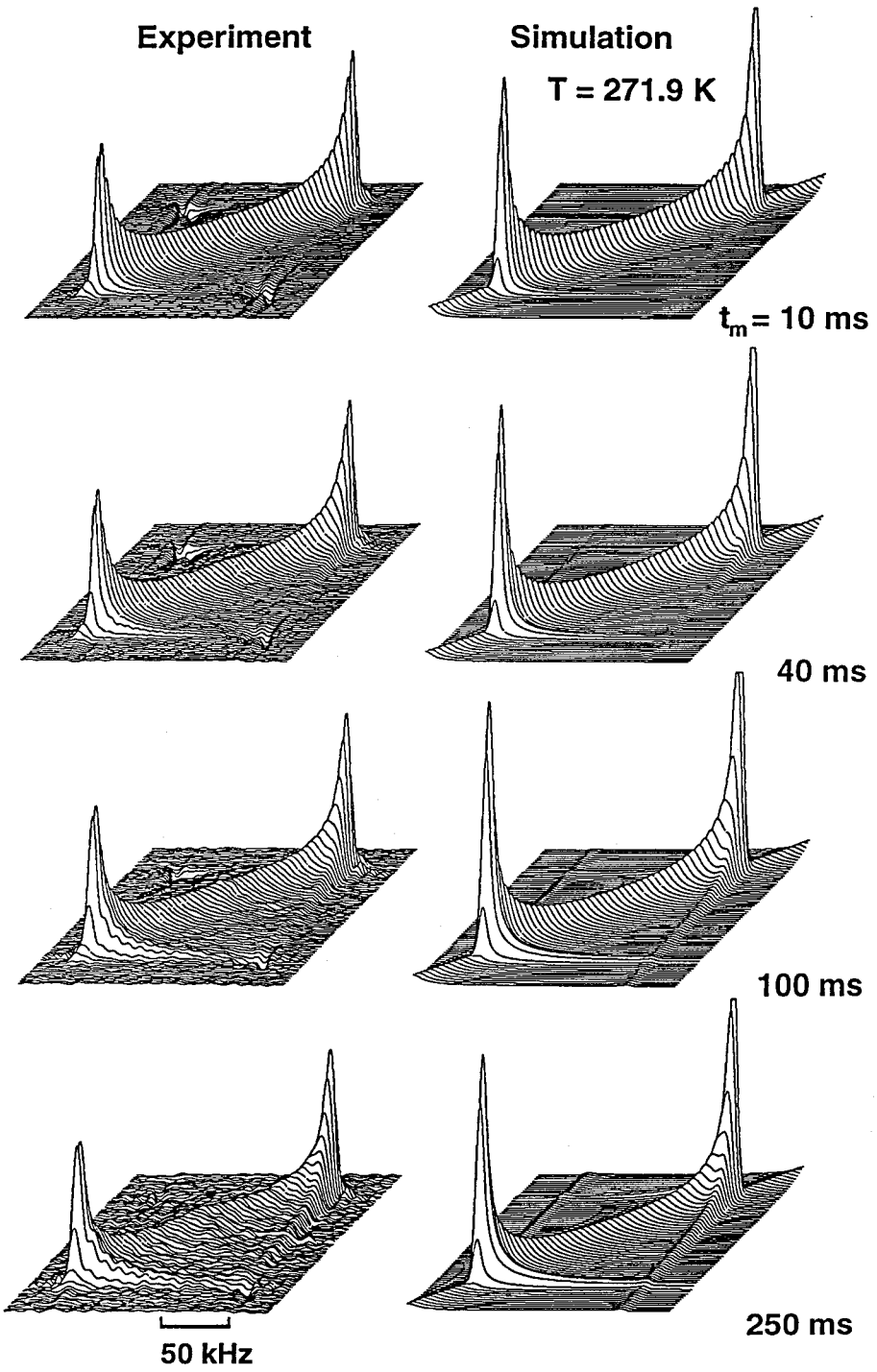

Figure 3.4: 2D NMR spectra of dPVE homopolymer obtained close to T_g.

Aside from these small artifacts, these two spectra exhibit the Pake-like diagonal and smooth off-diagonal lineshape. Two characteristic features of the underlying reorientation process can be inferred from the line-shape of the 2D spectra. First, symmetric ridges along the two frequency axis decaying away from the peaks are observed on the off-diagonal spectral plane. This lineshape is characteristic of isotropic reorientation spanning a large range of angles during t_m, especially from $\theta_i \sim \pi/2$ before the mixing time to any other angles away from the initial θ_i. The fact that the exchange signals from a particular initial frequency are spread out over the whole frequency range suggests that a given C-^{2}H bond can reorient from its initial orientation to any orientations. Second, the broadening of the Pake pattern is observed near the diagonal, suggesting that changes in the resonance frequency take place by small angular steps. This is interpreted as indicating that a diffusive isotropic reorientation by a small angular step is a dominant motional process, even though conformational changes accompanying a discrete jump by large angles also occur sporadically. The simple Brownian rotational diffusion of C-^{2}H bonds can capture these two features of 2D spectra of these and many other amorphous homopolymers. This is readily seen from **Figure 3.3, 3.4** by comparing the experimental spectra to the ones simulated by the motional model of Brownian rotational diffusion.

The evolution of spectra as a function of t_m is also consistent with the evolution of the orientation distribution simulated from the rotational diffusion model. Therefore, we fit the experimental spectra by simulating the 2D spectra arising from isotropic rotational diffusion, with the log-Gaussian distribution of correlation times

(eqn. 2.15). Other types of correlation time distributions may be equally justifiable. We have compared the quality of fit obtained with the log-Gaussian distribution to the asymmetric log-Gaussian that has been used by others to mimic the asymmetry of a stretched exponential distribution [41, 28]. We find that an asymmetric distribution does not improve the fit significantly, as was also observed by other studies [28, 42]. Furthermore, the mean and the full width of the distribution obtained using the asymmetric distribution are consistent with those determined using the simpler log-Gaussian distribution.

Some differences between the experimental and the simulated spectra are observed (**Figure 3.3, 3.4**), particularly near the two diagonal peaks and on an off-diagonal region where the ridges cross at large mixing times. Such differences in the shape of 2D spectra between the experimental and the simulated spectra can arise from many origins not directly related to the reorientation dynamics, such as an anisotropic relaxation of magnetization during the mixing time, a small deviation from axial symmetry of electric field gradient around C-^{2}H bonds, and more importantly, some experimental imperfections. Therefore, absolute height of the diagonal peaks and the small dips/peaks on the off-diagonal region can be neglected in the fit. Since the degree of exchange sensitively affects how signal along the off-diagonal ridges change relative to the diagonal intensity, the difference in appearance near the diagonal peaks and their off-diagonal cross region does not affect the accuracy of the fit parameters. The mean correlation times determined by the fits shown in **Figure 3.3** and **3.4** are 0.5 s and 1 s for dPI (at T_g+2.7K) and dPVE (at T_g+1.2K) respectively.

As temperature increases from T_g + 5K to T_g +13K, segmental reorientation becomes faster, and the evolution of 2D NMR spectra with mixing time also becomes much faster, as shown in **Figure 3.5**. As mixing time increases, the spectra capture the reorientation of progressively slower-moving populations in the overall distribution of correlation times, which may have appeared rigid (diagonal intensity) at smaller t_m. For the top three spectra, the exchange intensity on the off-diagonal region starts appearing at $t_m \simeq 5$ ms, and very small intensity remains along the diagonal except near the peaks at $t_m \simeq 200$ ms, suggesting that the exchange intensity grows almost completely in about 2 decades. With increasing temperature, similar degree of exchange is evidenced at much shorter mixing time. For example, three middle spectra show similar exchange pattern at $t_m = 20, 10, 1$ms respectively, suggesting that motional rates increase correspondingly with temperature. In addition, the evolution of the exchange pattern takes place in progressively shorter ranges of mixing times as temperature increases: at $T_g + 13$K, complete decay of diagonal intensity occurs in a little over a decade (**Figure 3.5a**), while at $T_g + 5$K similar evolution occurs in about 2 decades (**Figure 3.5c**).

The changes in the dynamics as a function of temperature can be examined more easily and quantitatively by comparing the changes in the mean τ_{c_0} and width σ of the correlation time distribution with temperature. We begin by considering the mean correlation times (**Figure 3.6**). The width of correlation time distribution σ will be discussed in comparison to those observed in blends. In order to check the validity of the mean correlation time, τ_{c_0}, we compare it with earlier 2D NMR result by other

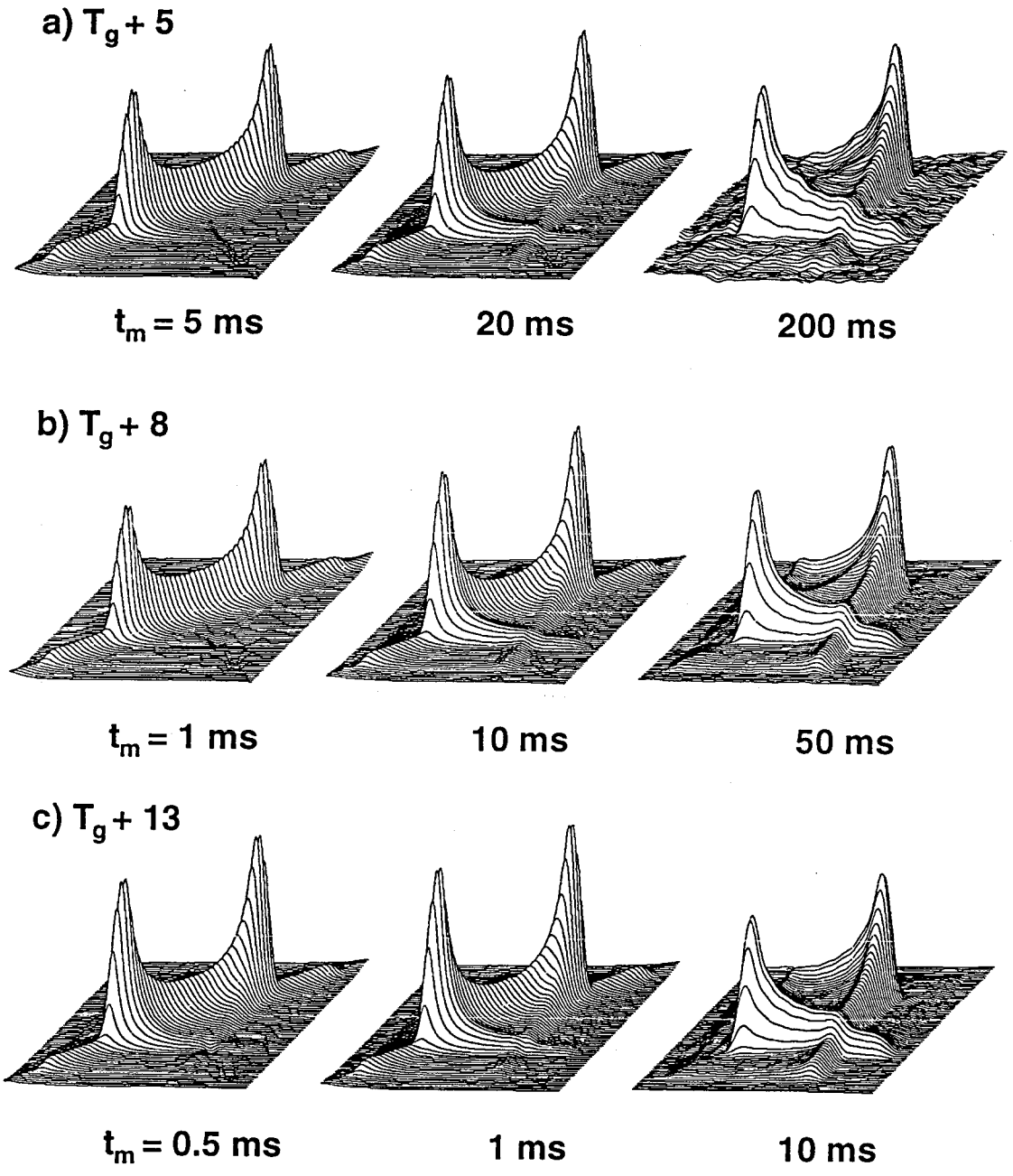

Figure 3.5: Changes in 2D NMR spectra of dPI as a function of temperature.

workers and also with other experimental results obtained from available literatures. Direct comparison of τ_{c_0} determined by 2D NMR is possible only for PI homopolymer, and the agreement is reasonable. In fact, the agreement would be nearly perfect if the other 2D ^{2}H NMR data were shifted by 5 K. The difference could be simply due to the instrumental imperfection, and similar discrepancy in temperature between the thermocouple and the sample is also observed in our laboratory if the thermocouple is placed in the probe as manufactured by Bruker.[1] The mean correlation time for pure PI also agrees very well with the previous photon correlation spectroscopy (*Box*) and the dielectric relaxation measurements (open $\diamond$, $\triangle$, and $+$)(**Figure 3.6**) [28, 45, 43, 44]. Similar comparison is also possible for PVE as well. The comparison is slightly less reliable for PVE because even a small difference in microstructure can cause a large change in T_g, but the agreement appears to be reasonable (**Figure 3.6**).

The comparison suggests that segmental reorientation probed by 2D ^{2}H NMR is a cooperative dynamic process coupled to the mechanical, dielectric, and density relaxation. This relaxation is often called the α-process underlying dynamic softening or glass-to-rubber transition. The temperature dependence of the correlation time for each pure component is also consistent with the Williams-Landel-Ferry (WLF)

[1]The variation from the set temperature is within 1K. However, the Bruker thermocouple reading is frequently very different from the sample temperature. To overcome this problem, an additional thermocouple is built in near the sample. The temperature measurement is further tested by placing another thermocouple at the center of the sample tube and comparing the readings from all three thermocouples. The reading from the new built-in thermocouple turned out to be more reliable, probably due to the smaller distance from the sample than the Bruker one. It is also noticed that the Bruker thermocouple reading is always higher than the test thermocouple reading by about 3 $\sim$ 5K when operating at temperatures below 0°C. In this work, the data are reported in reference to the temperature read by the new built-in thermocouple.

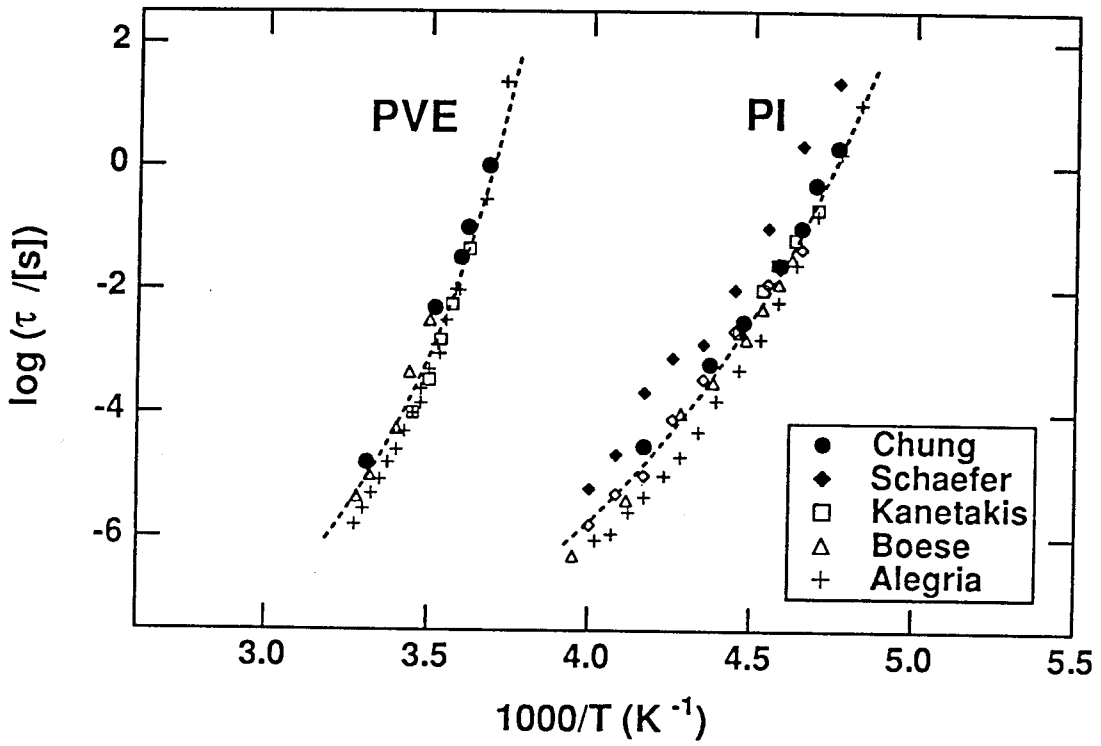

Figure 3.6: Comparison of τ_{c_0} with segmental mobilities obtained by other experimental methods. $\diamond$: 2D ^{2}H NMR (filled), dielectric measurement (open) [28], $\square$: photon correlation spectroscopy [45], $\triangle$: dielectric measurement [46] and $+$: dielectric measurement [44].

behavior established previously by dynamic mechanical measurements of the terminal relaxation (dashed curves, **Figure 3.6**) [9],

$$\log \tau_{c_0} = \log \tau_g - \frac{C_1^g (T - T_g)}{C_2^g + (T - T_g)}, \tag{3.1}$$

where C_1^g and C_2^g are WLF parameters, and τ_g is the mean correlation time at the DSC T_g. The WLF parameters (C_1^g, C_2^g) for the dashed curves are given in **Table 3.2**. The mean correlation time at the DSC T_g $\tau_g \simeq$ 1s for each pure species studied here. This correspondence between the mean correlation time and the DSC glass transition also appears to be valid in blends, and is used to describe the broad glass transition behavior in blends. Similar WLF temperature dependence of τ_{c_0} is also observed in previous 2D ^{2}H NMR studies on a number of amorphous homopolymers [26, 31, 28, 20]. Therefore, the mean correlation time τ_{c_0} can be used to probe the cooperative segmental motion, and its temperature dependence agrees well with that of viscoelastic response of amorphous polymers associated with longer length scale dynamics.

3.3.2 Segmental dynamics of individual species in PI/PVE blends

In PI/PVE blends, the individual species have significantly different mobilities at all experimental temperatures, which is evidenced in the obtained spectra at nearly identical conditions (**Figure 3.7- 3.12**). For the same blend composition and temperature, PI exhibits much faster reorientation than PVE. Direct inspection of the spectra enables one to estimate the relative rates of PI and PVE motion, and to observe that they differ by more than a decade at all three compositions. For exam-

Table 3.2: Comparison of best fit WLF parameters for segmental mobility with literature values for terminal relaxation times.

	species	C_1	C_2	T_g	reference
terminal relaxation	PVE	11.4	56		[9]
		13.8	39.8		[38]
	PI	12.0	53		[9]
		14.7	34		[47]
segmental motion	dPVE	12.3	45	270.4	
	dPI	13.0	50	210.6	

ple, in the 75/25 PI/PVE blends, the degree of exchange is more pronounced at a mixing time of 20 ms for dPI than for dPVE at mixing time of 200 ms (**Figure 3.7, 3.8**). Similarly, the second PI spectrum in **Figure 3.9** at t_m = 5ms shows more exchange intensity than the second PVE spectrum in **Figure 3.10**. Furthermore, for the 25/75 PI/PVE blends, the evidence of highly mobile PI units is observed even at temperatures where motion of PVE is so slow that 2D spectra for 25/75 PI/dPVE do not show significant exchange intensities (e.g., 250 K) (**Figure 3.11, 3.12**). Specifically, the dPI spectra exhibit a smeared out appearance which indicates a significant fraction of segments falling in the intermediate dynamic regime. In fact, the dPI spectra obtained at temperature, 5 K higher, exhibit not only a strongly smeared off-diagonal intensity, but also an asymmetrically distorted spectra with an isotropic peak at the center. These features have previously been observed in spectra obtained

in the middle of the intermediate dynamic regime ($\tau_{c_0} \sim 10\mu s$) [28]. Although the 2D spectra are obtained using the pair of selectively labeled blends (dPI/PVE and PI/dPVE with the same composition in wt.%), This significant difference between the mobilities of dPI and dPVE species represent the actual difference in the mobility between PI and PVE in PI/PVE blend. The possible effect of deuteration on the phase behavior of this blend and hence on the mobility of each species appears to be negligible at least for the compositions studied here and especially for the segmental level dynamics near the glass transition studied here. The deuteration effect on the segmental motion in blends is discussed further in the Appendix A.

As discussed earlier the mean correlation time, τ_{c_0}, and the width, σ, of the correlation time distribution are determined by fitting the series of experimental spectra at each temperature with calculated spectra. The mean correlation times obtained using a single log-Gaussian distribution are shown in **Figure 3.13** for the two homopolymers and each species in three blends. The temperatures at which $\tau_{c_0} \simeq 2/\delta$ are estimated from the minimum in solid echo intensity as a function of temperature. The mean correlation time estimated from the minimum in solid echo intensity is denoted by $\tau_{c,min}$. For dPVE, $\tau_{c,min}$ is approximately $16\mu s$, and for dPI $\tau_{c,min} \simeq 26\mu s$. For $\tau_{c,min}$ of dPI, weighted log-average of methyl and back bone deuterons is taken since the dPI has 3 methyl deuterons with $2/\overline{\delta} \simeq 54\mu s$ and 5 back bone deuterons with $2/\delta \simeq 16\mu s$. These data are also included as (+) and appear to be consistent with the 2D NMR data for the two homopolymers. Blends rich in PVE, however, exhibit mean correlation times estimated from 2D spectra, which are substantially

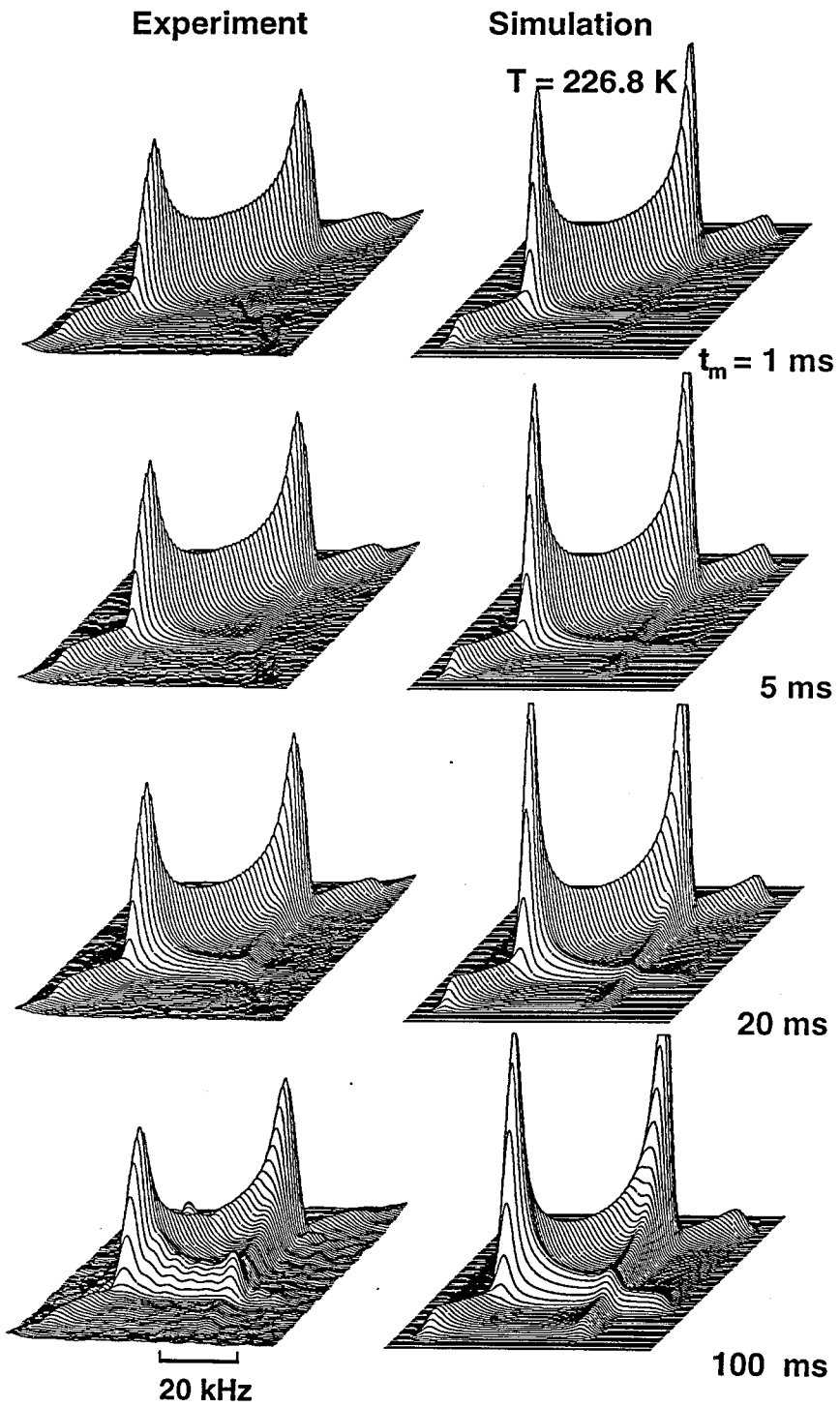

Figure 3.7: Experimental and simulated 2D NMR spectra of 75/25 dPI/PVE at $T = 226.8$ K obtained with mixing times of 1, 5, 20 and 100 ms. From the fit, we obtain $\tau_{c_0} = 12.5$ ms and $\sigma = 1.35$ decade. See also Figure 3.8 for comparison.

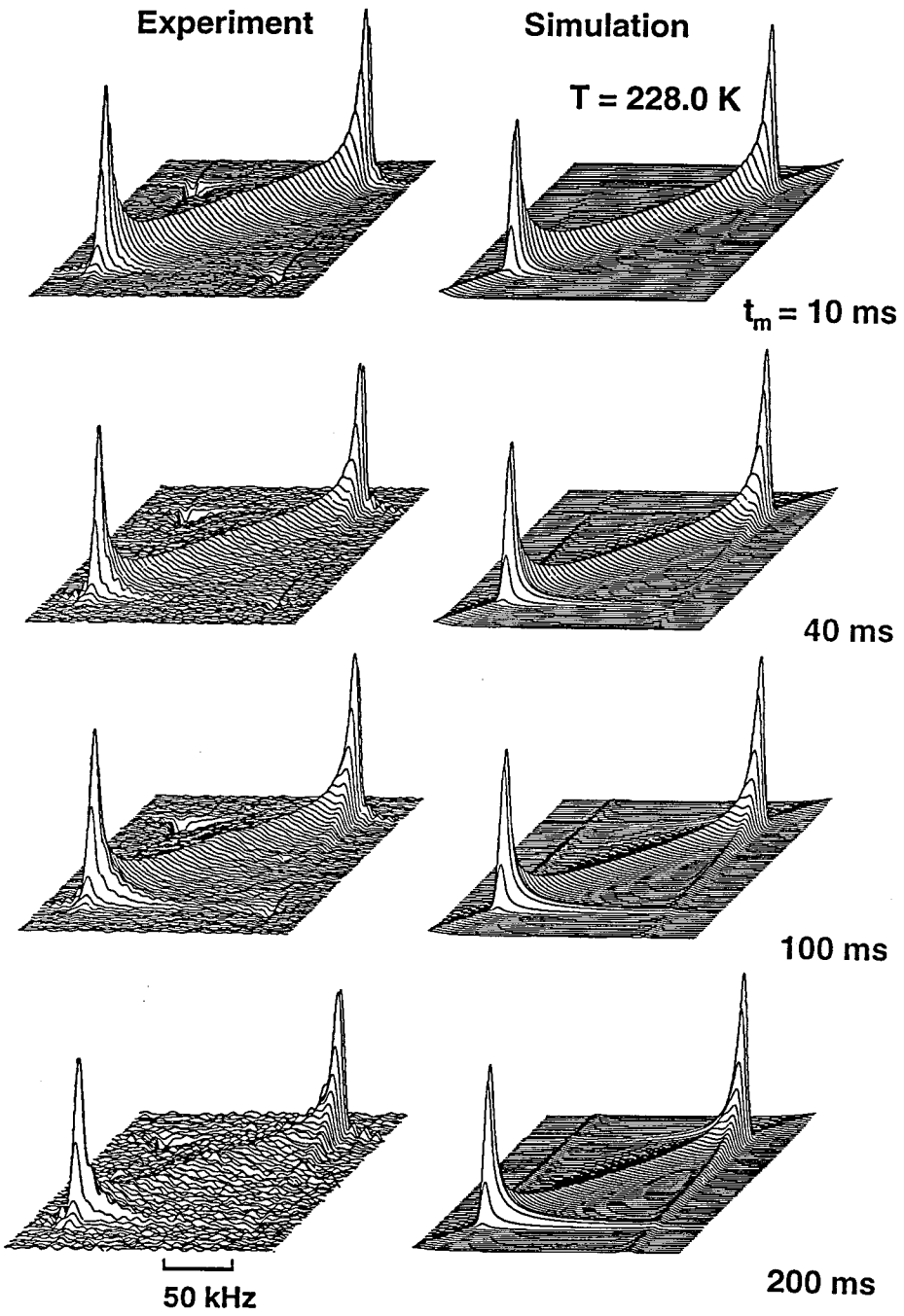

Figure 3.8: 2D NMR spectra for 75/25 PI/dPVE obtained at $T = 228.0$ K. ($\tau_{c_0} = 0.5$ ms and $\sigma = 1$ decade) See also Figure 3.7 for comparison.

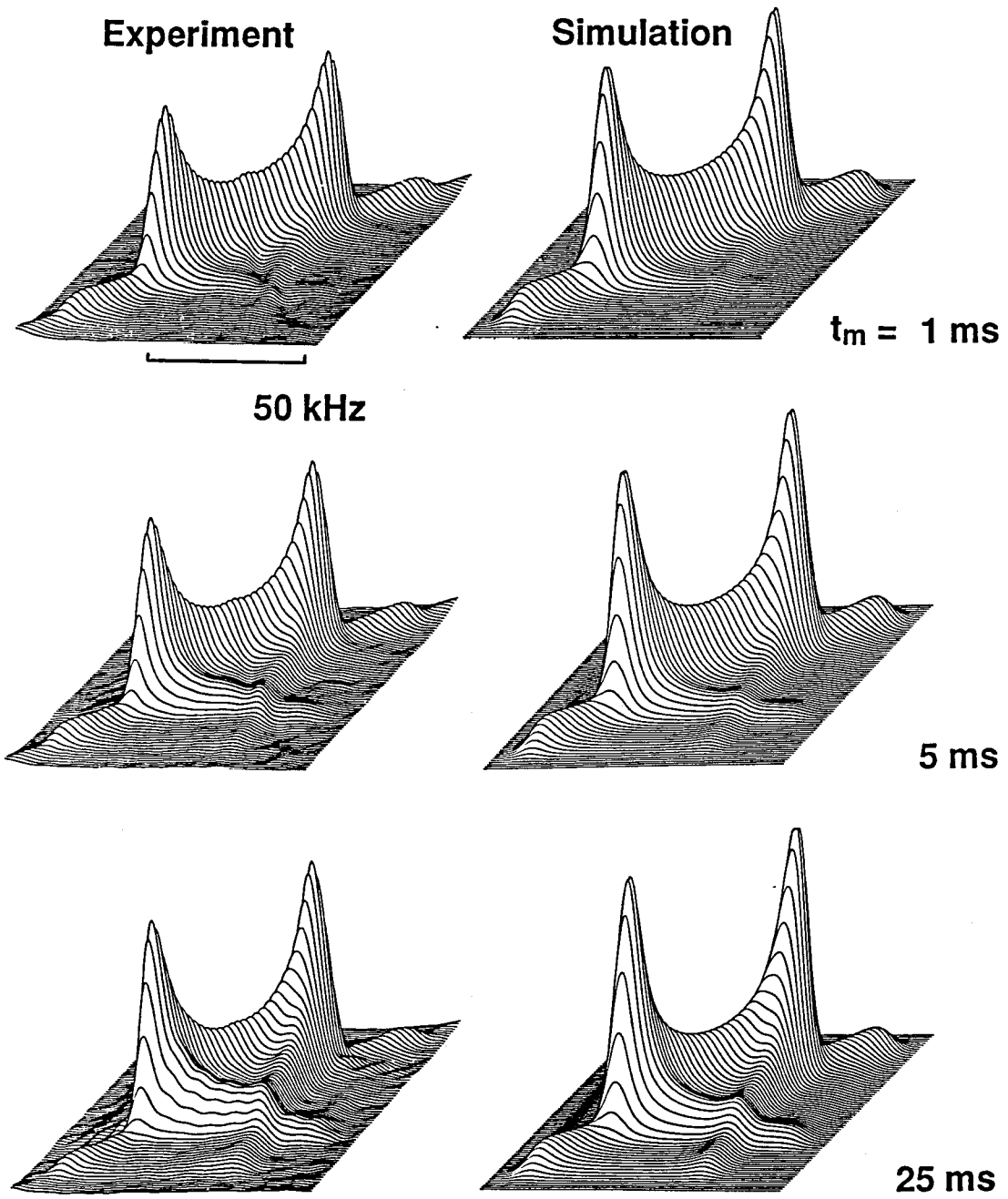

Figure 3.9: Experimental and simulated 2D NMR spectra for 50/50 dPI/PVE obtained at $T = 237.1$ K. ($\tau_{c_0} = 25$ ms and $\sigma = 1.5$ decade). See also Figure 3.10 for comparison.

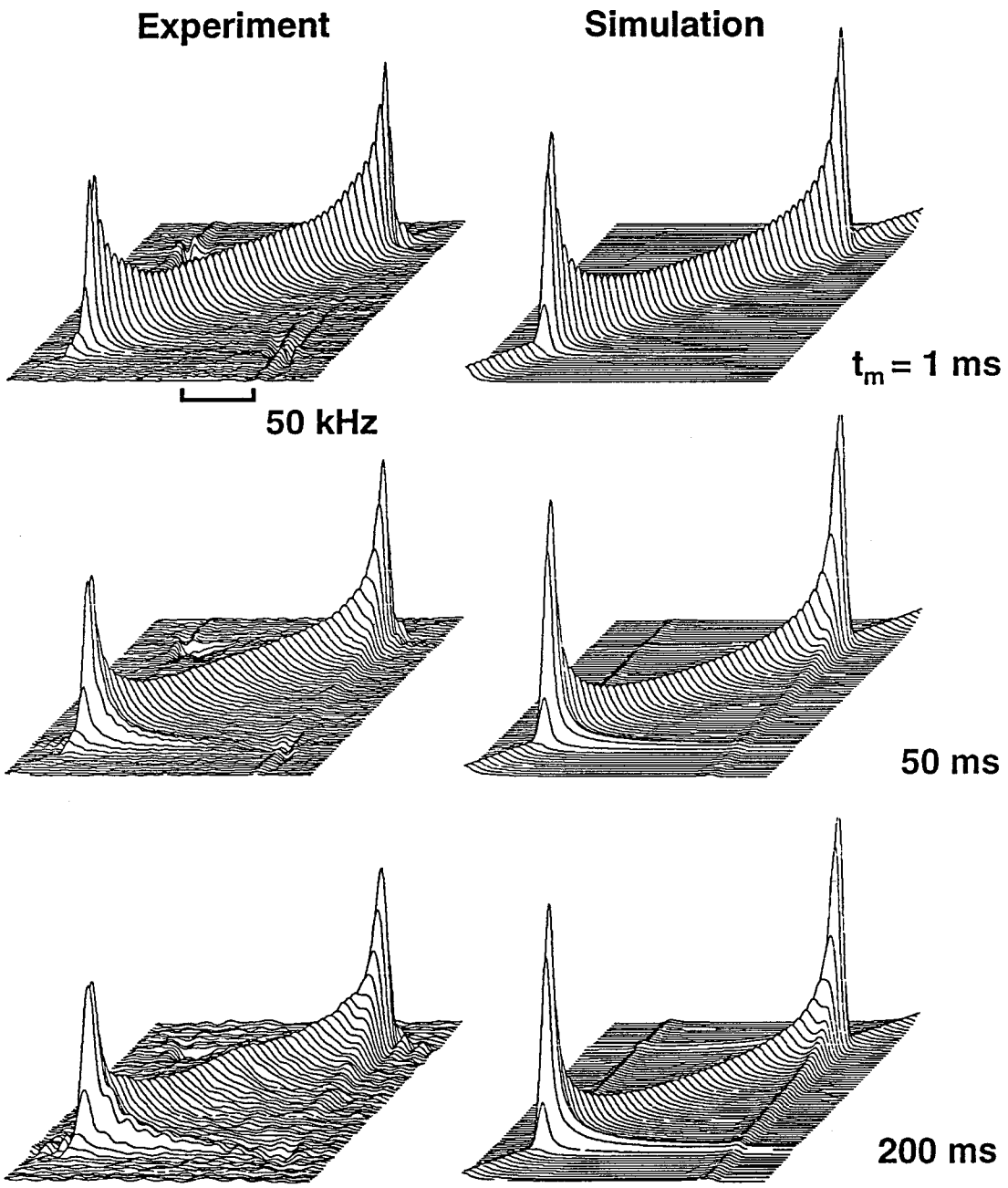

Figure 3.10: Experimental and simulated 2D NMR spectra for 50/50 PI/dPVE obtained at $T = 237.5$ K. ($\tau_{c_0} = 500$ ms and $\sigma = 1.5$ decade). See also Figure 3.9 for comparison.

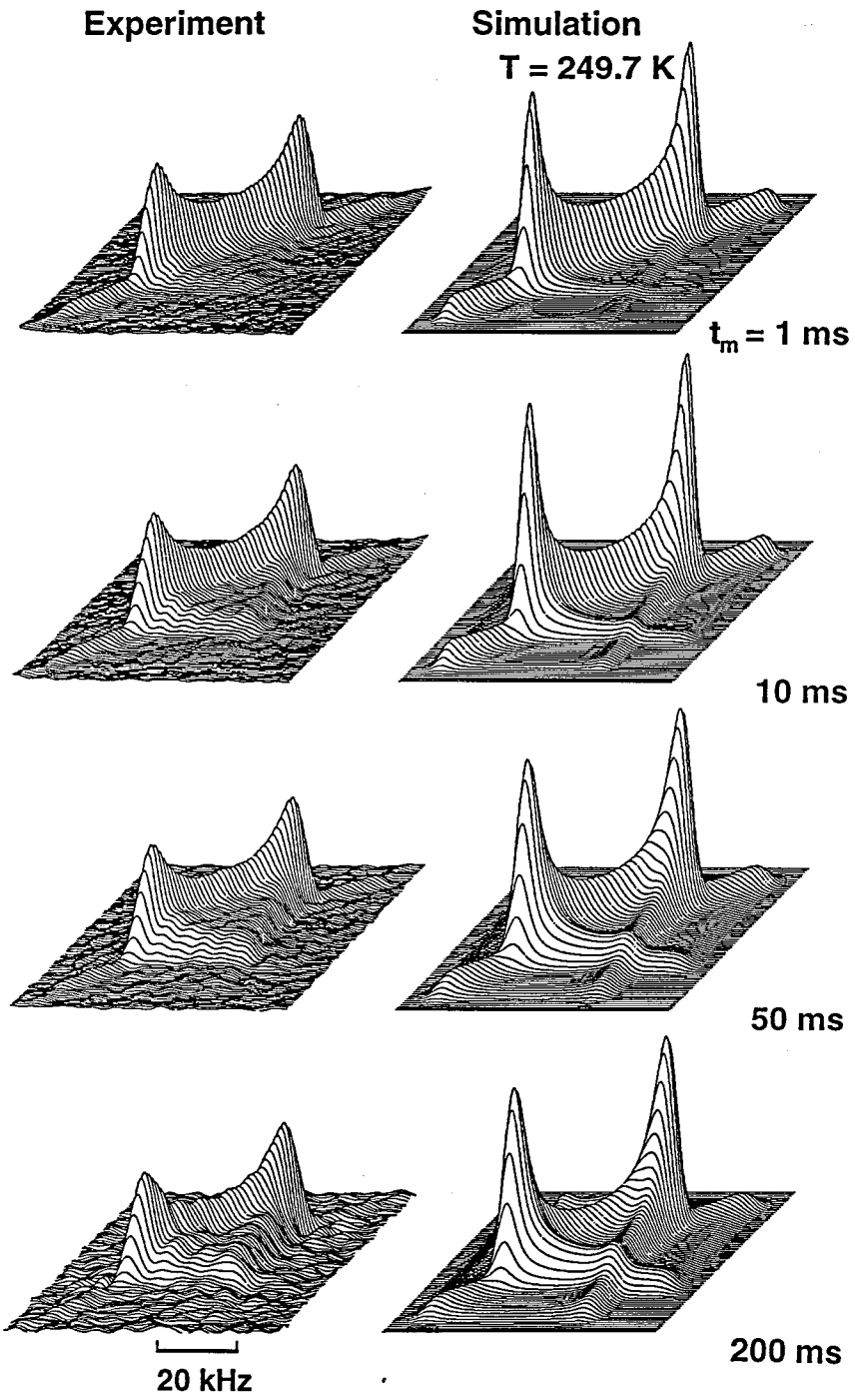

Figure 3.11: Experimental and simulated 2D NMR spectra for 25/75 dPI/PVE obtained at $T = 249.7$ K. ($\tau_{c_0} = 33$ ms and $\sigma = 1.85$ decade). See Figure 3.12 for comparison.

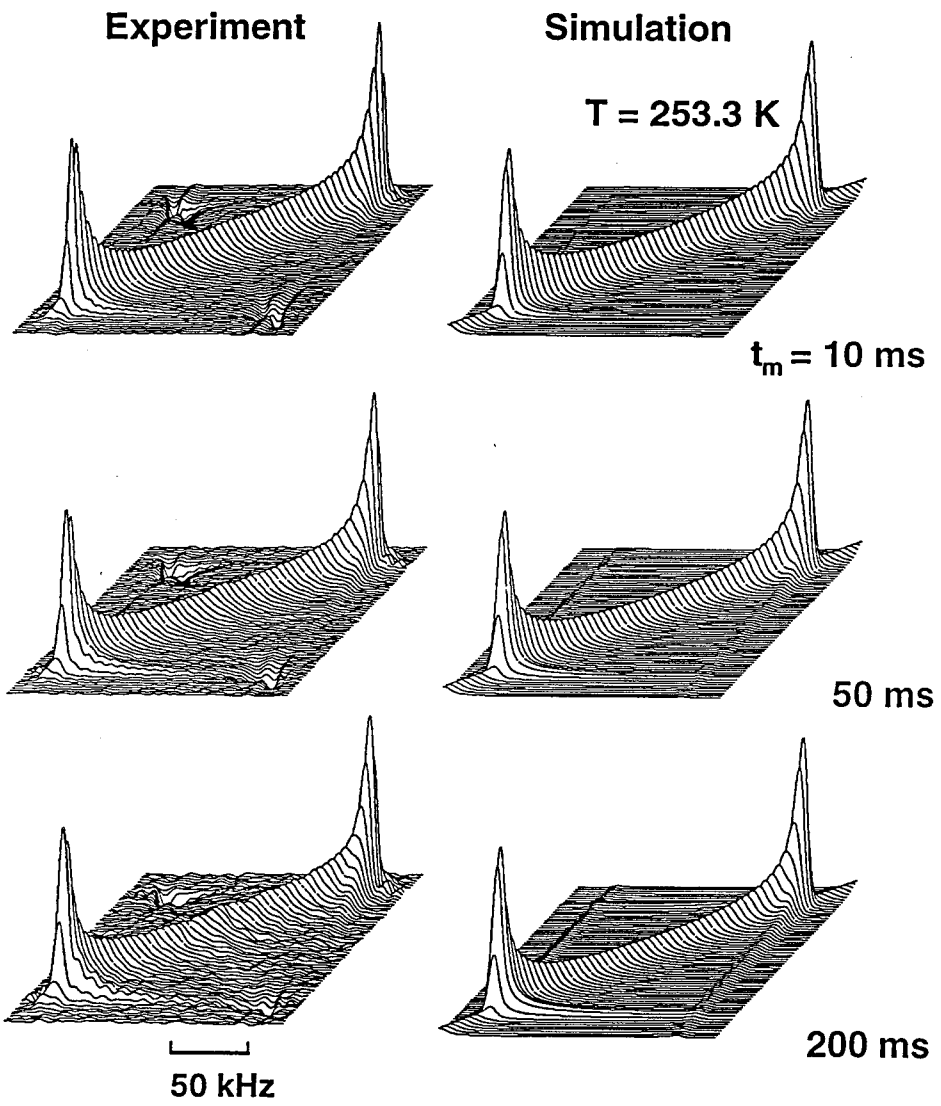

Figure 3.12: Experimental and simulated 2D NMR spectra for 25/75 dPI/PVE obtained at $T = 253.3$ K. ($\tau_{c_0} = 1.33$ s and $\sigma = 1.75$ decade). See Figure 3.11 for comparison.

larger compared to those obtained from the minimum in solid echo intensity. The deviation is particularly noticeable in 50/50 and 25/75 PI/PVE blends. This increase in the deviation appears to be related to the broad correlation time distribution and can be ascribed to the inhomogeneous reduction of signal in the intermediate dynamic regime (see Appendix B).

In order to assess the effect of signal loss in the intermediate dynamic regime, solid echo intensities and the transverse NMR relaxation time, T_2, have been measured as a function of temperature (**Figure 3.14**). Since the detection of the signal in the 5 pulse 2D exchange NMR experiment is done by solid echo, the loss of solid echo intensity essentially gives rise to an almost identical loss of signal in the 2D exchange NMR experiment. The intensities in **Figure 3.14a** are normalized by the Boltzman factor determining the temperature dependence of the spin population, and scaled with the intensity obtained well below the glass transition. The decrease in solid echo intensity with temperature can be explained by two mechanisms: the change in T_2 relaxation times and incomplete echo formation due to changes in magnetic resonance frequency during the echo delay time [50]. Both mechanisms give rise to a correlation time dependent reduction of spectral intensity, which is strongest at $\tau_c \simeq 2/\delta$ [23, 51]. Therefore, the 2D ^{2}H NMR spectra obtained near the glass transition tend to be insensitive to the mobile segments, whose mobilities lie in the intermediate dynamic regime. This leads to an overestimation of the mean correlation times and an underestimation of the width of the correlation time distribution. The effect of the loss of spectral intensity on the apparent correlation time distribution is

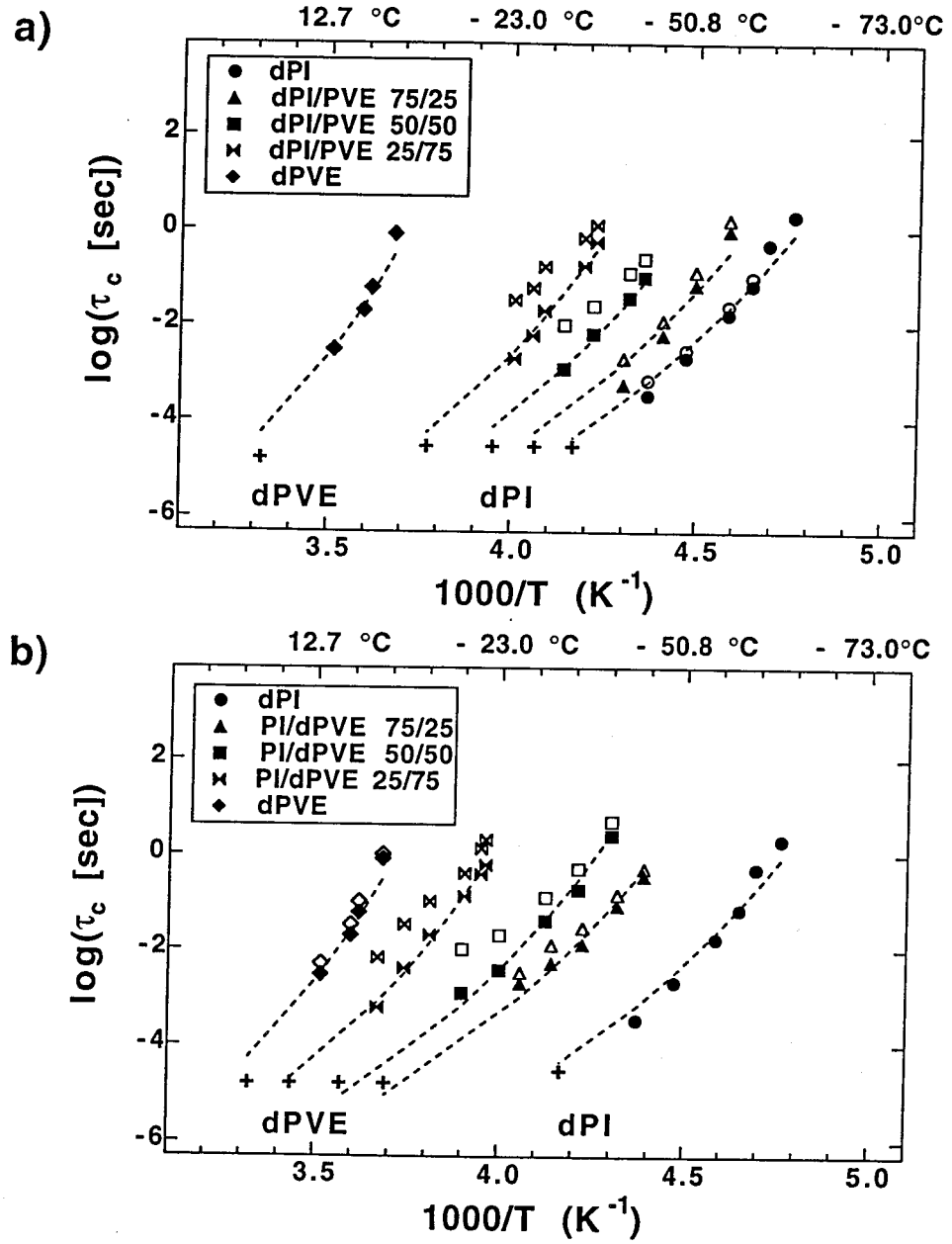

Figure 3.13: Log mean correlation times (open symbol) as a function of temperature obtained from 2D spectra for (a) dPI and (b) dPVE, and modified mean correlation times (filled symbol) after taking into account the effect of correlation time dependent reduction in spectral intensity. The + symbols are the mean correlation times estimated from the intensity/T_2 minima. The dashed lines are WLF curves for a rough qualitative comparison, obtained by using the WLF parameters C_1^g and C_2^g in the literature [9]. For dPI homopolymers, $C_1^g = 11.7$, $C_2^g = 52.9$. For dPVE, C_1^g =11.4, $C_2^g = 56$. The WLF parameters are assumed to be independent of composition. The $T_g(\phi)$'s obtained from the fit is nearly the same as the effective T_g shown in **Table 4.1**.

discussed in more detail in the Appendix B.

Taking into account the loss of signal during the solid echo detection period in a semi-quantitative way, values of the corrected mean, $\tau^*_{c_0}$, and the width of the correlation time distribution, σ^*, consistent with both the observed 2D spectra and the solid echo intensity may be estimated. The estimated $\tau^*_{c_0}$ are shown by (filled symbols) on **Figure 3.13**. For the literature values of WLF parameters C_1^g and C_2^g and the DSC T_g, reasonable WLF curves are obtained with $\log \tau_g \simeq 0$ (dashed curves, **Figure 3.13**). The mean correlation times of PI and PVE in all three blends are also compared with a WLF temperature dependence as shown by the dashed curves, where the WLF parameters for each species are assumed to be independent of composition. The agreement is reasonable when the effect of intensity loss is approximately taken into account (filled symbol). The restricted WLF fit of the correlation times with fixed values of C_1^g and C_2^g renders different $T_g(\phi)$ for each species.

The different $T_{g,i}(\phi)$ for each species i obtained from the restricted WLF fit describe the significant differences in their average mobilities and their temperature dependence. The difference in the mean correlation times between the two components close to the macroscopic T_g increases from 1.5 to more than two orders of magnitude as the PVE content increases. Alternatively, when we compare the $T_{g,i}(\phi)$ obtained from the fit, $T_{g,PVE} - T_{g,PI}$ increases from about 8 K for 75/25 PI/PVE to 15 K for 25/75 PI/PVE. This increased difference in mobilities between the two species with increasing PVE content is in accord with the more pronounced thermorheological complexity observed in blends rich in PVE [12]. This observation suggests that

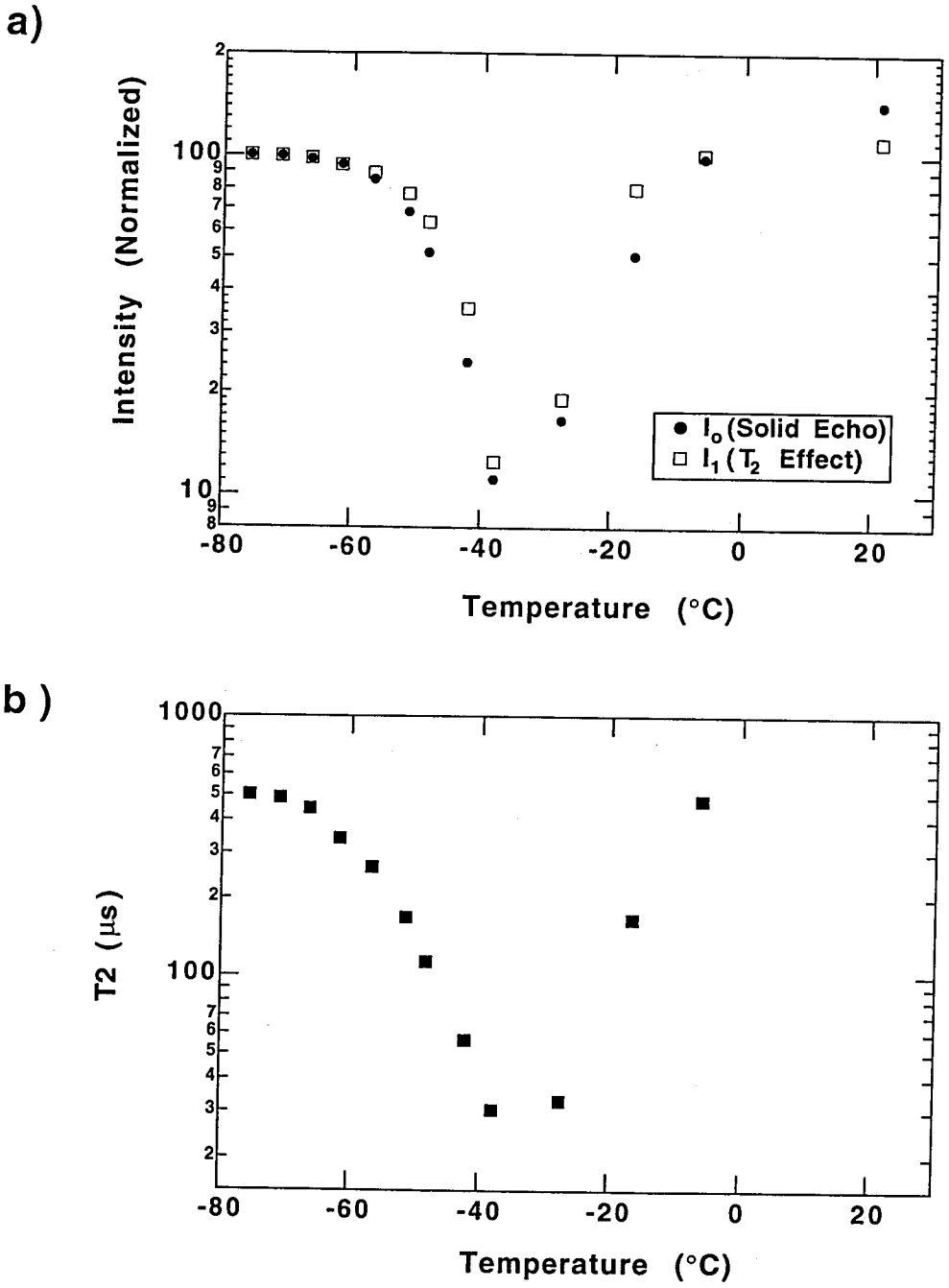

Figure 3.14: Temperature dependence of the absolute solid echo intensity and the effective T_2 relaxation time. (a) Normalized solid echo intensity of dPI as a function of temperature, and the estimated decay of signal intensity due to the change in T_2 relaxation time. (b) The apparent T_2 relaxation time. It appears to exhibit a minimum where intensity becomes minimum.

thermorheological complexity is directly related to differences in segmental mobilities of individual species near the glass transition.

Another quantity that is relevant to understanding the broad glass transition is the width of log-Gaussian distribution, σ, which is related to the distribution of mobilities and can be obtained from the fit of 2D NMR spectra (top). The width of distribution determined from the 2D spectra and the corrected value, σ^*, that takes the reduction into account are presented as vertical bars in **Figure 3.15-3.18** (bottom). The 2σ is often used as the full width of correlation time distribution [20, 28], and corresponds to the full scale of the vertical bars, which is $\pm\sigma$ from τ_{c_0}.

As temperature decreases, σ gradually increases for both homopolymers. Similar behavior is also observed for PI and other homopolymers [28], and can be attributed to the heterogeneity gradually frozen in near the glass transition. This is also observed for both components in the blend. The magnitude of σ at comparable values of τ_{c_0} differs significantly between the homopolymers and blends and also varies with composition. For example, σ of the dPI in 50/50 blend is much larger than that of pure dPI, when compared at comparable mean correlation time (**Figure 3.15**). Similar behavior is also observed for dPVE components (**Figure 3.17**). Even in blends, the magnitude of σ changes strongly with composition. The σ is much larger for 25/75 PI/PVE blends than for 75/25 PI/PVE blends, as evidenced in **Figure 3.16** and **3.18**. For 50/50 and 75.25 PI/PVE blends, NMR data could be obtained at nearly identical conditions, allowing direct comparison of τ_{c_0} and σ. In contrast to the significant differences in the mean mobility, the σ obtained at a common temperature

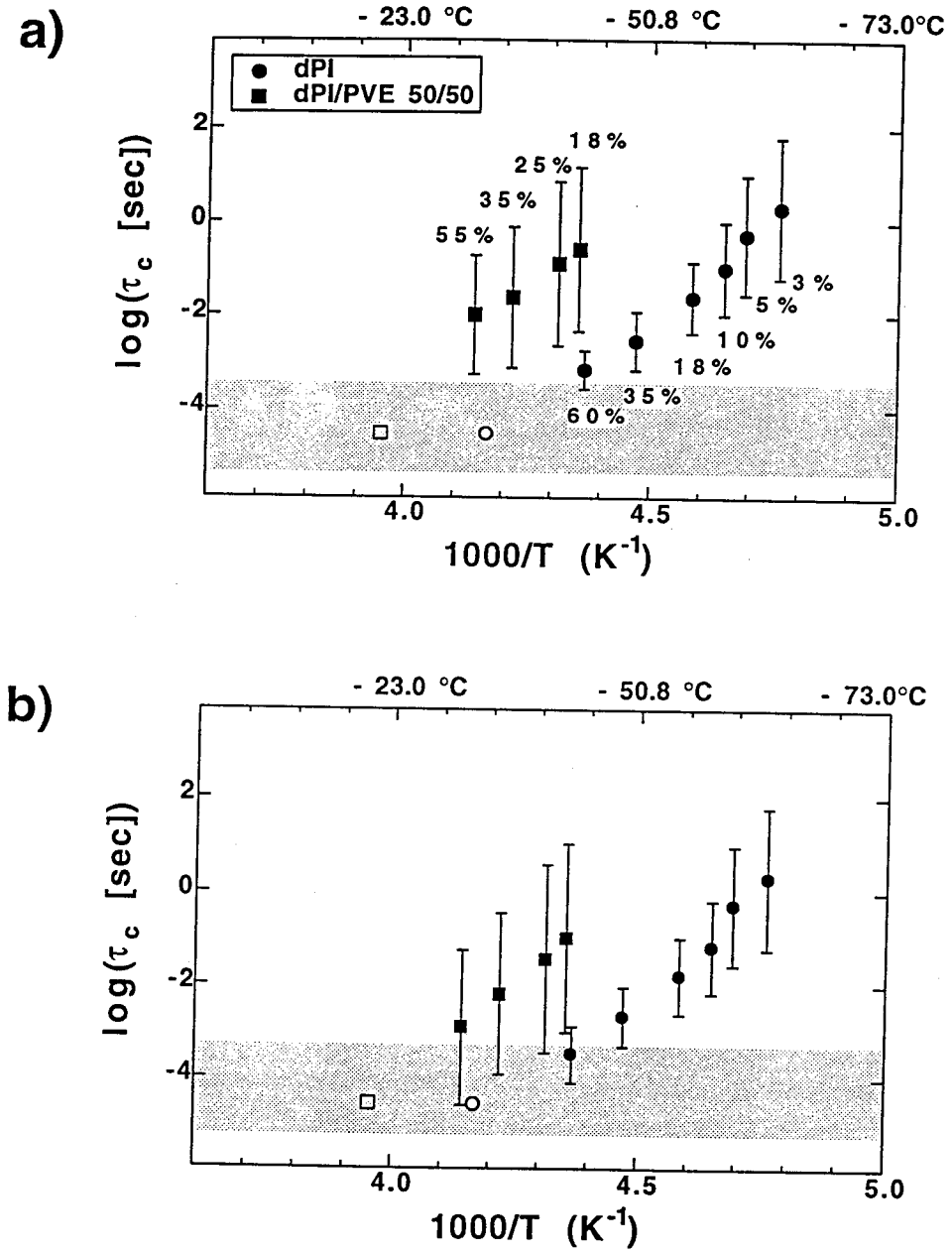

Figure 3.15: Effect of reduction on the mean and width of the correlation time distribution. (a) Apparent mean (symbol) and width (vertical bars corresponding to $\pm\sigma$) obtained without accounting for intensity reduction (percent reduction observed from solid echo are indicated). (b) Modified mean and width of the correlation time distribution in accord with the observed τ_{c0}, σ and $\overline{R}$. The shaded area corresponds to the range of correlation times that undergo more than 80 % reduction. Open symbol corresponds to the mean correlation times obtained from the intensity/T_2 minimum.

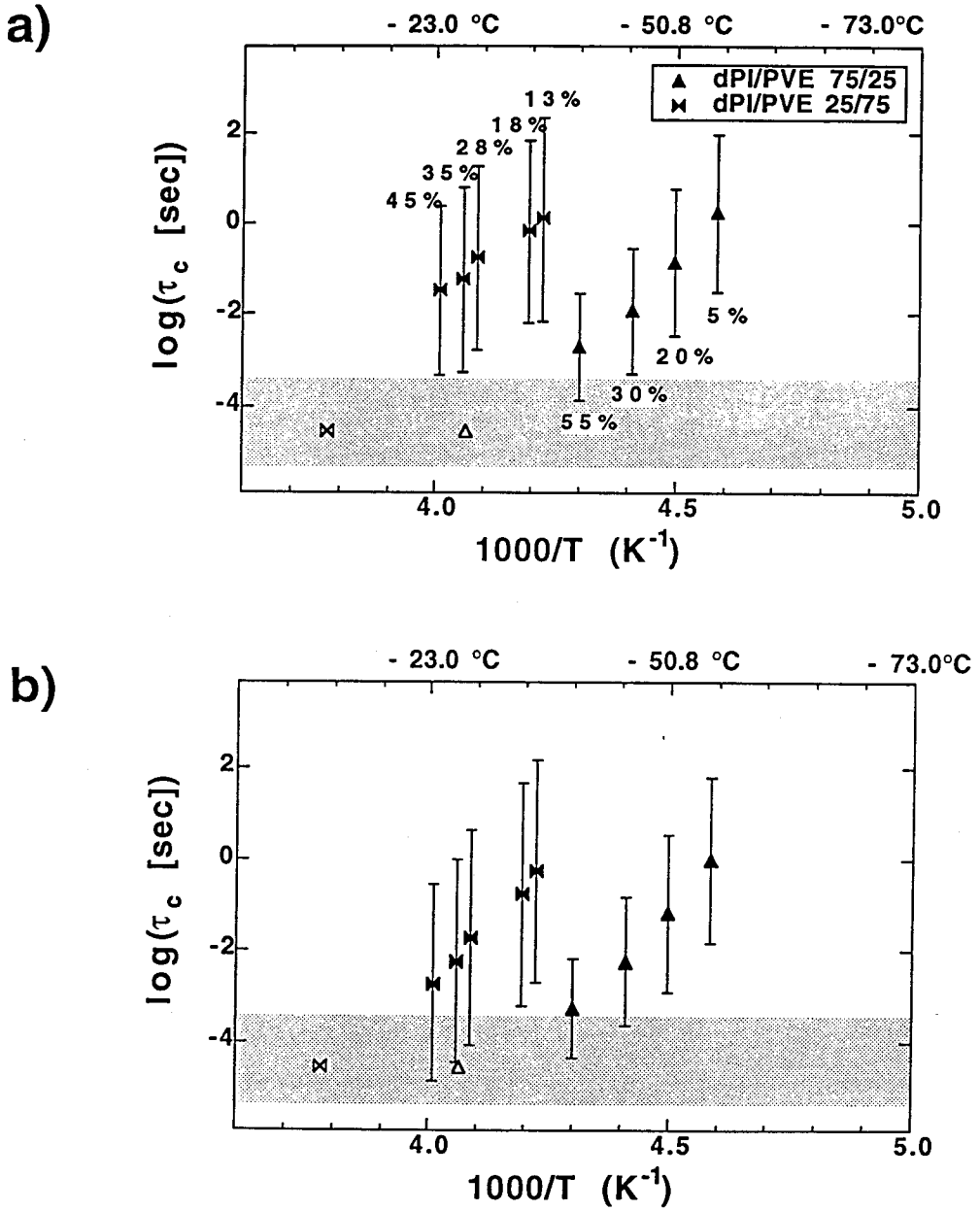

Figure 3.16: Effect of reduction on the mean and width of the correlation time distribution of PI: 75/25 and 25/75 dPI/PVE. See Figure 3.15 for symbol codes.

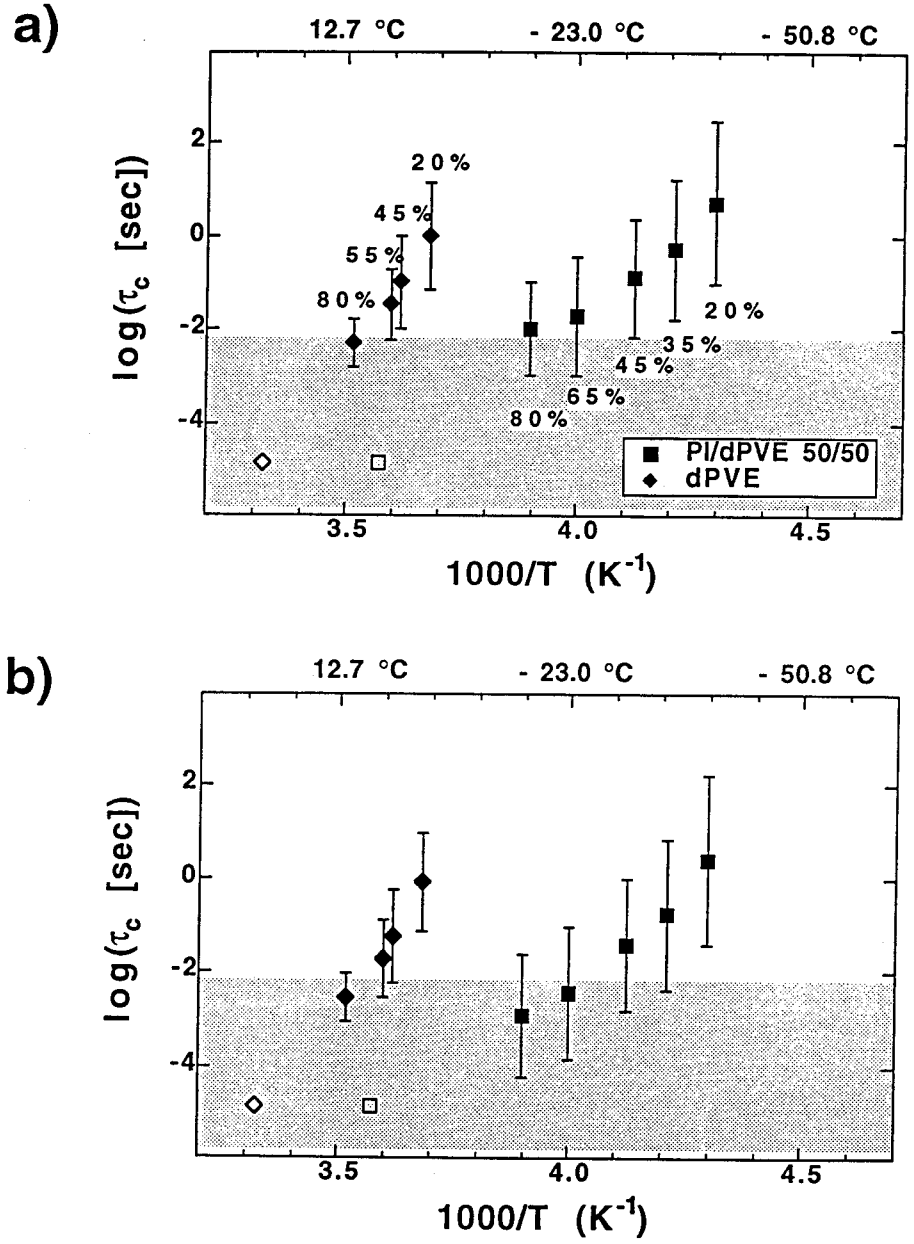

Figure 3.17: Effect of reduction on the mean and width of the correlation time distribution of PVE: dPVE and 50/50 PI/dPVE. See Figure 3.15 for symbol codes.

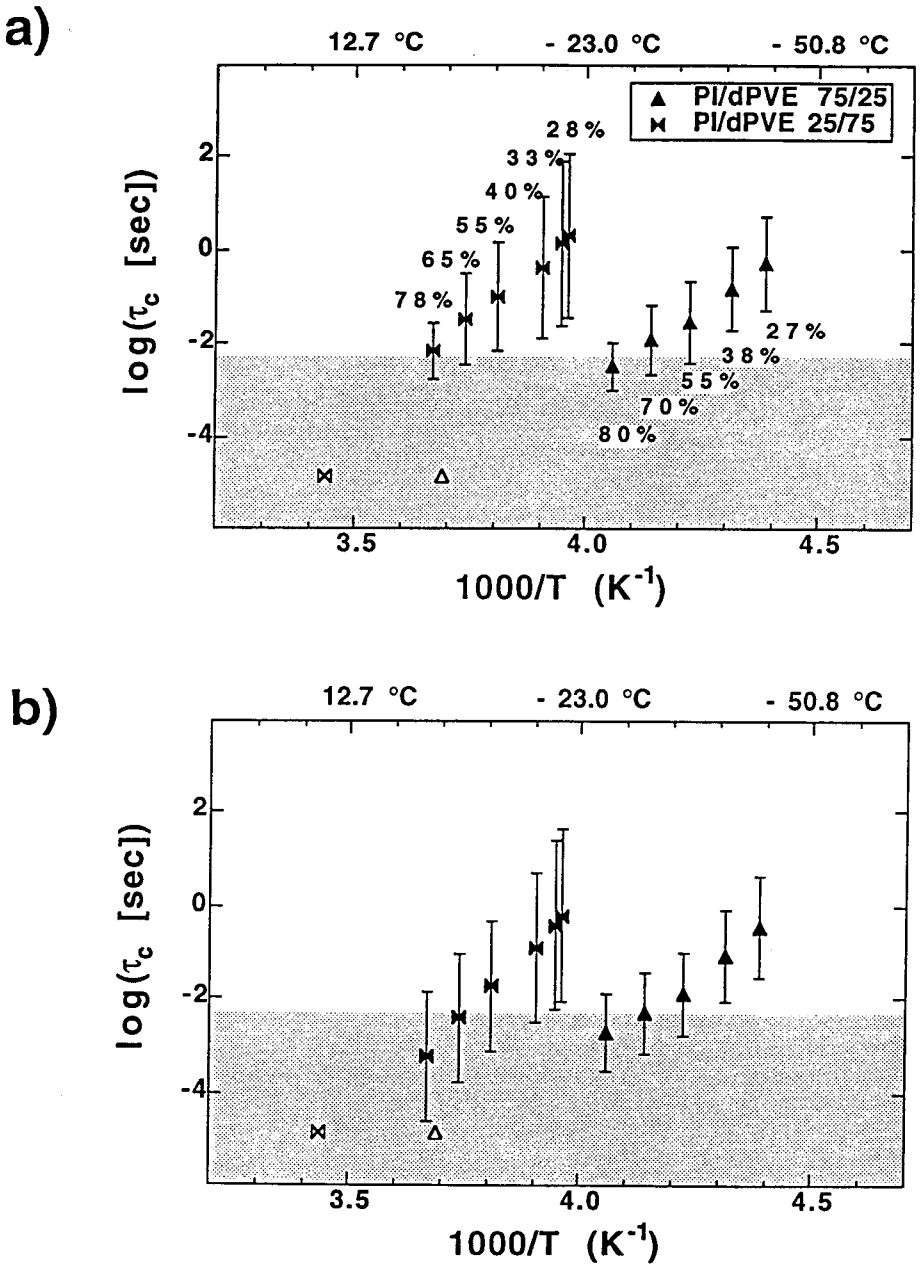

Figure 3.18: Effect of reduction on the mean and width of the correlation time distribution of PVE: 75/25 and 25/75 PI/dPVE. See Figure 3.15 for symbol codes.

appears to be quite close for both components at all compositions examined. It is inferred from this similarity in σ, despite the wide differences in τ_{c_0}, that the broadening of dynamics for both components arises from some structural heterogeneities that are shared by both components.

Chapter 4

Dynamic heterogeneities in miscible polymer blends

In light of our deuteron NMR results, a unified view of the dynamic heterogeneity in blends is suggested. Variety of previous observations on the dynamic heterogeneity can be summarized by three qualitative features: broadening of the dynamic responses, thermorheological complexity, and complex compositional dependence of the mean mobilities of each species. These features have been observed by different experimental methods and have been discussed separately, due to the difficulty associated with resolving the dynamics of each component and probing the complete spectrum of mobilities of each species at the same time. The quantitative information on the mobilities of each component provided by 2D ^{2}H NMR is unique in allowing us to assess the importance of both the broadening of the dynamics and the difference between their mean motional rates. Our results can be used to describe the broad macroscopic glass transition as well as the complex temperature and compositional

dependence of the viscoelastic properties of blends. The broad distribution of motional rates plays the dominant role in explaining the broad glass transition. On the other hand, the different mean motional rates for each species and their distinct temperature dependence give rise to the thermorheological complexity. This differences in mean motional rates can be described in terms of the separate effective glass transition temperatures, which cannot be neglected in a quantitative description of the broad glass transition. In order to clarify the origin of the dynamic heterogeneities at a molecular level, we examine simplistic pictures of cooperative segmental dynamics.

4.1 Broad glass transition of miscible polymer blends

Some of the distinctive and potentially useful (or deleterious) macroscopic properties of miscible blends, particularly the anomalously broad glass transition evident in DSC [52, 53] and mechanical measurements [33], originate in a broadening of the distribution of segmental motional rates upon mixing. To control these properties, it is necessary to understand how they are related to underlying molecular motions. A number of spectroscopic methods have been applied to observe the segmental dynamics of each species underlying the glass transition. In blends in which the dielectric response is dominated by one component, dielectric spectra have shown that blending can significantly broaden the motional spectrum of an individual component [54, 55]. However, these results lacked information on the difference between the dynamics of the two component, or the relationship between the broadening of the spectrum of one component to that of the other. Similar limitations apply to 2D ^{13}C NMR studies of

only one component in a miscible blend, which provide information on the spectrum of motional rates for only the labeled species [48]. Researchers focusing on these results have emphasized the effect of compositional heterogeneity as the dominant mechanism of broadening the dynamics and hence producing the broad macroscopic glass transition.

Other spectroscopic methods have provided information on particular averages of the motional spectrum. Relaxation times and line widths for distinct ^{13}C NMR lines provide information on the mean motional rate of each species in a blend, and have shown that they can be well separated [17, 18]. However, these experiments provide little information on the distribution of motional rates for each species because NMR linewidths and relaxation times are coupled to the dynamics only at particular frequencies of motion. Perhaps as a consequence, researchers focusing on this type of information have emphasized the differences in mean motional rates between the two components in explaining the broad glass transition. Then, the broad glass transition is understood as a result of two separate glass transitions for individual species.

The ^{2}H NMR results on the mobilities of each species enable us to assess the importance of both the broadening of the dynamics and the difference between their mean motional rates simultaneously. For example, the difference in mean correlation time, τ_{c_0}, between the two components in a 50/50 PI/PVE blend leads to a difference of approximately 10 K in their effective glass transition temperature, T_g^*. This cannot completely explain the overall width of the DSC glass transition, which is roughly 30 K (**Figure 3.1** 217 K $\sim$ 247 K). However, the observed width of the correlation time

distribution, σ, shows that, for each component, the temperature range over which motions reach the rate correlated with the DSC glass transition ($\tau_{c_0}(T) \simeq 1$ s) is very broad for each component in the blend. It turns out that the temperatures that are swept across by $\log \tau_{c_0} + \sigma \simeq 0$ and $\log \tau_{c_0} - \sigma \simeq 0$ corresponds to the bounds of DSC glass transition reasonably well.From **Figure 3.15-3.18**, we estimate the ranges of effective glass transition to be roughly from 217 K to 233 K for PI and from 227 K to 244 K for PVE. The similarity between the DSC glass transition and the effective glass transition estimated from the observed correlation time distribution are also observed for homopolymers and for other blend compositions. It is also noteworthy that the increase in the width of glass transition with PVE content parallels the increase in σ of both species in those blends.

In light of these results, the broad mobility distribution of each species plays the major role in explaining the broad glass transition in blends like PI/PVE. On the other hand, the difference in mean motional rates between the two species cannot be neglected in a quantitative description of the broad glass transition. In addition, the difference in mean motional rates also has far reaching consequences in the complex temperature and composition dependence of viscoelastic properties of blends.

4.2 Molecular origin of thermorheological complexity

The glass transition temperature is a useful reference temperature, with which the temperature dependence of the viscoelastic properties is discussed. This is due to the fact that the glass transition temperature corresponds to a well defined dynamic

state for homopolymers. Although miscible blends exhibit a single broad glass transition, the underlying dynamics are not as simple as in homopolymers. In particular, dynamics of individual species differ significantly at a given temperature. Therefore, the glass transition temperature measured by DSC and likewise determined from any other macroscopic properties does not represent a well-defined dynamic state. However, consistent dynamic state for each species is invoked in interpreting the dynamics observed in blends.

When the effective glass transition temperature is defined as an iso-correlation time temperature, it is consistent with the DSC glass transition for homopolymers. Similarly, the definition of the effective glass transition temperatures represents a well-defined dynamic state for individual species in the blends. The separate effective glass transition that is underlying the broad glass transition appears to be a more reliable reference state in miscible blends. Complex composition and temperature dependence of viscoelastic properties observed in blends are reinterpreted in terms of the complex glass transition behavior and the effective glass transition temperatures for individual species. In order to further examine the nature of thermorheological complexity in miscible blends, the mean correlation times are compared with the monomeric friction coefficient obtained in our laboratory from simultaneous mechanical and birefringence measurements.

4.2.1 Distinct glass transition temperatures of each species

In many glass forming systems, the glass transition is accompanied by sharp changes in viscosity and relaxation times, as well as many thermodynamic properties (*i.e.*,

heat capacity, thermal expansion coefficient, etc.) [56]. A consistent definition of the glass transition temperature can be given in terms of certain relaxation times. For example, the temperature at which the macroscopic enthalpy relaxation time reaches $\simeq$ 100 s can be defined as glass transition temperature and is known to be correlated with the conventional onset temperature for many glass forming systems observed in a DSC measurement [56]. Although it seems consistent in many small molecular glasses and pure polymers, it becomes ambiguous for miscible blends in which the two components can exhibit widely different mobilities, even though the blend as a whole shows a single glass transition. In a 50/50 PI/PVE blend, for example, the mean reorientational correlation times of the two components can differ by more than an order of magnitude. Therefore, it seems reasonable to define an effective glass transition temperature, T_g^*, for individual species, based on mean correlation times. Here, we define T_g^* as the iso-correlation-time temperature at which τ_{c_0} reaches 1 s. It can be obtained by direct inspection of the observed τ_{c_0} or from the WLF fit of the correlation times by requiring $\log \tau_g = 0$.

The T_g^* obtained from the corrected mean correlation times (filled symbol in **Figure 3.13, 4.3**) are plotted against the PI weight fraction (**Figure 4.1**). The T_g^* is almost identical to the conventional DSC T_g for both pure components. In the blends, the T_g^*'s for the two components differ by more than 10 K, and the difference increases with increasing PVE fraction. However, the two individual T_g^*'s fall well within the DSC glass transition, except that the T_g^* of PVE in 75/25 PI/PVE blend appears to fall outside the glass transition region. Close inspection of the DSC traces

for blends with high PI fraction (e.g. 75/25 PI/PVE in **Figure 4.2**) reveals that there is indeed a distinct but weak shoulder at temperatures corresponding to the T_g^* of PVE [9, 57][1].

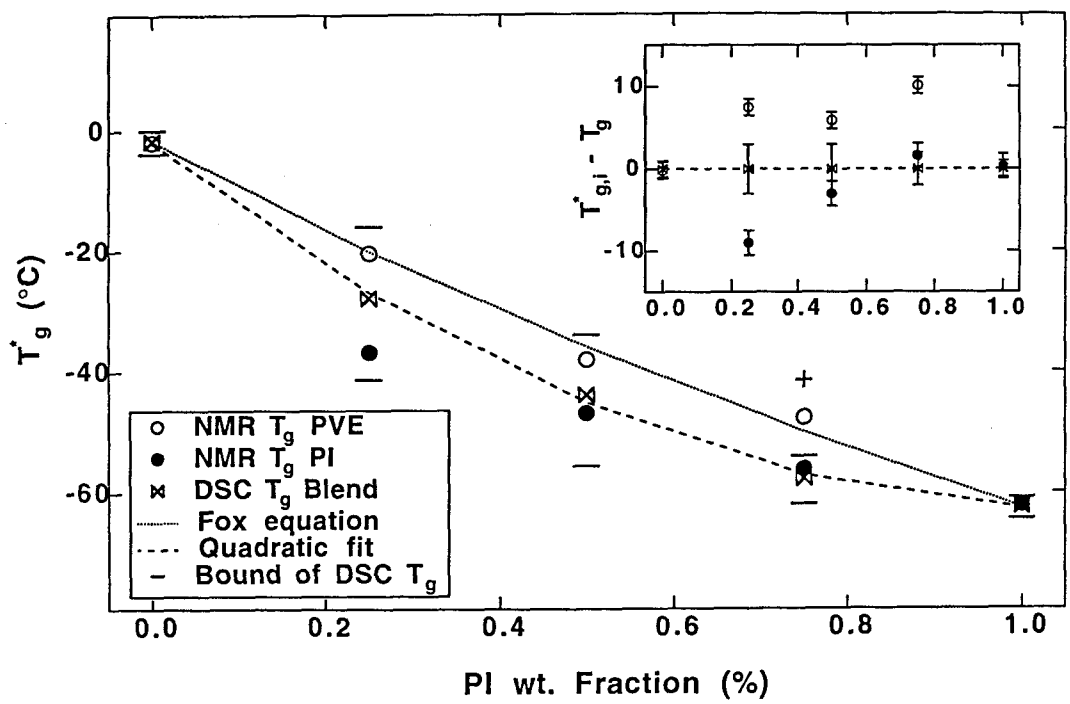

Figure 4.1: Compositional dependence of the effective glass transition temperature, T_g^*. The – symbol corresponds to the bound of the glass transition by tangent method. The + at 75/25 PI/PVE blend corresponds to the width with the weak shoulder of heat capacity change taken into account (see **Figure 4.2**). Inset: The differences between the T_g^* and the DSC T_g is also displayed. The vertical bars correspond to the uncertainties in determining T_g and T_g^*.

[1]The relative magnitude of the heat capacity change at the high temperature shoulder is about 10% or less of the total, which is much less than the PVE weight fraction. This can be partially accounted for by the relative magnitude of the heat capacity change at the glass transition of the two pure components. (PI shows about 50% more heat capacity change than PVE.) Further, the broad hump similar to that observed for 90/10 PI/PVE blend may also be present with smaller magnitude to the actual changes in heat capacity for 75/25 blend. This may have affected the appearance of the DSC trace and hence reduce the apparent heat capacity changes at the high temperature shoulder.

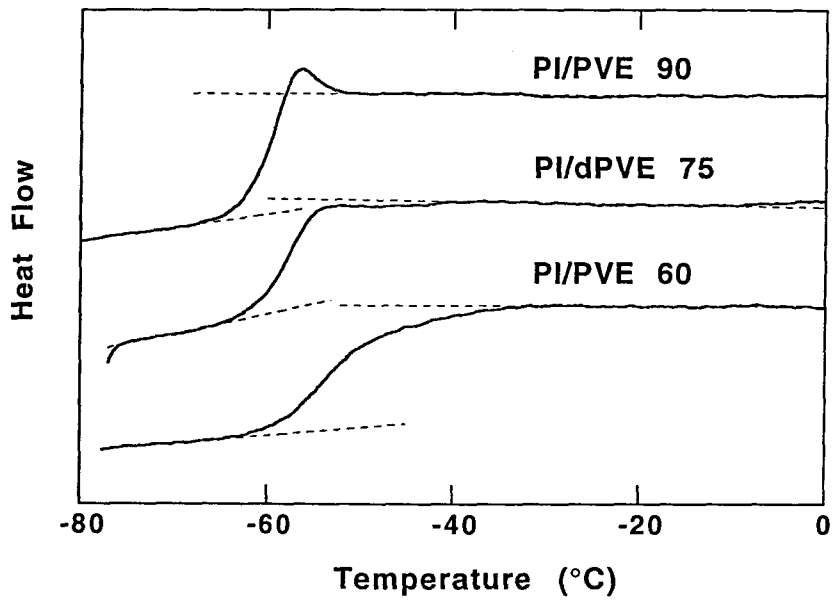

Figure 4.2: DSC traces for PI rich blends. As PVE fraction increases, the DSC traces show the development of the weak high temperature shoulder.

The two T_g^*'s show different compositional dependence from each other and from the macroscopic DSC T_g. In particular, the difference between the DSC T_g and the T_g^* of PVE is nearly constant at least for the compositions studied here, while the difference for PI goes through a weak maximum and decrease almost monotonically with increasing PVE content (**Figure 4.1** inset). This implies that the dynamics in miscible blends near the glass transition cannot be characterized solely in reference to the macroscopic T_g of the blend. When the mobility ratio of the two components obtained at various compositions is compared at temperatures with fixed $T - T_g$, the ratio varies with composition. For the particular choice of T_g based on the conventional calorimetric glass transition, the ratio of mobilities between PVE and PI would exhibit a distinct maximum near the PI weight fraction of 25%. Similar behaviors

have been observed by tracer diffusion, chain relaxation, and segmental motions manifested in T_1 NMR relaxation times [8, 58, 18] when compared at fixed $T - T_g$. This often complicates the diffusion studies in miscible blends because the compositional dependence of tracer diffusivities due to the change in matrix glass transition cannot be compensated by simply shifting the measurement temperature with respect to the blend T_g. Significant discrepancies between the experimental and theoretical studies on the compositional dependence of the monomeric friction coefficient of each species seem to be related to this complex glass transition behavior [8, 58, 59].

When we compare the T_g^* with simple empirical relations for the compositional dependence of T_g, we notice that the T_g^* of PVE agrees reasonably well with the Fox-Flory relation, while the T_g^* of PI increases close to linearly at PI fractions higher than 50%. Further studies are required to determine whether or not this behavior is typical in miscible blends with weak interactions.

4.2.2 Failure of time-temperature superposition

The thermorheologically complex behavior observed in a number of miscible blends [13, 9] can be explained in terms of distinct temperature dependence of the monomeric friction coefficient, $\zeta_{0,i}$, where i indexes each component. In light of our NMR results, a qualitative analogy between the $\zeta_{0,i}$ and $\tau_{c_0,i}$ can be invoked to understand the failure of time-temperature superposition. It is reasonable to expect that distinct $T_{g,i}^*$'s for the two species underlying the broad DSC glass transition can describe the different temperature dependence of $\tau_{c_0,i}$, and perhaps $\zeta_{0,i}$.

Here, the $\tau_{c_0,i}$ is directly compared with $\zeta_{0,i}$ obtained from the same set of polymer

blends using simultaneous mechanical and optical measurements [12](**Figure 4.3**). The two sets of data are compared quantitatively by introducing one adjustable constant for each pure component, which accounts for the ratio of $\zeta_{0,i}/T$ to τ_{c_0}. The connection is made using the general relationship between the shortest Rouse-relaxation time of species i, $\tau_{R,i}$, and its friction coefficient, $\zeta_{0,i}$:

$$\tau_{R,i} = \frac{A_i}{k_B T}\zeta_{0,i}, \tag{4.1}$$

where $A_i = \frac{a_i^2}{3\pi^2}$, a_i is the length of a Rouse chain segment, and k_BT is the thermal energy. For comparison purposes, the value of A_i is adjusted so that the pure component data for both $\tau_{R,i}$ and $\tau_{c_0,i}$ can be best described by a common WLF fit. The same values of A_i are used for species i in the blends as well. The dotted lines shown in **Figure 4.3** are the common WLF fits and the parameters are listed in **Table 4.1**, where $\log \tau_g$ is fixed to be 0, consistent with the definition of T_g^*. For the WLF curves, C_1^g is also fixed for each species, since we expect the extrapolated mobility at infinite temperature to be controlled by intra-chain dynamic constraints, independent of composition. Furthermore, both C_1^g and C_2^g cannot be determined unambiguously, within the experimental uncertainties. The proportional factors, A_i, determined empirically from $\frac{\tau_{c_0,i}k_BT}{\zeta_{0,i}}$ are much smaller than A_i directly calculated from the literature values of the statistical segment lengths. This is consistent with the fact that the segmental motion observed by the ^{2}H NMR is more local than the Rouse chain dynamics.

The common WLF curves can describe both NMR and rheological data reasonably well over eight decades for both homopolymers. For a given species i in a blend,

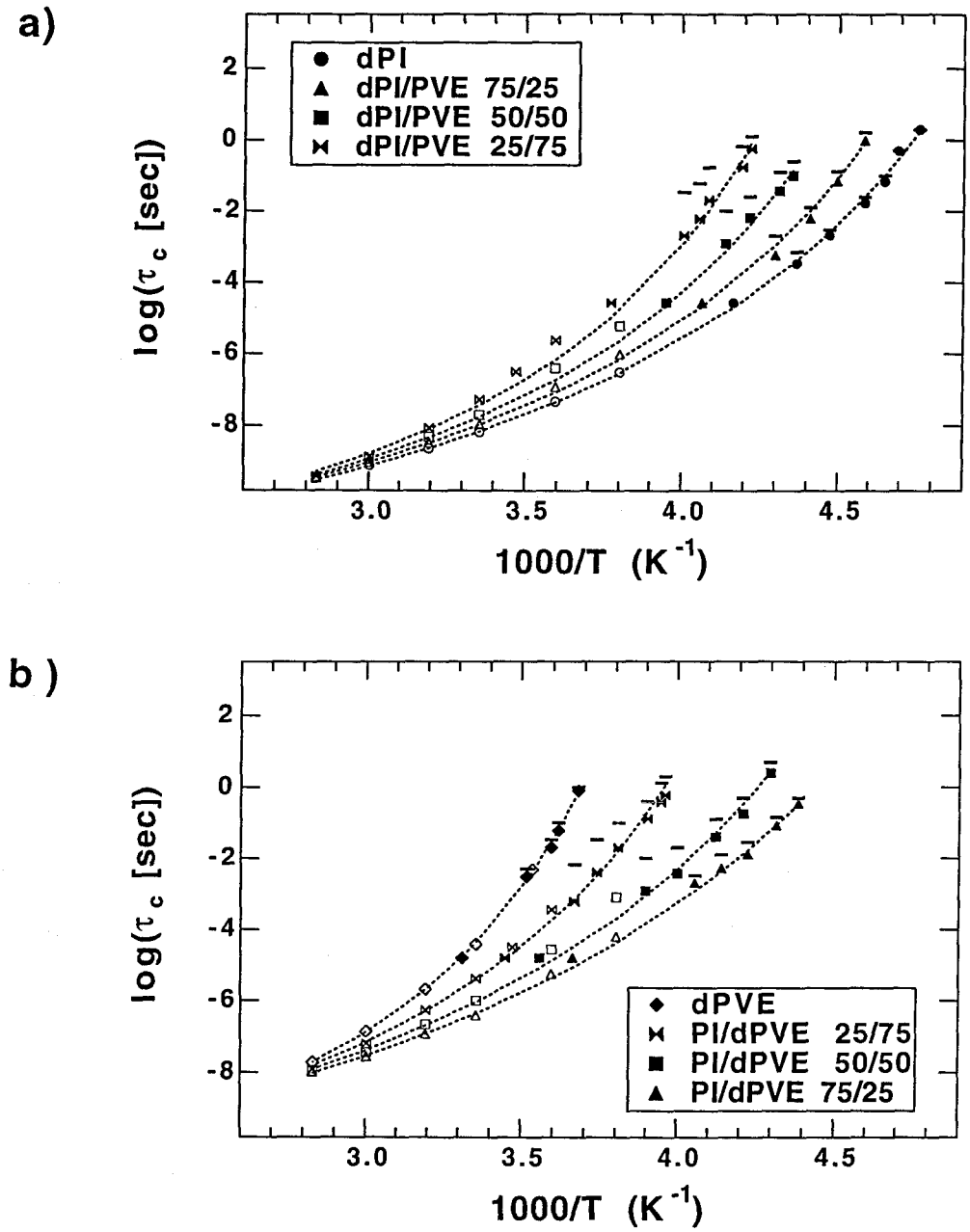

Figure 4.3: Comparison of τ_{c_0} and ζ_0 for each component in the same blend. The solid symbols are the mean correlation times obtained after accounting for the reduction of intensity (see Appendix B), and the open symbols are the shortest Rouse-like relaxation time τ_R evaluated from the monomeric friction, ζ_0. The $-$ symbols correspond to the mean correlation times from 2D spectra before accounting for the intensity loss. The dotted lines are the best fit WLF curves that pass through both the τ_{c_0} and τ_R, and the parameters are listed in **Table 4.1.**

Table 4.1: The WLF parameters that best fits both the τ_{c_0} and τ_R.

species	composition (PI/PVE)	C_1^g	C_2^g	T_g^*
PI	100/0	12.85	49.6	210.9
	75/25	12.85	49.7	216.8
	50/50	12.85	46.9	226.3
	25/75	12.85	44.8	236.5
PVE	75/25	12.3	68.0	225.3
	50/50	12.3	65.4	234.4
	25/75	12.3	57.5	252.7
	0/100	12.3	48.6	271.2

$\tau_{R,i}$ and τ_{c_0} can roughly be described by a common WLF fit. As suggested previously [60, 9], the failure of time-temperature superposition can be described in terms of the different temperature dependence of component dynamics. Though the dominant feature still seems to be the distinct individual T_g^*, the other two parameters (C_1^g, C_2^g) also appear to have a weak compositional dependence, in spite of the similarity between these parameters for each pure component. Although experimental uncertainties limit our ability to quantitatively determine C_1^g and C_2^g, it is impossible to achieve a reasonable fit if they are both held fixed, independent of composition.

Although common WLF curves can approximately describe both rheological and NMR data for blends as well, some deviation is noticed in the blend. The deviation

from the best fit is more pronounced when the correlation time distribution is very broad (*i.e.*, in 50/50 and 25/75 PI/PVE blends). In particular, for 50/50 and 25/75 PI/PVE blends, the rheological results for $\tau_{R,i}$ (open symbols) rise more strongly with decreasing temperature than the common WLF fit does. A WLF fit to the rheological data alone would lie above the mean correlation times but within the distribution of correlation times observed by NMR (see also **Figure 3.15-3.18**). The NMR measurement probes segmental motion that appears to correlate well with the monomeric friction coefficient in homopolymers. However, the rheological measurement probes ζ_0, which is highly averaged in the scale of the entanglement molecular weight. Therefore, the systematic discrepancies between the temperature dependence of $\tau_{R,i}$ and τ_{c_0}, evidenced most strongly in blends, suggest that the ζ_0 measured rheologically may be a biased average of locally heterogeneous friction. This behavior is perhaps related to the way that the heterogeneity in segmental dynamics is propagated to the chain dynamics at a Rouse or reptation level.

4.3 Origin of dynamic heterogeneities

In light of the deuteron NMR results, dynamic heterogeneities in miscible blends can be reduced to two different types: the broad range of mobilities associated with spatial heterogeneity, and distinct mobilities between individual species. These dynamic heterogeneities have not been observed simultaneously by previous workers because the dynamics of individual species could not be resolved or because only particular averages of the complete motional spectrum could be probed. In terms of the two

dynamic heterogeneities, a unified view is suggested that interrelates the segmental dynamics to macroscopic properties such as the broad glass transition and the thermorheological complexity of blends.

To further advance the understanding of the dynamic heterogeneity in blends, we should examine the effect of the two hypothesized origins of the dynamic heterogeneities: difference in intrinsic dynamic constraints of each component [9, 17], and local compositional heterogeneity [13, 55, 19]. The concept of intrinsic dynamic differences between the two components alone cannot explain the observed broadening of correlation time distribution for each species. Local compositional heterogeneity in the absence of intrinsic dynamic differences, however, can qualitatively explain both a difference in mean correlation time between the two species and an increase in width of the correlation time distribution for both species. Therefore, the effect of spatial heterogeneity must be examined [52, 55, 19] more closely to see if it can explain the observed behavior of the mean and the width of the correlation time distribution for each component. To do so, we consider a simple model of compositional heterogeneity that is appropriate for the case of $\chi \simeq 0$.

4.3.1 Effect of statistical composition variation: simplistic model

While the mobilities of the two species in the blend differ significantly from one another, this difference is small compared to the change in their mobilities with respect to their pure states. This suggests that the dynamics of both species are strongly dependent on the composition of their surroundings. This is also consistent with the pronounced broadening of the distribution of segmental mobilities for both species,

which suggests that their dynamics are very sensitive to variations in the local composition.

In a real system, the dynamics of a test segment depend on its intramolecular dynamic constraints and on the coupling of its dynamics with its neighbors. It is expected that the dynamics of a test segment would be strongly coupled to its neighbors both because of connectivity along its backbone and because its neighbors are densely packed around it. Near the glass transition temperature, in particular, it has been speculated that the dynamic coupling extends much beyond the nearest neighbors [16]. Although it is not unambiguously established, the local segmental dynamics of a flexible chain appear to be sensitive to the neighboring chains lying within a distance that has been estimated to be 2-7 nm [55, 19, 61]. Obviously, the influence of the immediate neighbors is the greatest, with the interactions decaying with distance. A primitive statistical model that takes into account only the nearest neighbors on a cubic lattice has been used to explain 2D NMR lineshapes in a miscible blend and polymer-diluent systems [48, 62]. As a crude yet more realistic approximation, one can assume that the dynamics of a test segment are coupled to all neighbors within a certain distance or critical radius r_c. In this simple model, we represent this dynamic coupling by a local glass transition that depends only on the local composition within a critical radius r_c .

In the presence of local composition variations, this simple physical picture predicts a distribution of local glass transitions and hence a distribution of motional rates. The difference in average motional rates between the two components in a

blend can also arise, since the test segment biases the composition of a local volume around it toward that of the test chain. This simple model is useful in showing how much of the observed broadening and difference in mobility between the two species can be ascribed to random variations in the local composition. The effects of *intrinsic* differences in the dynamics between the two species are not included in the model (*i.e.*, differences in dynamic coupling or intramolecular barriers to conformational rearrangement). When these are neglected, it turns out that this simple model cannot explain both the observed mean mobility difference and the width of the mobility distribution simultaneously.

In a blend of two polymers A and B with very weak interactions ($\chi \simeq 0$), one can assume that the neighbors of a particular chain are chosen randomly. Thus, the composition of its neighbors will have some distribution about the mean. The composition of a subvolume is biased toward that of the test chain, since it occupies a certain fraction of the subvolume due to connectivity. The rest of the space is filled by either 'A' or 'B' randomly. The compositional distribution of the neighbors is approximated to be Gaussian, with mean equal to the macroscopic composition, $\tilde{\phi}$, and variance, σ^2, estimated from the statistics of Bernoulli Trials. The size of the region that influences the dynamics naturally affects the distribution of local composition: as the r_c decreases, the number of neighboring units within r_c decreases and the width of the distribution of local composition increases.

To connect this distribution of composition with the distribution of motional rates, one must adopt some mapping of composition to mobility. Here we adopt the ap-

proach suggested by Fischer and co-workers [55]. Their model of dynamic heterogeneity in a mixture of polymers denoted by A and B is based on the following assumptions:

1. The local dynamics are taken to be sensitive to the composition within the subvolume of a given size. The volume fraction of component A in each subvolume is ϕ. The distribution of ϕ is assumed to be Gaussian with a variance $\langle \delta\phi^2 \rangle$.

2. The value of ϕ in each subvolume remains constant on the time scale of the α relaxation.

3. A subvolume has a local glass transition temperature T_g^{loc} that depends only on ϕ; and the ϕ dependence of $T_g^{loc}(\phi)$ is assumed to be the same as that of the macroscopic T_g.

4. The correlation time of a subvolume $\tau(\phi, T)$ is calculated by the WLF-equation, with the parameters (C_1^g, C_2^g) taken as the average of the pure components' values, and using the empirical $T_g^{loc}(\phi)$.

Fischer has used this model to quantitatively describe the gradual broadening of the α relaxation spectra by using $\langle \delta\phi^2 \rangle$ as a temperature dependent fitting parameter [55]. The temperature dependence of $\langle \delta\phi^2 \rangle(T)$ was interpreted as arising from the temperature dependence of the subvolume size. The radius of the subvolume was estimated to be approximately 7 nm at T_g + 20K and decreases with temperature [55]. The subvolume was interpreted as the cooperatively relaxing unit [16].

Our goal is to see if this physical picture is capable of describing the observed

correlation time distribution for both components simultaneously. Although we adopt the mapping of local composition to mobility introduced by Fischer and co-workers, our calculation differs from theirs in a few respects. In Fischer's model, the sample is divided into small subvolumes and all segments in a subvolume have the same mobility. Here, the subvolumes are constructed around every test segment and the mobility of that test segment is obtained from the composition of its subvolume. Instead of using $\langle \delta\phi^2 \rangle$ as a temperature-dependent fitting parameter and using it to estimate the size of subvolumes, we start with a simple statistical model to estimate $\langle \delta\phi^2 \rangle$ and the composition distributions as a function of the subvolume size. The temperature dependence of the subvolume size is neglected in our calculation. We assume that the mixing is random at a molecular level with $\chi = 0$, which is consistent with the observation that PI/PVE is miscible without any specific interaction between the species [33]. We also neglect the effects of slight densification (*circa* 0.1%) and any difference in the packing efficiency of the blend compared to the homopolymers [32, 33]. The correlation time distributions of the components in a blend are then calculated by following the assumptions 1)–4) introduced by Fischer and co-workers

In this model, the subvolumes around each test segment are constructed as illustrated in **Figure 4.4**. In a subvolume with diameter $N \cdot b$, there are N^3 sites for segments, each with a volume of $\frac{4\pi}{3}(b/2)^3$, where b is the size of the statistical segment. A given subvolume is identified as an A- or a B-subvolume depending upon the type of test segment at the center of the subvolume. The test chain that contains this central segment is assumed to occupy $N^2/2$ sites, i.e., the average number occupied

by two random walks that begin at the origin and end a distance $r_c = N\,b/2$ away from it. The remaining $N^3 - N^2/2$ sites are filled by either A or B randomly. Thus, the composition in the subvolume is biased toward that of the test chain due simply to connectivity of segments along the chain [52, 48, 62]. When the volume fraction of A for the macroscopic sample is $\tilde{\phi}$, the mean composition of subvolumes centered on an A segment is

$$\langle\phi\rangle_A = \frac{1}{2N} + (1 - \frac{1}{2N})\,\tilde{\phi}, \tag{4.2}$$

and the mean volume fraction of A in the subvolumes centered on a B segment is

$$\langle\phi\rangle_B = (1 - \frac{1}{2N})\,\tilde{\phi}, \tag{4.3}$$

where the subscript (A or B) denotes the identity of the test segment for the subvolumes included in the average.

The width of the ϕ distribution depends on the number of independent units that participate in filling the $N^3 - N^2/2$ empty sites. The estimation of the composition variation is particularly simple when the empty sites are filled by independent units of equal size. In selecting this fixed size, there are two extreme cases, as illustrated in **Figure 4.4b)**; the independent unit is taken in one case to be a single segment (case **I**) and in the other a strand of $N^2/2$ segments, like the test chain (case **II**). The composition variation $\langle\delta\phi^2\rangle$ estimated from case **I** denoted by $\sigma^2_{\phi,1}$ gives a lower bound on $\langle\delta\phi^2\rangle$, whereas the composition variation from case **II** ($\sigma^2_{\phi,N}$) sets a practical upper bound. The variance of the volume fraction is the same for both the A- and B-subvolumes and is obtained by applying the statistics of Bernoulli Trials. In the case that $N^3 - N^2/2$ remaining sites are filled by independent segments, the variance

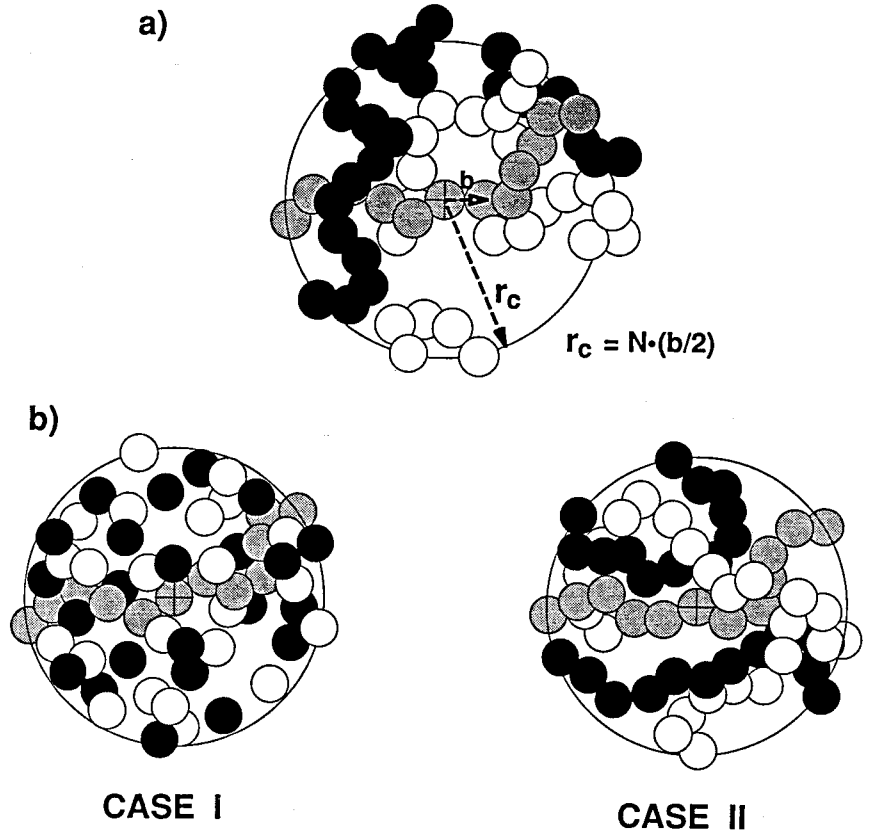

Figure 4.4: Schematic description of local compositional variations in a model miscible blend of A and B, denoted by black and white beads. The central gray chain can be either A or B, with a probability of $\tilde{\phi}$ of being A. Each subvolume of radius $r_c = N(b/2)$, where b is the size of a statistical segment, contains N^3 sites for monomer segments. **a)** One possible realization of an actual subvolume. Each strand that is residing in the subvolume is varied in length. **b)** Case **I**: The subvolume is assumed to be filled by independent segments. Case **II**: The subvolume is filled by independent strands of uniform length of $N^2/2$. The composition variation becomes larger than most realizations.

of ϕ is

$$\sigma^2_{\phi,1} = \frac{\tilde{\phi}(1-\tilde{\phi})}{N^3 - N^2/2}, \tag{4.4}$$

and in the case that sites are filled by $2N-1$ independent strands of $N^2/2$ segments, the variance is

$$\sigma^2_{\phi,N} = \frac{\tilde{\phi}(1-\tilde{\phi})}{2N-1}, \tag{4.5}$$

where the subscript 1 or N denotes filling by single segments or strands of $N^2/2$ segments. The composition distribution of each subvolume $P_i(\phi)$ is further approximated as Gaussian with the mean and the variance of composition obtained above, *i.e.*,

$$P_{i,n}(\phi) = \frac{1}{\sqrt{2\pi\sigma^2_{\phi,n}}} \exp[-(\phi - \langle\phi\rangle_i)^2/2\sigma^2_{\phi,n}], \tag{4.6}$$

where $P_{i,n}(\phi)$ is the probability that a subvolume have a given value of ϕ given that the test segment is type i (A or B) and the mode of 'filling' is designated by n (1 or N).

Under the assumptions introduced by Fischer and co-workers, the composition of a subvolume, ϕ, is directly mapped onto the correlation time for segmental motion of all chains in that subvolume, $\tau(\phi, T; T_g^{loc}(\phi))$:

$$\log\{\tau(\phi, T; T_g^{loc}(\phi))\} = \log\tau_g - \frac{C_1(T - T_g^{loc}(\phi))}{C_2 + (T - T_g^{loc}(\phi))}, \tag{4.7}$$

where τ_g is the correlation time for the motion at $T = T_g^{loc}$. Here, we use the empirical value $\tau_g = 1$ s as described earlier. In our calculation, we take τ to be that of the test segment, rather than that of all segments in the subvolume. Although $\tau(\phi, T; T_g^{loc}(\phi))$ is taken to be the same for both species in a blend, the mean correlation times of

the two species can differ significantly due to the bias in the composition distribution toward that of the test chain (eqn. 4.2 and 4.3). And the width of the distribution of correlation times for the two components can also differ, due to the non-linear dependence of τ on ϕ through T_g. We let A denote the higher T_g component and B the lower T_g component, corresponding in our experiments to PVE and PI respectively. The composition dependent glass transition temperature, $T_g^{loc}(\phi)$, is approximated by the quadratic fit of the DSC T_g of PI/PVE blends.

We calculate the correlation time distribution of A and B-subvolumes directly from the above composition distribution. The log mean correlation times, $\log \tau_{i,n}$, and the distribution widths, $\sigma_{i,n}$, are subsequently calculated as averages over the subvolumes:

$$\log \tau_{i,n} = \int_0^1 [\log\{\tau(\phi, T; T_g^{loc}(\phi))\}]\, P_{i,n}(\phi)\, d\phi, \tag{4.8}$$

and

$$\sigma_{i,n}^2 = \int_0^1 [\log\{\tau(\phi, T; T_g^{loc}(\phi))\} - \log \tau_{i,n}]^2\, P_{i,n}(\phi)\, d\phi, \tag{4.9}$$

where i is A or B according to the identity of the test segment and n is 1 or N specifying case **I** or **II**.

A. Comparison of model and experimental results: 50/50 blend

The results of the model calculations are presented for 50/50 blend, and compared with the mean and the width of correlation time distribution observed in a 50/50 PI/PVE blend. The behavior of the $\log \tau_i$'s and σ_i's agree qualitatively with the experimental observations, for both cases **I** and **II**. At all temperatures, the mean

correlation times of A and B are biased toward that in their pure state. The differences between the mean correlation times and the distribution widths of both A and B chains increase with decreasing temperature. However, neither of the two cases can capture the relative magnitude of the difference in mean correlation times and the width of the distribution.

In case **I** the width of the composition distribution decreases strongly with subvolume size [$\sigma^2_{\phi,1} \sim N^{-3}$, eqn. 4.4], so even a very small size ($N \approx 3$) cannot capture the observed width of the distribution of motional rates. Further, when the subvolume is this small, the bias in composition toward that of the test chain is very large and produces a bimodal distribution of motional rates overall contrary to experimental observations. Finally, the A-subvolumes (rich in the high-T_g component) have a significantly broader distribution of motional rates than the B-subvolumes due to the increasing sensitivity of T_g to the volume fraction of the high-T_g component ϕ as $\phi \rightarrow 1$. Thus, case **I** cannot describe the observed distribution of motional rates.

For case **II**, since the subvolumes are filled by independent strands of $N^2/2$ segments, the width of the composition distribution for a given N is much wider than in case **I**. The subvolume size that gives $\sigma^2_{\phi,N}$ in accord with the experimental results is $N \simeq 10$ (**Figure 4.5b**). For this size, the segments of the test chain constitute a minor fraction of all the segments in the subvolume, and the difference between the mean composition and associated motional rate for the A- and B-subvolumes is relatively small. As a result, the composition distributions of A- and B-subvolumes are strongly overlapped and the overall correlation time distribution becomes unimodal,

in accord with experiment. In addition, for $N \geq 10$, $\sigma_{A,N}$ and $\sigma_{B,N}$ become similar to each other, which is also in agreement with experiment. However, for a subvolume size that captures the approximate magnitudes of σ_A and σ_B and their relative magnitude, the difference between the mean correlation times is much smaller than is observed experimentally (see **Figure 4.5b**). To capture the observed difference between the mean correlation times, the size of the subvolume must be reduced to $N \simeq 5$ (**Figure 4.5a**). This results in an increase in the distribution widths and an increase in $\sigma_{A,N}$ relative to $\sigma_{B,N}$ for the reasons discussed earlier in relation to case **I**. Thus, the present physical picture cannot capture simultaneously the separation in the mean correlation times *and* the two distribution widths for any choice of the subvolume size.

B. Model calculation: 25/75 and 75/25 B/A blends

For the other two compositions (*i.e.*, 75/25 and 25/75 PI/PVE blends), the same model calculation is repeated. The calculation and the experimental results are compared in **Figure 4.6**. In the calculation, the width of the correlation time distribution is governed by the mapping of variations in composition onto mobility distributions through the compositional dependence of the local $T_g(\phi)$. The size of the normalized critical radius $N = 2r_c/b$ is chosen to capture the observed broadening of T_g and the correlation time distribution for the 50/50 blend. The model does not account for the intrinsic width of the correlation time distribution in the homopolymers; therefore it is not surprising that in the 75/25 PI/PVE blend, in which the distribution width is comparable to that of the homopolymers, the model underpredicts the distribution

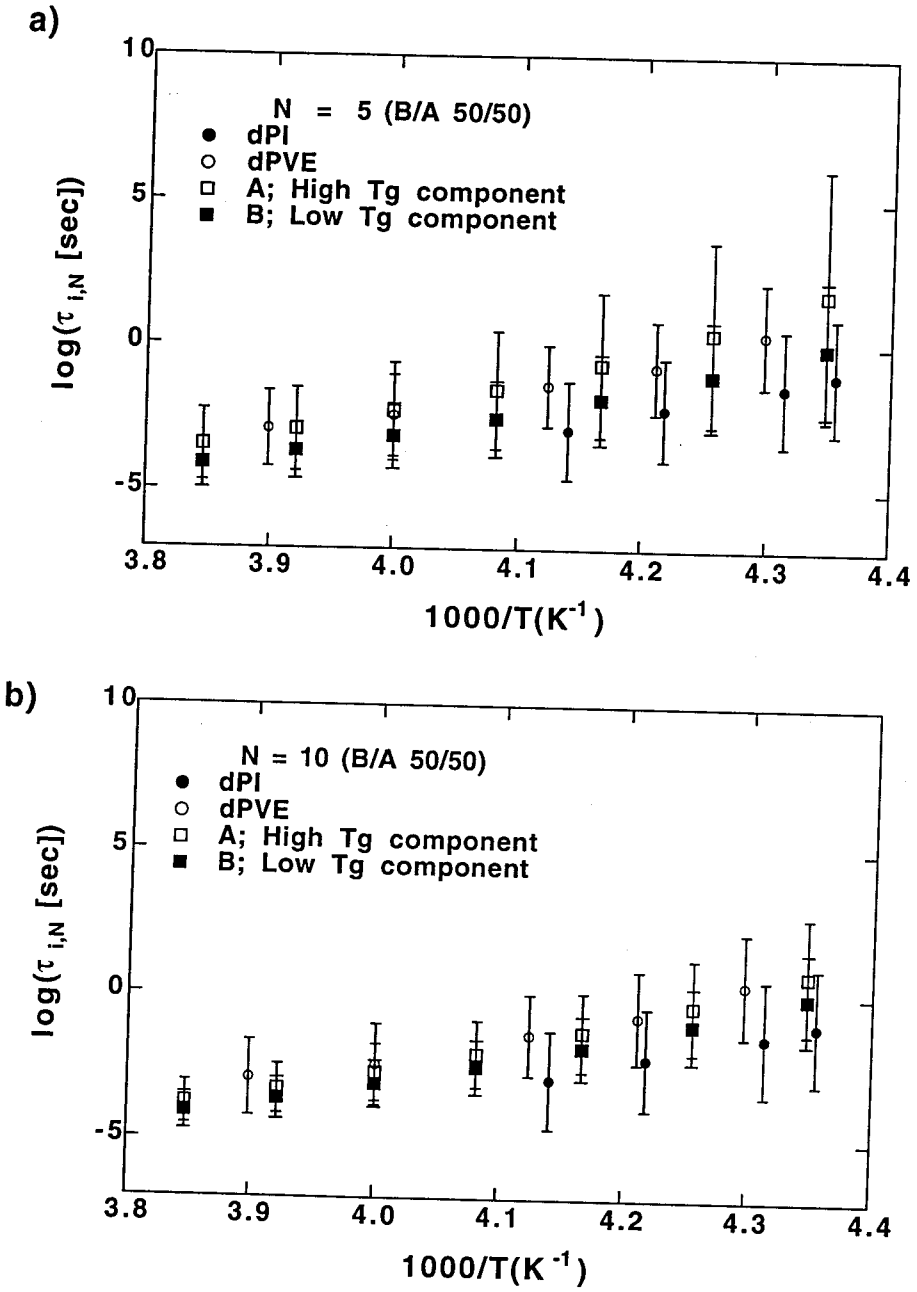

Figure 4.5: Mean and width of the correlation time distribution ($\log \tau_{i,N}$, $\sigma_{i,N}$) that are calculated for case **II**, where i is the identity of the chain A or B. (a) for a subvolume size of $N = 5$, the difference in the mean correlation times, $\tau_{A,N} - \tau_{B,N}$ is comparable to the experiments. (b) for $N = 10$, the distribution width of the correlation time σ_A and σ_B are comparable to the experimental values.

width.

For the value of N that best reproduces the width of correlation time distribution, the separation between the mean motional rates of A and B is much smaller than the experimental difference at all compositions. The separation between the mean motional rates would increase if the bias in the composition of each subvolume is increased. This could be achieved by reducing the subvolume size, so the test chain occupies a larger fraction of it. However, increasing the bias in composition toward the test chain makes the σ of the two species differ significantly, because σ increases more strongly when the mean composition is richer in high T_g component. This behavior implies that the observed segmental dynamics cannot be completely explained by local compositional variation alone. The remaining differences in the mean correlation times between the two species are probably due to the intrinsic dynamic differences between the two species.

C. Effect of statistical composition variation on the broad glass transition

In the previous chapter, compositional dependence of the glass transition broadening is discussed qualitatively. It is noted that the width of the glass transition increases with increasing content of high T_g component (PVE), which is also correlated with the steep compositional dependence of T_g. In light of our simple model, this compositional dependence of the glass transition broadening can be partially explained by the effect of random compositional variation.

Under the assumption of one-to-one correspondence between local composition and T_g^{loc}, the broad T_g arises from the compositional variation through the mapping

a)

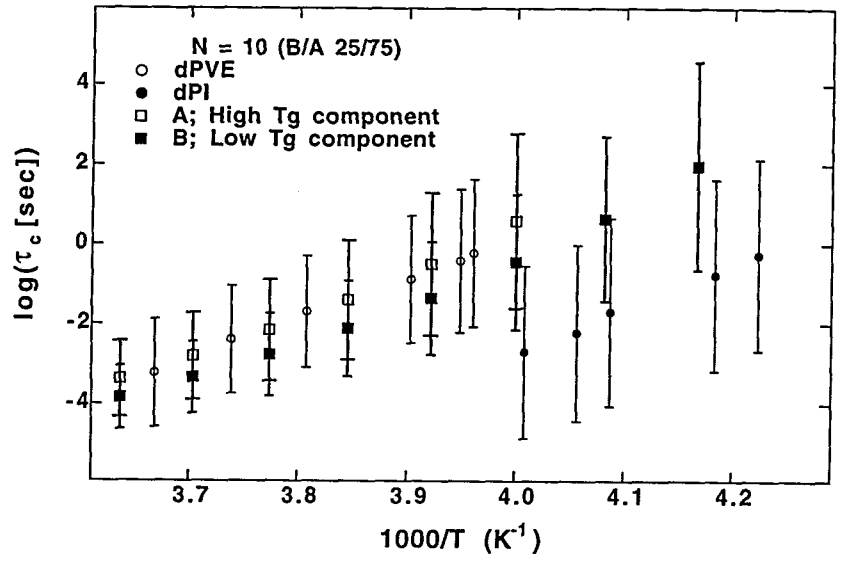

b)

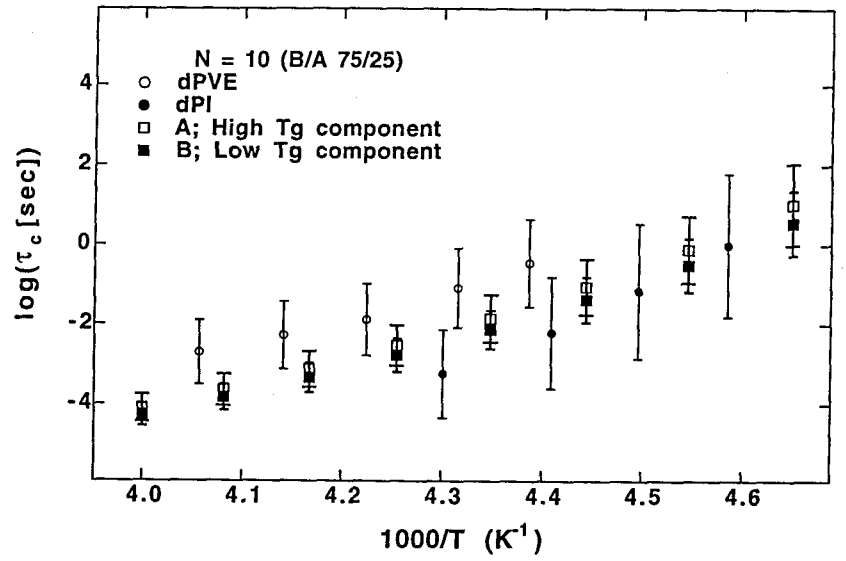

Figure 4.6: Mean and width of the correlation time distribution from the experiment and from the model calculation for a subvolume size of $N = 10$, (a) for 25/75 PI/PVE and (b) for 75/25 PI/PVE.

between ϕ and $T_g^{loc}(\phi)$. For blends where random mixing is a reasonable assumption, local compositional variation becomes maximized at $\tilde{\phi} = 0.5$. The variation then falls off away from the maximum as $\langle \delta\phi^2 \rangle \propto \tilde{\phi}(1-\tilde{\phi})$ (eqn. 4.4 and 4.5). This alone would predict maximum width of glass transition at around $\tilde{\phi} = 0.5$ and narrower width away from this composition, which is not consistent with the DSC traces shown in **Figure 4.7a**. The increased broadening toward blends rich in high T_g component results from the greater sensitivity of T_g^{loc} to compositional variations as $\tilde{\phi} \rightarrow 1$ (**Figure 3.2**). Consequently, the calculated width of the glass transition is broadest for $\tilde{\phi} \simeq 0.75$, which corresponds to 25/75 PI/PVE blend (**Figure 4.7**). For the model calculation, the heat capacity changes at T_g, ΔC_p's, are assumed to differ by 50%, *i.e.*, $\Delta C_{p,B}/\Delta C_{p,A} = 1.5$, in accord with experiments for PI and PVE homopolymers. The size of the subvolume is fixed to $N = 10$, which is previously shown to reproduce the width of correlation time distribution reasonably well. The simple model can describe the changes in glass transition broadening in a semi-quantitative way. However, the model underestimates glass transition width, perhaps because the broadening associated with the distinct individual mobilities is neglected.

4.3.2 Phenomenological model of cooperative segmental dynamics

In the condensed state, polymer segments cannot relax independently of their intermolecular neighbors. This intermolecular cooperativity causes a large increase in the apparent activation energy from that of the conformational rearrangement of a single backbone bond. For example, apparent activation energy of a typical homopolymer

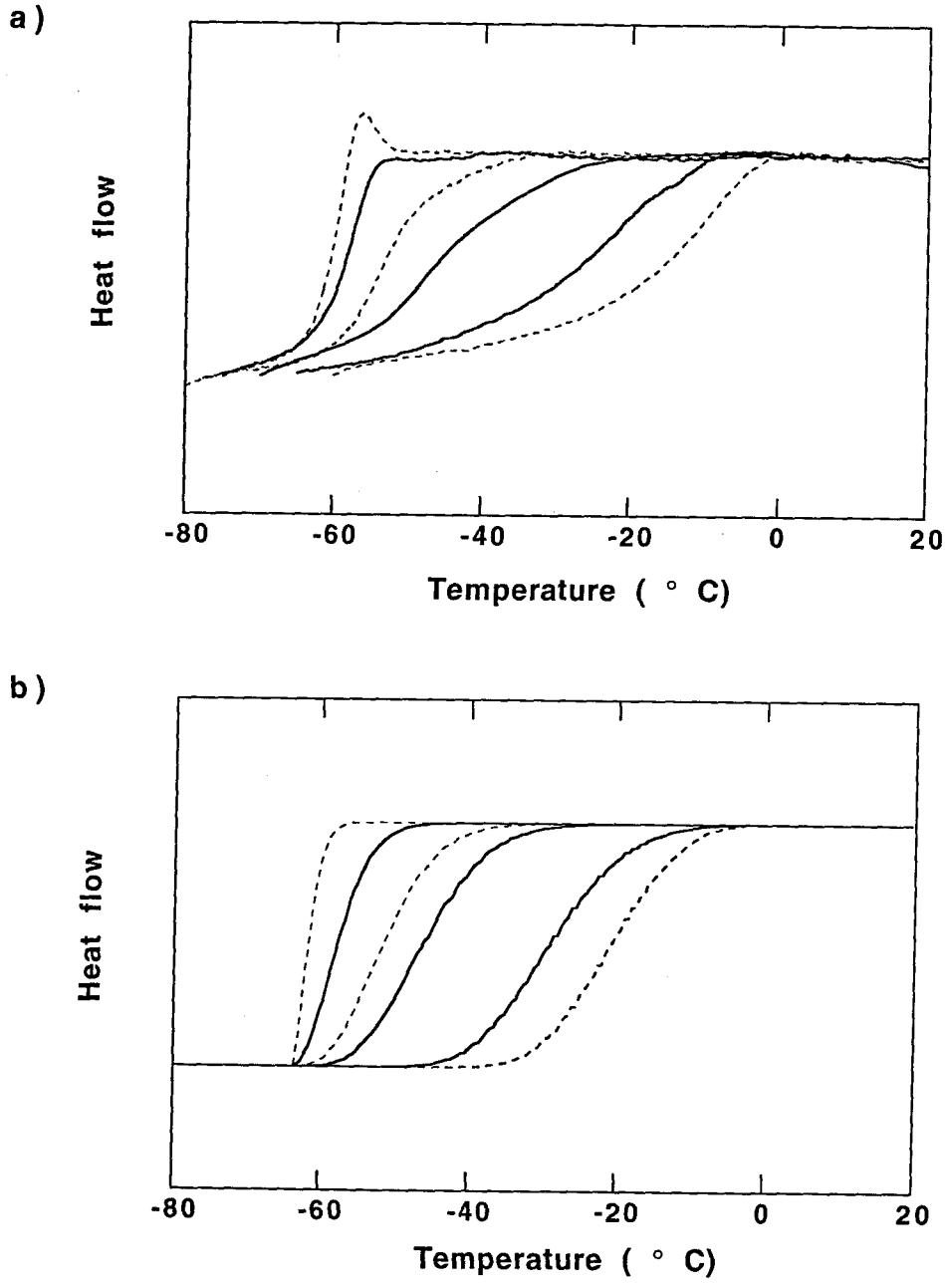

Figure 4.7: Effect of compositional variation on the width of glass transition. The experimental DSC traces are compared with simple model calculation for $N = 10$. (a) Experimental DSC traces from 90/10, 75/25, 60/40, 50/50, 25/75 and 15/85 PI/PVE blends. (b) Calculated DSC traces for $\tilde{\phi} = 0.1$, 0.25, 0.4, 0.5, 0.75 and 0.85.

at its glass transition is 200 kcal, whereas activation energy for a single bond rotation is about 3.5 kcal. The WLF temperature dependence is also considered to arise from such intermolecular cooperativity. The WLF parameters are, in principle, related to the molecular properties of polymers as well as the nature of cooperative dynamics. Although WLF parameters cannot be predicted from molecular architectures, a number of phenomenological models can predict the WLF temperature dependence based on simple physical pictures of cooperativity as described briefly in the Introduction.

In miscible blends, intermolecular cooperativity changes with composition without affecting the intramolecular dynamic constraints. Therefore, changes in the WLF parameters with composition may be understood/predicted based on a simple physical picture of cooperative dynamics. One basic property of the WLF equation is the divergence of relaxation times at the Vogel temperature, $T_0 = T_g - C_2^g$. In phenomenological models, the Vogel temperature is identified as the temperature at which segmental dynamics become infinitely cooperative or free volume vanishes.

Suppose the Vogel temperature is indeed associated with infinitely cooperative motion, then the two species in the same blend have to share a common T_0. Also based on simple models, certain constraints are placed on the WLF parameters for each species in the same blend. The consistency of some phenomenological models can be tested using the combined NMR and rheological data. Due to the limited temperature range of the data and uncertainties associated with combining the NMR and rheological data, unambiguous determination of all the WLF parameters is impossible. Therefore, instead of examining the WLF parameters for each species at all

compositions, we will first seek a possibility for a common T_0 governing the dynamics of both components. Further WLF analysis will be performed based on a number of constraints suggested from models.

A. Free volume model

Cohen and Turnbull have derived the mobility of a condensed hard sphere liquid by assuming that a distribution of hole sizes exists and the jump probability is determined only by the chance of finding an adjacent local free volume of sufficient size [15]. They obtained the total probability of finding a free volume exceeding a given size v^*,

$$P(v^*) = \exp(-bv^*/v_f), \tag{4.10}$$

where b is a numerical constant, and v_f is the average free volume per molecule. Fujita's free volume model postulates that the mobility is proportional to the jump probability. By approximating v_f as $f\,v_0$ where f is the fractional free volume and v_0 is the molecular volume and lumping bv^*/v_0 into a constant that depends on the structure of a given molecule, he has derived the mobility [63],

$$m = \tilde{A}\exp(-\tilde{B}/f). \tag{4.11}$$

For the hard sphere liquids, the molecular volume, v_0, and the free volume, v_f are well defined in terms of the volume fraction of the hard sphere. However, for real molecules and polymers, v_0, v_f and v^* are not defined clearly and serve as phenomenological parameters that preserves the original definition only qualitatively.

Similarly, we can assume that the correlation time is inversely proportional to the

jump probability and that both species share the same fractional free volume in a miscible blend. The mean correlation time of segmental motion is

$$\log \tau_{c,i} = \log(A_i) + B_i / f(T, \phi), \tag{4.12}$$

where i indexes each species and $B_i = 0.434\, b_i v_i^* / \overline{v_0}$ and $\overline{v_0}$ represents average unit size of the blend. When we further assume the linear temperature dependence of $f(T, \phi)$, eqn. 4.12 becomes

$$f(T, \phi) = \alpha(\phi)[T - T_0(\phi)] \tag{4.13}$$

$$\log \tau_{c,i} = \log(A_i) + \frac{B_i}{\alpha(\phi)[T - T_0(\phi)]}, \tag{4.14}$$

where $\alpha(\phi)$ is the thermal expansion coefficient of free volume, and the fractional free volume vanishes at $T_0(\phi)$.

In the conventional free volume model, B_i is assumed to be fixed for all polymers since the segmental volume and the critical free volume size are relatively insensitive to the specific polymers. Also, the iso-free volume state is considered to be a dynamically consistent state, at which all polymers exhibit similar mobility. In miscible blends, such approximations would predict a constant mobility ratio independent of temperature and composition, which is not consistent with our NMR results. On the other hand, when the critical free volume size can depend on the intramolecular structure, mobility of each species can have different temperature dependence. The free volume model can be used to completely specify compositional dependence of WLF parameters based on the compositional dependence of $\alpha(\phi)$ and $T_0(\phi)$, which can, in principle, be obtained from a volumetric measurement. Additional two intramolecular

parameters, $\log(A_i)$ and B_i, can be determined from two homopolymers. The Vogel temperature T_0 cannot be obtained directly from a simple volumetric measurement alone, but can be estimated by using the relationship between the volumetric glass transition temperature and T_0, *i.e.*, $T_0(\phi) = T_g^{Vol}(\phi) - f(T_g, \phi)/\alpha(\phi)$, where T_g^{Vol} represents the glass transition temperature obtained by volumetric measurement. The rough approximation of T_0 is possible once we know $\alpha(\phi)$ and $T_g^{Vol}(\phi)$ by assuming the value of $f(T_g^{Vol})$, which is known to be insensitive for wide range of polymers.

B. Adam-Gibbs model of cooperative motion

Adam and Gibbs have postulated that the cooperative transition probability $W(T)$ is proportional to the number of subsystems that is in states permitting rearrangement [16]. The transition probability of a cooperative region of a given size z is given by

$$W(T) = A \exp(-z\Delta\mu/kT), \tag{4.15}$$

and the average transition probability is given for the critical size of cooperative region, z^*,

$$\overline{W}(T) = \overline{A} \exp(-z^*\Delta\mu/kT). \tag{4.16}$$

The critical size of the cooperatively rearranging unit, z^*, can further be related to the configurational entropies [64] and its temperature dependence can be approximated as $z^* = \bar{c}\frac{T}{T-T_0}$ [65]. As temperature approaches T_0, the critical size of cooperatively rearranging unit diverges and the constant $\bar{c}$ that depends only on the intramolecular structure controls the intermolecular cooperativity.

This model can also be extended to each species in a miscible blend by assuming

that both species share a common T_0. Since the correlation time is reciprocally related to the transition probability,

$$\tau_c(T) \propto 1/\overline{W}(T) \tag{4.17}$$

$$\log \tau_{c,i}(T,\phi) = \log \overline{A_i} + \frac{\Delta\mu(c)_i}{k}\frac{c_i}{T-T_0}, \tag{4.18}$$

where $c_i = 0.434\,\overline{c_i}$. Suppose we assume that the rearrangement of all segments is completely coupled within the region of cooperativity, the potential barrier of transition per unit segment, $\Delta\mu(c)_i$, can be further assumed to be the same for both species. Under these approximations, both the free volume model and the Adam-Gibbs model predicts nearly identical temperature dependence of correlation time (eqn. 4.14 and eqn. 4.18).

C. Composition dependence of WLF parameters

Both phenomenological models examined above lead to the same WLF behavior, whose compositional dependence are governed by $T_0(\phi)$ and $\alpha(\phi)$ or $\Delta\mu(\phi)$. For the sake of concreteness, subsequent discussion will rely on the common form of the WLF equation,

$$\log \tau_{c,i}(T,\phi) = \log C_i + \frac{D_i}{T - T_0(\phi)}, \tag{4.19}$$

where C_i and D_i can be related to the parameters in each phenomenological model. The conventional WLF equation can also be rewritten in a form similar to eqn. 4.19,

$$\log \tau_{c,i} = -C^g_{1,i} + \frac{C^g_{1,i}C^g_{2,i}}{T - T_{0,i}}, \tag{4.20}$$

where $T_{0,i} = T_{g,i} - C^g_{2,i}$. In light of the phenomenological models, it is expected that $C^g_{1,i}$ is independent of composition, $T_{0,i}$ is the same for both species in the same

blend and the ratio of $C^g_{1,i}C^g_{2,i}$ is constant independent of composition. Thus, we first estimate the composition independent quantity based on the motional rates obtained from both NMR and rheological measurements. The possibility of the common T_0 in miscible blends is sought based on the composition independent mobility C_i. The uncertainty in the parameter T_0 is relatively large and is sensitive to small changes in C_i that we assume to be fixed for each species. The best fit parameters for a given value of C_i are summarized in **Table 4.2**. Since good fits can be obtained for a range of C_i's for both PI and PVE, similar results are also included for other values of C_i's.

Typical uncertainties in T_0 and D are about ± 5 K ($\sim 7\%$) and ± 40 K ($\sim 11\%$) respectively. Within the uncertainties, common T_0 can be found at all three compositions with given values of C_i. In the analysis, the range of C_i is taken such that the WLF fit for homopolymer data yield mean square error not exceeding 50% of the minimum error. Similarly, the range of T_0 is taken within 100% of the minimum error. For 50/50 and 75/25 PI/PVE blends, the range of T_0's overlap significantly, while for 25/75 PI/PVE, very narrow T_0 range is common for both species. This is perhaps related to the effect of compositional variation that can increase the difference in mean correlation times between the two species. We then use the values of C_i and constrain T_0 to be unique in a blend. One result of such constrained fitting is summarized in **Table 4.2c**. The ratio between D_i's is fairly constant in accord with the models. This ratio can be directly interpreted as the ratio of the critical size of fractional free volume, v^*/v_0, or the intermolecular dynamic cooperativity, c_i, between the two species.

The primitive WLF analysis for the combined NMR and rheological data suggests that significant differences in component mobilities can arise from small difference in intramolecular parameters (e.g., A_i and B_i in free volume model). In terms of the phenomenological models, such intramolecular properties are represented as the critical size of free volume or intermolecular cooperativity. In the case of this free volume model, all the intramolecular and intermolecular parameters can be obtained from the properties of both homopolymers and from an independent volumetric measurement. This approach can be useful in estimating the compositional dependence of monomeric friction coefficient, and hence in predicting the thermorheological behavior of miscible blends. The validity of these phenomenological models in the blend, however, is not conclusive, due to the limited range of temperature and composition covered in this study. Further study of the temperature dependence of segmental and chain relaxation times for more composition ranges can allow more solid understanding.

Table 4.2: The WLF fit parameters constrained based on the phenomenological models of cooperative dynamics.

(a)

	PI %	*C*	*D*	*To*	
dPI	100	-13.0	674	159	
	75	-13.0	667	166	(166+-5)
	50	-13.0	680	173	(173+-4)
	25	-13.0	650	186	(186+-4)
dPVE	75	-12.3	854	156	(156+-5)
	50	-12.3	850	165	(165+-8)
	25	-12.3	750	191	(191+-5)
	0	-12.3	594	223	

(b)

	PI %	*C*	*D*	*To*	
dPI	100	-13.3	720	156	(156+-4)
	75	-13.3	720	163	(163+-4)
	50	-13.3	730	171	(171+-3)
	25	-13.3	700	184	(184+-4)
dPVE	75	-12.1	816	161	(158+-5)
	50	-12.1	810	170	(167+-7)
	25	-12.1	710	188	(193+-5)
	0	-12.1	560	223	(225+-2)

(c)

	PI %	*C*	*D*	*To*	*ratio*
dPI	100	-13.19	687	159	
	75	-13.19	732	161	1.10
	50	-13.19	727	170	1.10
	25	-13.19	644	188	1.20
dPVE	75	-12.25	802	161	
	50	-12.25	800	170	
	25	-12.25	772	188	
	0	-12.25	591	223	

Chapter 5

Conclusion

5.1 Summary

We have presented quantitative measurements on the segmental mobility of PI and PVE in their neat form and in PI/PVE miscible blends. The mean reorientational correlation times of the two homopolymers agree well with segmental mobilities measured by various other methods, suggesting that the motion of C-^{2}H bonds probed by ^{2}H NMR is directly related to the cooperative backbone reorientation. The temperature dependence of this segmental mobility also seems to be consistent with that of terminal relaxation for PI and PVE. The effects of blending on the component dynamics have been examined by measuring the mean and distribution of motional rates as a function of temperature and composition. Near the glass transition of blends, we have been able to characterize two types of dynamic heterogeneity simultaneously: different mean mobilities between the two species and broadening of the mobility distribution for both species. The mean mobilities of the two species can

differ by two orders of magnitude at identical conditions, suggesting that the glass transition of miscible blends does not represent a dynamically simple state. Different mean mobilities and their distinct temperature dependence can be described in terms of an effective glass transition temperature, T_g^*, which differs for each species. The increase in the width of the correlation time distribution and the separation between the species' effective glass transitions produce the broad glass transitions of blends.

Segmental mobilities of the two species change sensitively with composition. As the content of high T_g component (PVE) increases, both the difference in mean motional rates and the width of mobility distribution increase. Such enhancement in dynamics heterogeneities observed for blends rich in high T_g species seems to cause the anomalously broad glass transition and the more pronounced thermorheological complexity, observed in these blends for high PVE fraction. In addition, the individual T_g^*'s show different compositional dependence from each other and from the macroscopic DSC T_g. As the relative difference between $T_{g,PVE}^* - T_g$ and $T_g - T_{g,PI}^*$ changes, the mobilities observed at a given $T - T_g$ vary significantly. Thus, viewing the dynamics with respect to the macroscopic T_g can lead to a complex non-monotonic dependence of mobilities on composition.

Further, two possible origins of the dynamic heterogeneities are examined by comparing the experimental results with simple model calculations that take into account the effect of composition variations in a blend. Based on a simplistic model, local composition variations can give rise to the observed broadening of the mobility distribution. The broadening is pronounced when the glass transition temperature changes

rapidly with composition, which is often the case in blends rich in the high T_g species. Although this model can explain the observed σ and its compositional dependence, the observed difference in the mean mobilities cannot be explained at the same time. This may be due to the intrinsic dynamic differences between the two species which are neglected in the simplistic model. Such intrinsic dynamic differences can be considered, using phenomenological models of cooperative local dynamics. In terms of these models, compositional dependence of segmental mobilities and perhaps the monomeric friction coefficients can be estimated.

To determine the relationship between the local segmental dynamics and the macromolecular relaxation processes, the mean correlation times have been compared with monomeric friction coefficients obtained by rheo-optical measurements [12]. The comparison suggests that both NMR and rheo-optical results can be described reasonably by a common temperature dependence. However, monomeric friction coefficients exhibit deviation from a common temperature dependence when the correlation time distribution becomes significantly broader than that of homopolymers. Whenever it deviates, the monomeric friction coefficient appears to have steeper temperature dependence than the mean correlation times, suggesting that the average monomeric friction coefficient represents an average biased toward slower segments within the distribution of locally heterogeneous motional rates.

The results show how significant dynamic heterogeneity arises in a single-phase polymer blend in which the pure components have widely separated glass transition and have sufficiently weak interactions that statistical composition variation is

significant. These conditions lead to separate effective glass transition for the two components which contributes to the broad glass transition and underlies the failure of time-temperature superposition. In addition, in the presence of such spatially heterogeneous mobility distribution, the average monomeric friction coefficient manifested in the longer length scale chain relaxations appear to be biased toward slower motions.

5.2 Further Studies

Some of the observations made in this work may be specific to this system, or may be readily extended to compatible polymer mixtures in general. A number of assumptions also have been made based on empirical results, which may be specific to this system. In order to gain deeper insight into the effect of blending on component dynamics and the macroscopic mechanical properties, a number of aspects need to be examined further.

1. In order to confirm that the dynamic heterogeneities observed in PI/PVE blends depend solely on local properties and the intramolecular dynamic characteristics, similar NMR and rheo-optical studies on PI-co-PVE block copolymers are under way. In addition, this study will reveal how different dynamics of each block give rise to an average friction coefficient manifested by terminal relaxation of the whole chain.

2. The comparison between the monomeric friction coefficient and the segmental correlation times is based on the assumption that both level of dynamics

have common temperature dependence in the absence of any local dynamic heterogeneities. In PVE homopolymer, the assumption appears to be reasonable, because the NMR and rheological results performed at overlapping temperature ranges seem to be consistent with each other. In order to make the comparison more reliable, NMR relaxation time measurements can be applied to homopolymers and each species in the blend, which will expand the range of correlation times to 10^{-7} s.

3. In the context of the phenomenological models discussed in Chapter 4, the temperature dependence of component dynamics and monomeric friction coefficients can be described in terms of the thermal expansion coefficient of free volume. By measuring the thermal expansion coefficient, we can further test this possibility. The thermal expansion coefficient of free volume is calculated as the difference in thermal expansion coefficients above and below the glass transition. It is implicitly assumed that the fractional free volume of the blend at the glass transition is the same as that of two homopolymers.

4. Similar NMR and rheo-optical measurement can also be extended to blends that are miscible due to stronger attractive interactions. The bias in the composition of neighboring chains arising from such favorable interaction can influence the extent of compositional variations. The coupling between the motions of the two components is also of interest.

Appendix A

Deuteration effect on segmental mobility

In this study, blends containing a labeled polymer have been used to resolve dynamics of individual species. It has been implicitly assumed that the dynamics observed from deuterated species are identical to that of unlabeled counterpart. However, it is known that deuterium labeling can have a significant effect on the thermodynamics of mixing. It has been shown recently that, indeed, phase separation can arise in isotopic blends [66, 67, 57, 68]. The isotopic effect has been attributed to the reduction in bond length when C-H bond is replaced by C-^{2}H bond, which then alters segment polarizabilities [57]. It is an important question whether such an isotopic effect can partially explain the observed differences in mean correlation times of each labeled species.

First of all, deuteration does not alter the miscibility of PI/PVE blends as drastically as observed for many isotopic blends. It has been observed from recent SANS

measurement on PI/dPVE blends containing a volume fraction of 52% PI that the interaction parameter is negative at all accessible temperatures [32]. This is consistent with observations made on normal (unlabeled) blends [69, 36]. Such miscibility behavior suggests that the favorable interaction between PI and PVE is much stronger than the isotope effect, which give rise to a small positive χ interaction parameter by inducing difference in solubility parameter [57],

$$\chi \propto [\delta_1 - \delta_2]^2 \tag{A.1}$$

$$\delta_i = (\frac{\hat{\alpha}}{V})_i. \tag{A.2}$$

The parameter δ is called the solubility parameter, $\hat{\alpha}$ is the polarizability and V is the segment volume. Since an additional positive component in the χ interaction parameter due to labeling is not the dominant effect in PI/dPVE blends, similar miscibility is expected for dPI/PVE blend as well. Furthermore, the DSC traces from dPI/PVE and PI/dPVE look almost the same with that of PI/PVE, except for some differences that seem to arise from small discrepancy in volume% due to molecular weight change upon deuteration and microstructural difference between PVE and dPVE.

We can also examine the deuteration effect on the segmental dynamics directly by studying the blends with different deuteration content. If the deuteration effect is significant, dynamics of deuterated species would change as the deuteration density varies. The labeling density can be controlled by either using polymer with different deuteration content or by diluting completely deuterated polymer with unlabeled counterpart. Due to the availability of the sample, the second approach is taken.

Two samples are prepared; 50/25:25 PI/dPVE:PVE and 25:25/50 dPI:PI/PVE. The segmental motion is probed by 2D ^{2}H NMR experiment and the NMR spectra are directly compared with those for 50/50 dPI/PVE and 50/50 PI/dPVE blends. Due to the reduced deuterium content, the experiment takes significantly longer. The experiment is performed at one temperature for 50/25:25 PI/dPVE:PVE blend, and at two temperatures for 25:25/50 dPI:PI/PVE. The spectra obtained at similar temperatures are directly compared in **Figure A.1** and **Figure A.2**. The changes in off-diagonal intensities with mixing time are very similar for both sets of blends. Only slight differences are observed for PVE labeled blends, perhaps because of small temperature difference. We conclude from the similarity that the difference in segmental mobilities between the two species and the extent of compositional variations are not influenced significantly by the isotope effect.

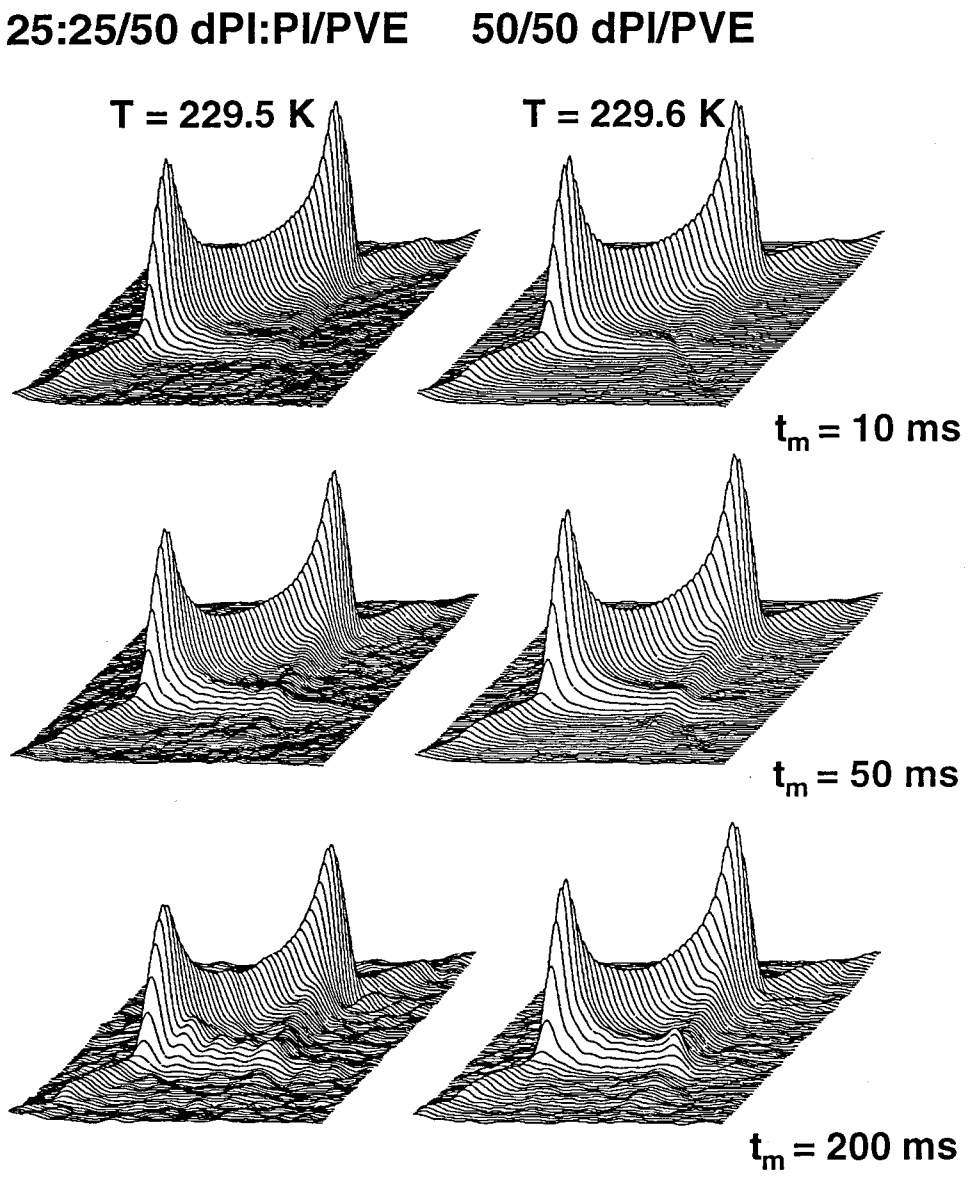

Figure A.1: Deuteration effect on the segmental dynamics of dPI: comparison of 2D ^{2}H NMR spectra for 50/50 dPI/PVE and 25:25/50 dPI:PI/PVE blends.

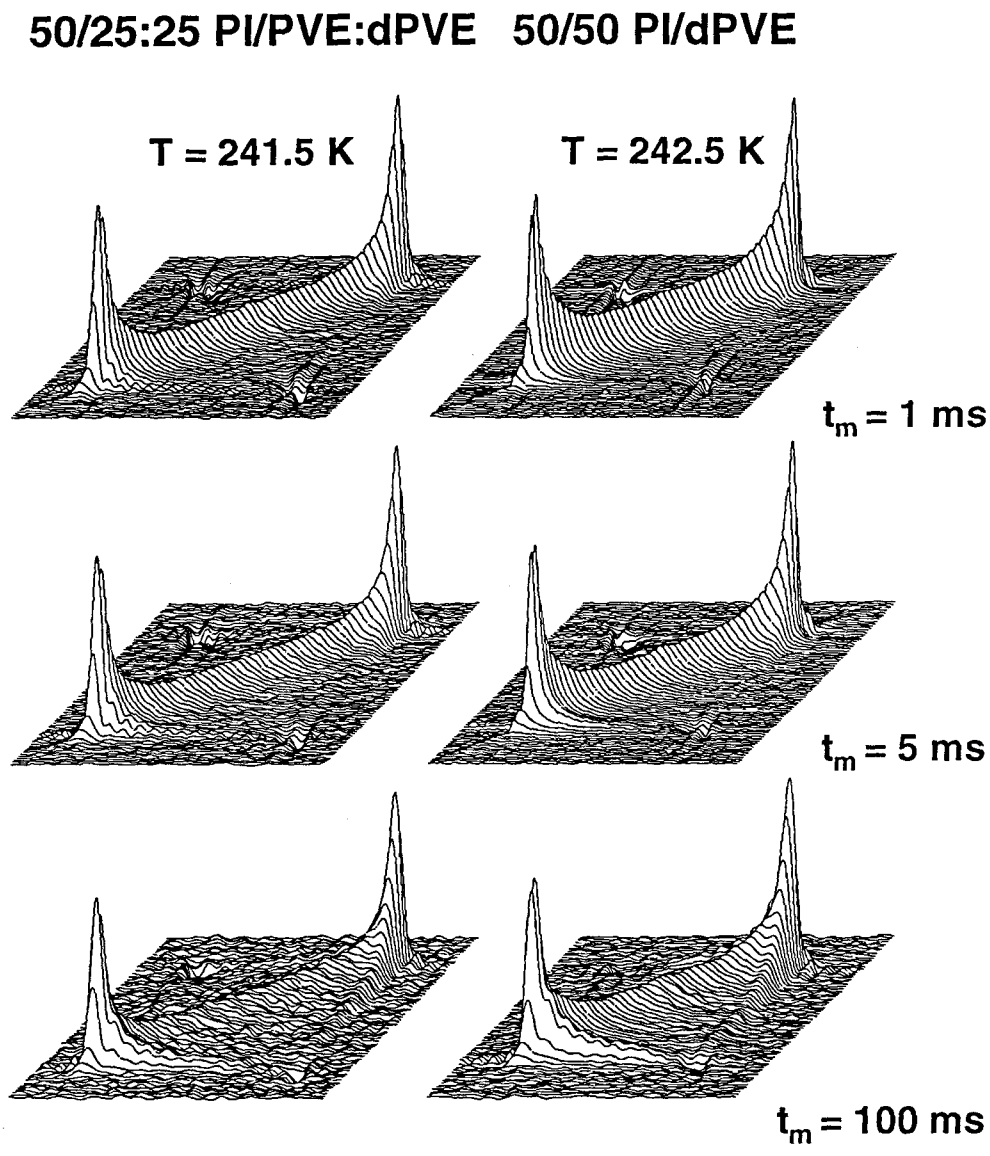

Figure A.2: Deuteration effect on the segmental dynamics of dPVE: comparison of 2D ^{2}H NMR spectra for 50/50 PI/dPVE and 50/25:25 PI/PVE:dPVE blends.

Appendix B

Correction for the reduction of spectral intensity

The systematic experimental errors in τ_{c_0} and σ are discussed, in terms of the inhomogeneous reduction of spectral intensities. An approximate procedure for correcting the errors is suggested, based on the solid echo 1D NMR experiment. The apparent bimodality of correlation time distribution is also discussed.

When the solid echo intensity is measured as a function of temperature, it exhibits a broad minimum at about 30 K above the glass transition (**Figure B.1**). This behavior has been observed in many systems and has also been used to determine the nature of segmental dynamics in a number of polymer systems [22, 23, 51, 42]. This reduction of signal is often described in terms of a minimum in the effective T_2 relaxation time and/or the incomplete refocussing of the magnetization (**Figure**

B.1). Both effects appear to have a strong dependence on correlation times, with the reduction becoming strongest at correlation times $\tau_c \simeq 2/\delta$. Although this reduction of signal is most intense in the intermediate dynamic regime ($1\ \mu s \leq \tau_c \leq 1$ ms), some reduction is observed even for a significantly larger correlation times. In particular, the reduction is significant even at such low temperatures where the 2D NMR spectra are obtained. Thus, it is possible that the correlation time distribution determined from 2D spectra is biased toward slower motion, since the correlation time dependent reduction is stronger for C-^{2}H bonds lying in the fast tail of the actual correlation time distribution. We suggest an approximate procedure, based on solid echo intensity measurements, to correct for the effect of correlation time dependent reduction of spectral intensity.

The reduction of spectral intensity at a single correlation time, $R(\tau_c)$, can, in principle, be obtained from a detailed calculation of the solid echo spectrum as a function of a single correlation time, τ_c[22, 23]. Alternatively, this relationship between the reduction and the correlation time can be approximately obtained by measuring the average reduction as a function temperature, $\overline{R_i}(T)$, for each species i. For two homopolymers, the inherent correlation time distribution is relatively narrow, and it is expected that the measured average reduction over the distribution of correlation times, $\overline{R_i}(\sigma, \tau_{c_0}; T)$, is similar to the reduction at the mean correlation time, $R_i(\tau_{c_0}; T)$. The observed temperature dependence of the mean correlation times, $\tau_{c_0,i}(T)$, is used to obtain $R_i(\tau_c)$ from the measured reduction $\overline{R_i}(T)$ for each species i. The continuous representation of the correlation time dependent reduction is obtained by fitting

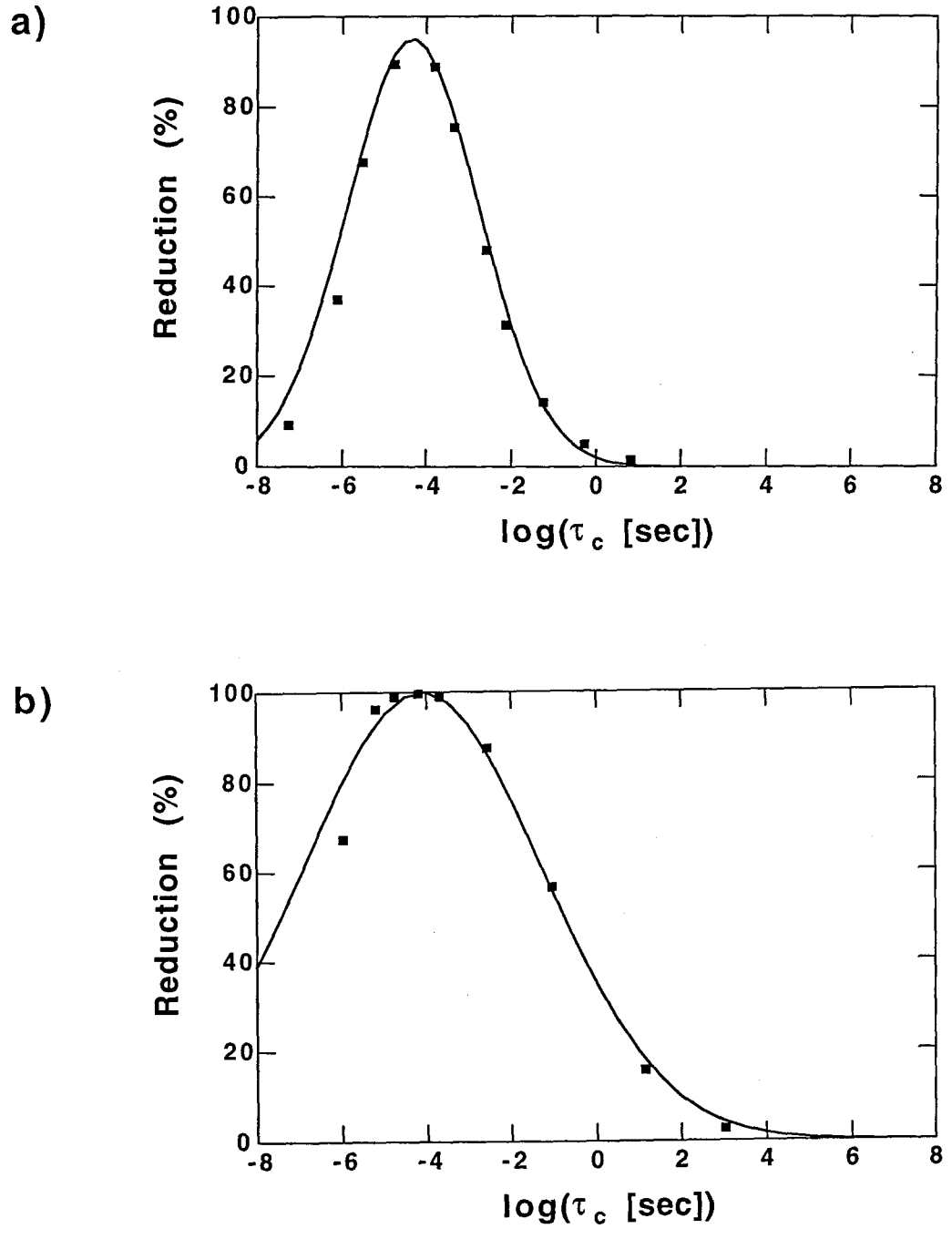

Figure B.1: Average reduction of solid echo intensity as a function of mean correlation times for each homopolymer. The Gaussian fit through the data is used as the correlation time dependent reduction $\overline{R_i}(\tau_c)$ for each species i. (a) dPI and (b) dPVE.

the measured reduction with a Gaussian function (**Figure B.1**).

Once we have $R_i(\tau_c)$, we can calculate the effect of the correlation time dependent reduction on the apparent correlation time distribution determined from the 2D NMR spectra. Suppose the actual underlying correlation time distribution is $P_i^*(\tau_c;\phi,T)$, then the apparent correlation time distribution, $P(\tau_c;\phi,T)$, can be evaluated via

$$P(\tau_c;\phi,T) = (1 - R(\tau_c)) \cdot P^*(\tau_c;\phi,T), \tag{B.1}$$

and the average reduction, $\overline{R}(\phi,T)$, is given by

$$\overline{R}(\phi,T) = \frac{\int [P^*(\tau_c;\phi,T) - P(\tau_c;\phi,T)] d\tau_c}{\int P^*(\tau_c;\phi,T) d\tau_c}. \tag{B.2}$$

Now, we want to estimate the mean and width of the actual correlation time distribution based on the experimentally measured quantities, which are the apparent mean and width of the correlation time distribution determined from the 2D NMR spectra, and the average reduction measured by solid echo intensity measurement. As a first approximation, we assume that the actual correlation time distribution can be represented as log-Gaussian distribution,

$$P^*(\tau_c) = \frac{\exp[-(\log \tau_c - \log \tau_{c0}^*)^2 / 2\sigma^{*2}]}{\sqrt{2\pi\sigma^{*2}}}, \tag{B.3}$$

where $\tau_{c0}^* = 10^{\langle \log \tau_c^* \rangle}$ is the log-mean correlation time and σ^* is the width of the correlation time distribution. The apparent $P(\tau_c)$ is calculated from $P^*(\tau_c)$ by subjecting it to the reduction via equation B.2. The set of values (τ_{c0}^*, σ^*) are taken as the modified mean and the width of correlation time distribution, when the average reduction, the apparent mean and the variance of the correlation time distribution after the reduction are consistent with the observed $\overline{R}, \tau_{c0}$ and σ. The $\overline{R}, \tau_{c0}$ and σ

obtained experimentally (top) are compared with the $\tau_{c_0}^*, \sigma^*$ determined by the correction procedure outlined above (bottom) (**Figure 3.15-3.18**). The modified mean correlation time is also included in **Figure 3.13, 4.3**. The range of correlation times that undergo more than 80% of the reduction is also shaded to make the comparison easier. The difference between (τ_{c_0},σ) and ($\tau_{c_0}^*, \sigma^*$) is most pronounced for the PVE rich blend, where the correlation time distributions are very broad.

When the width of the correlation time distribution is sufficiently broad, this reduction of intensities can also give rise to an apparent bimodality, as previously observed by other workers [42]. This apparent bimodality is manifested most dramatically by the presence of a central peak, while the rest of the 2D spectrum still exhibits a solid line-shape (**Figure B.2**). The bimodality in correlation time distribution, however, disappears at lower temperatures, as can be seen from the absence of the fast segments that give rise to a significant exchange even at small mixing times (**Figure B.3, B.4**). This qualitative change in the shape of correlation time distribution can be demonstrated by using the above scheme of correcting for the effect of reduction at the intermediate dynamic regime (**Figure B.5**). The apparent bimodality can arise (solid line) from a single log-Gaussian distribution of correlation times (dotted line), due to the reduction of exchange intensity at the center of the actual correlation time distribution. The narrow central peak arises from the small tail at high correlation time ($\tau_{c_0} \leq 10^{-6}$).

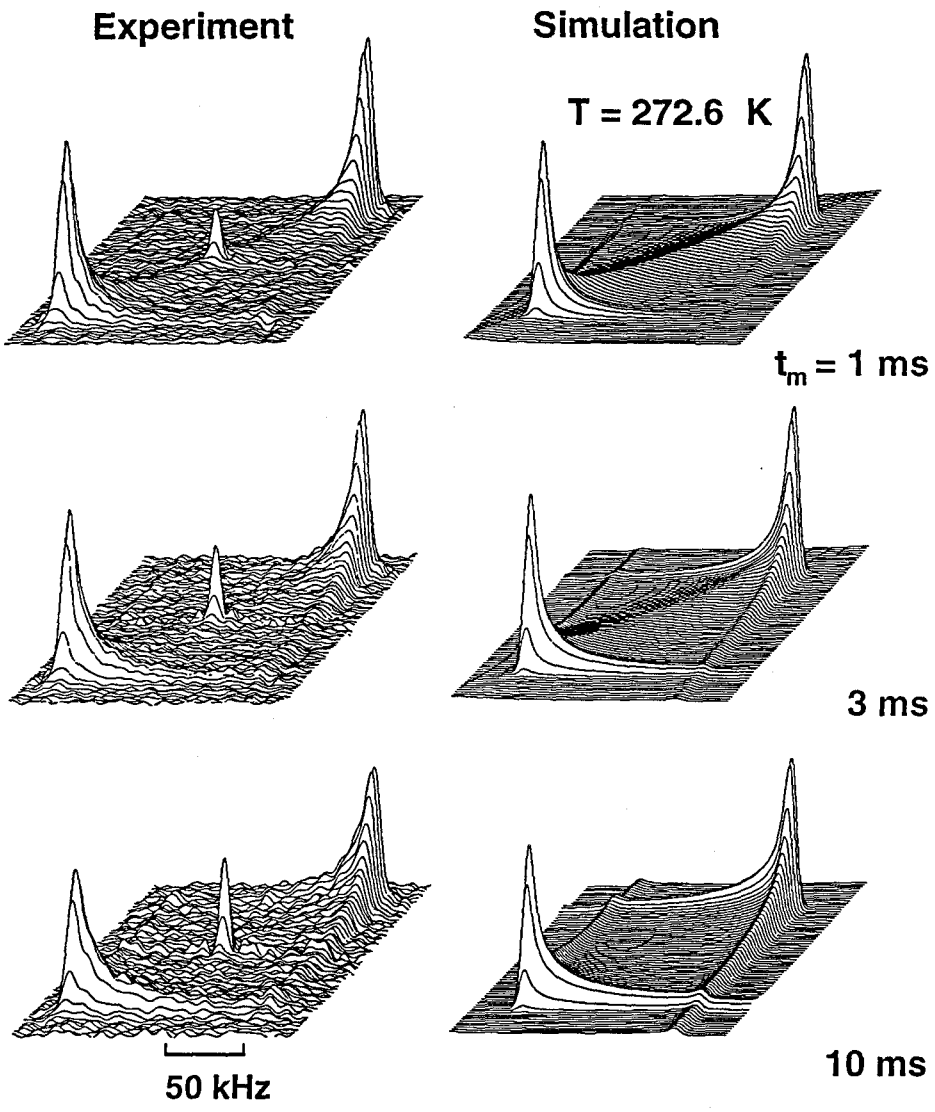

Figure B.2: Experimental and simulated 2D ^{2}H exchange NMR spectra for 75/25 PI/dPVE obtained at 272.6 K. Simulated spectra are calculated with $\tau_{c_0} = 6.7$ ms and $\sigma = 0.625$ decade. The narrow isotropic peak is neglected in the fit. This apparent bimodal character can arise from a single unimodal correlation time distribution due to the reduction in intensity (see **Figure B.5**).

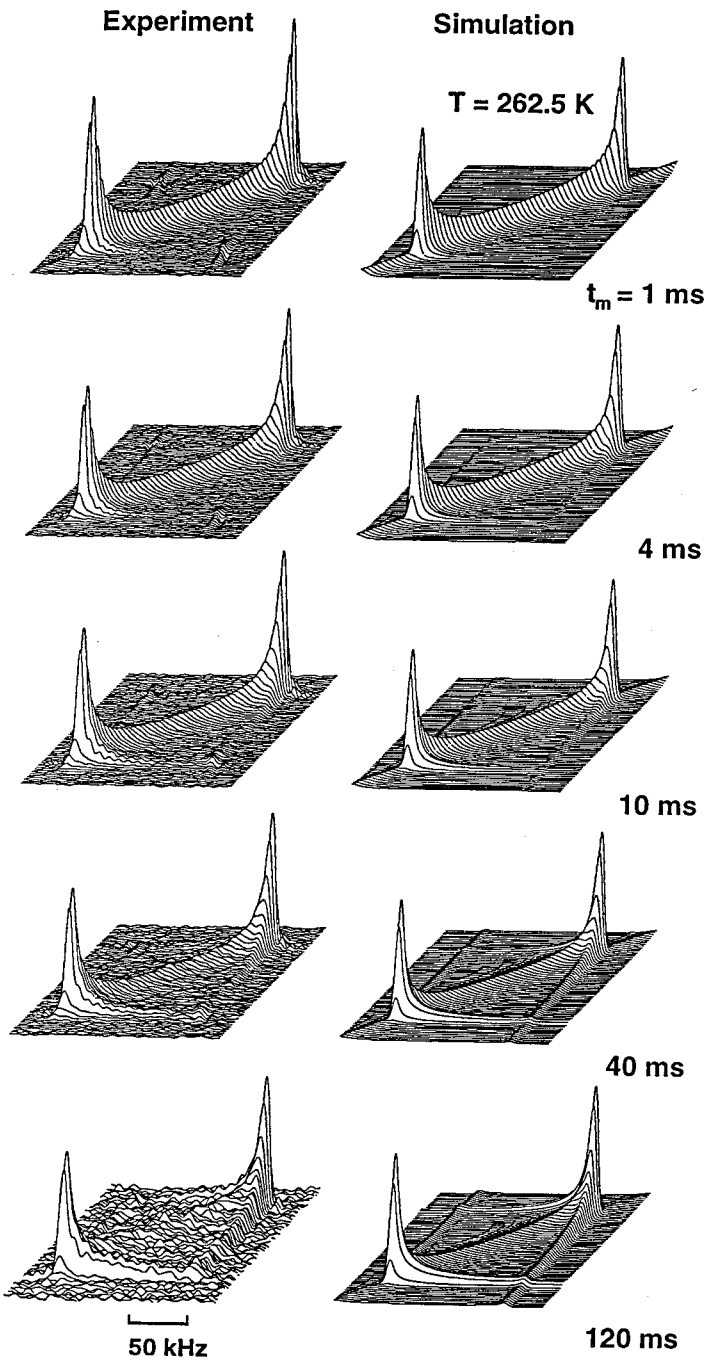

Figure B.3: Experimental and simulated 2D ^{2}H exchange NMR spectra for 75/25 PI/dPVE obtained at 262.5 K. Simulated spectra are calculated with $\tau_{c_0} = 100$ ms and $\sigma = 1.15$ decade.

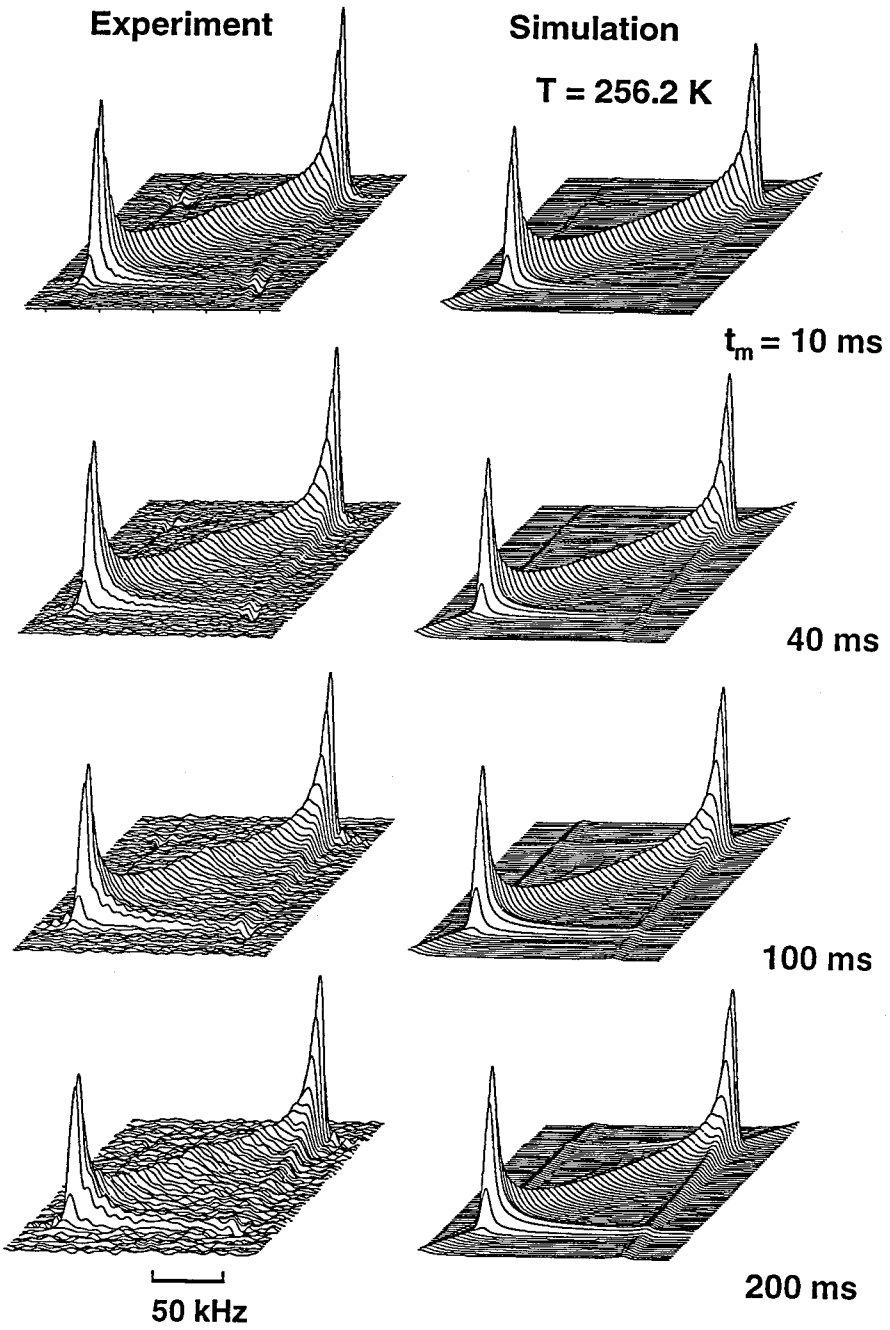

Figure B.4: Experimental and simulated 2D ^{2}H exchange NMR spectra for 75/25 PI/dPVE obtained at 256.2 K. Simulated spectra are calculated with $\tau_{c_0} = 200$ ms and $\sigma = 1.5$ decade.

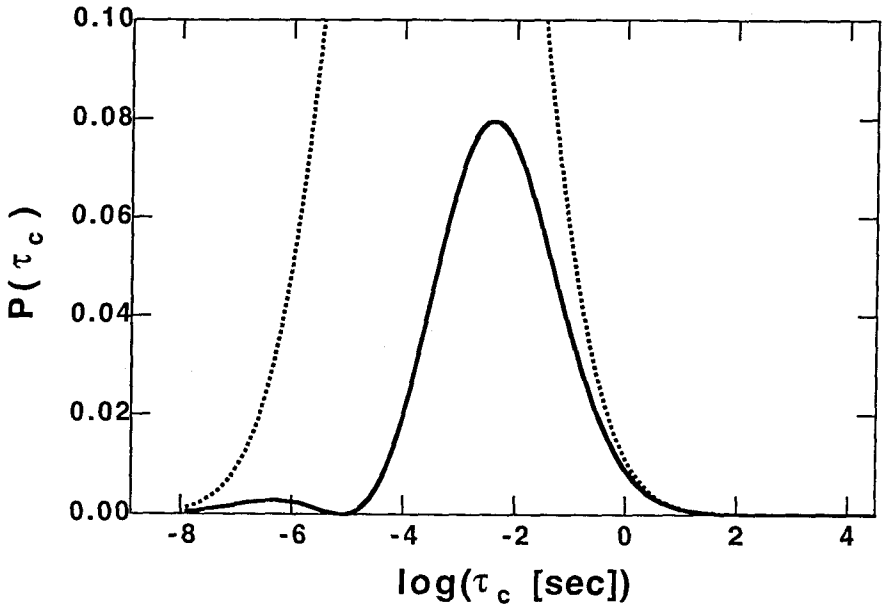

Figure B.5: Apparent bimodal distribution resulting from the loss of spectral intensity at the intermediate dynamic regime. The dotted line is the actual underlying correlation time distribution that is consistent with the measured τ_{c_0}, σ, and average reduction of signal $\overline{R}$. The peak height of the dotted line is about 0.295, and is truncated to emphasize the bimodal character of the solid curve.

Bibliography

[1] Macknight, W. J.; Stoelting, J.; Karasz, F. E. *Mult. Polymer Sys.* **1970**, 29

[2] Prest, W. M.; Porter, R. S. *J. Polymer Sci.* **1972**, *10*, 1639

[3] Zoller, P.; Hoehn, H. H. *J. Polymer Sci.* **1982**, *20*, 1358

[4] Fox, T. G. *Bull. Am. Phys. Soc.* **1956**, *1*, 123

[5] Gordon, M.; Taylor, J. S. *J. Appl. Chem.* **1952**, *2*, 493

[6] Wood, L. A. *J. Polymer Sci.* **1958**, *28*, 319

[7] Tsenoglou, C. *J. Polymer Sci.* **1988**, *26*, 2329

[8] a) Composto R. J.; Kramer E. J.; White D. M. *Macromolecules* **1988**, *21*, 2580,
b) Composto R. J.; Kramer E. J.; White D. M. *Polymer* **1990**, *31*, 2320

[9] Roovers, J.; Toporowski, P. M. *Macromolecules* **1992**, *25*, 3454

[10] Struglinski, M. J.; Graessley, W. W. *Macromolecules* **1985**, *18*, 2630

[11] Zawada, J. A.; Fuller, G. G.; Colby, R. H.; Fetters, L. J.; Roovers, J. *accepted to Macromolecules*

[12] a) Arendt, B. A; Kannan, R. M.; Zewail, M.; Kornfield, J. A.; Smith, S. D. *accepted to Rheologica Acta* b) Arendt, B. A; Krishnamoorti, R *to be published*

[13] Colby R. H. *Polymer* **1989**, *20*, 1275

[14] Brochard-Wyart, F. *C. R. Acad. Sci.* **1987**, *305*, 657

[15] Cohen, M. H.; Turnbull, D. *J. Chem. Phys.* **1959**, *31*, 1164

[16] Adam, G.; Gibbs, J. H. *J. Chem. Phys.* **1965**, *76*, 139

[17] Miller J. B.; McGrath K. J.; Roland C. M.; Trask C. A.; Garroway A. N. *Macromolecules* **1990**, *23*, 4543

[18] Le Menestrel, C.; Kenwright, A. M.; Sergot, P.; Laupretre, F.; Monnerie, L. *Macromolecules* **1992**, *25*, 3020

[19] Schmidt-Rohr, K.; Clauss, J.; Spiess, H. W. *Macromolecules* **1992**, *25*, 3273

[20] Pschorn, U.; Rössler, E.; Sillescu, H.; Kaufmann, S.; Schaefer, D.; Spiess, H. W. *Macromolecules* **1991**, *24*, 398

[21] Jelinski, L. W. *High Resolution NMR Spectroscopy of Synthetic Polymers in bulk*; Komoroski, R. A., Ed.; VCH Publishers: Deerfield Beach, FL, 1986

[22] Spiess, H. W.; Sillescu, H. *J. Magn. Res.* **1981**, *42*, 1981

[23] Woessner, D. E.; Snowden, B. S.; Meyer, G. H. *J. Chem. Phys.* **1969**, *51*, 2968

[24] Schmidt, C.; Wefing, S.; Blümich, B.; Spiess, H. W. *Chem. Phys. Lett.*, **1986**, *130*, 84

[25] Schmidt, C.; Blümich, B.; Spiess, H. W. *J. Magn. Res.*, **1988**, *79*, 269

[26] Kaufmann, S.; Wefing, S.; Schaefer, D.; Spiess, H. W. *J. Chem. Phys.* **1990**, *93*, 197

[27] Wefing, S.; Kaufmann, S.; Spiess, H. W. *J. Chem. Phys.* **1988**, *89*, 1234

[28] Schaefer, D.; Spiess, H. W. *J. Chem. Phys.* **1992**, *97*, 7944

[29] Spiess, H. W. *Chem. Rev.* **1991**, *91*, 1321

[30] Schaefer, D. *Ph.D. Thesis, University of Mainz* **1992**

[31] Schaefer, D.; Spiess, H. W.; Suter, U. W.; Fleming, W. W. *Macromolecules* **1990**, *23*, 3431

[32] Tomlin, D. W.; Roland, C. M. *Macromolecules* **1992**, *25*, 2994

[33] a) Roland, C. M. *Macromolecules* **1987**, *20*, 2557, b) Roland C. M. *J. Polym. Sci. Polym. Phys. Ed.* **1988**, *26*, 839

[34] Bates, F. S.; Rosadale, J. H.; Bair, H. E.; Russel, T. P. *Macromolecules* **1989**, *21*, 2557

[35] Sakurai, S.; Jinnai, H.; Hasegawa, H.; Hashimoto, T.; Han, C. C. *Macromolecules* **1991**, *24*, 4839

[36] Roland, C. M.; Miller, J. B.; McGrath, K. J. *Macromolecules* **1993**, *26*, 4967

[37] Roovers, J.; Wang, F. *submitted to J. Non-Cryst. Solids*

[38] Carella, J. M.; Graessley, W. W.; Fetters, L. J. *Macromolecules* **1984**, *17*, 2775

[39] Ferry, J. D. *Viscoelastic Properties of Polymers, 3rd ed.*; John Wiley & Sons: New York, 1980

[40] Roovers, J.; Wang, F. *submitted to J. Non-Cryst. Solids*

[41] Schmidt-Rohr, K.; Spiess, H. W. *Phys. Rev. Lett.* **1991**, *66*, 3020

[42] Wehrle, M.; Hellmann, G. P.; Spiess, H. W. *Colloid & Polymer Sci.* **1987**, *265*, 815

[43] Kanetakis, J.; Fytas, G.; Kremer, F.; Pakula, T. *Macromolecules* **1992**, *25*, 3484

[44] Alegria, A.; Colmenero, J.; Ngai, K. L.; Roland, C. M. *To be published*

[45] Kanetakis, J.; Fytas, G.; Hadjichristidis, N. *Macromolecules* **1991**, *24*, 1806

[46] Boese, D.; Kremer, F. *Macromolecules* **1990**, *23*, 829

[47] Gotro, J. T.; Graessley, W. W. *Macromolecules* **1984**, *17*, 2767

[48] Chin, Y. H.; Zhang, C.; Wang, P.; Inglefield, P. T.; Jones, A. A.; Kambour, R. P.; Bendler, J. T.; White, D. M. *Macromolecules* **1992**, *25*, 3031

[49] Chin, Y. H.; Inglefield, P. T.; Jones, A. A. *Macromolecules* **1993**, *26*, 5372

[50] Rössler, E.; Sillescu, H.; Spiess, H. W. *Polymer* **1985**, *26*, 203

[51] Schmidt, C.; Kuhn, K. J.; Spiess, H. W. *Prog. Colloid & Polymer Sci.* **1985**, *71*, 71

[52] Lau, S.; Pathak, J.; Wunderlich, B. *Macromolecules* **1982**, *15*, 1278

[53] Lin, J. L.; Roe, R. J. *Polymer* **1988**, *29*, 1227

[54] Zetsche, A.; Kremer, F.; Jung, W.; Schulze, H. *Polymer* **1990**, *31*, 1883

[55] Fischer, E. W.; Zetsche, A. *ACS Poly. Prepr.* **1992** Spring, San Francisco, 78

[56] Angel, C. A.; *J. Non-Cryst. Solids* **1991**, *131-133*, 13

[57] Bates, F. S.; Fetters, L. J.; Wignall, G. D. *Macromolecules* **1988**, *21*, 1086

[58] Zawada J. A.; Ylitalo C. M.; Fuller G. G.; Colby R. H.; Long T. E. *Macromolecules* **1992**, *25*, 2896

[59] Meire, G.; Fytas, G.; Momper, B.; Fleischer, G. *Macromolecules* **1993**, *26*, 5310

[60] Chung, G. -C.; Kornfield, J. A.; Smith, S. D. *Macromolecules* **1994**, *27*, 964

[61] Donth, E. *J. Non-Cryst. Solids* **1982**, *53*, 325

[62] Cauley, B. J.; Cipriani, C.; Ellis, K.; Roy, A. K.; Jones, A. A.; Inglefield, P. T.; McKinley, B. J.; Kambour, R. P. *Macromolecules* **1991**,*24*, 403

[63] Fujita, H. *Adv. Polymer Sci.* **1961**, *3*, 1

[64] Gibbs, J. H.; DiMarzio, E. A. *J. Chem. Phys.* **1958**, *28*, 373

[65] Matsuoka, S. *Relaxation Phenomena in Polymers*; Hanser Publishers, 1992

[66] Bates, F. S.; Wignall, G. D.; Koehler, W. C. *Phys. Rev. Lett.* **1985**, *55*, 2425

[67] Bates, F. S.; Dierker, S. B.; Wignall, G. D. *Macromolecules* **1986**, *519*, 1938

[68] Schwahn, D.; Hahm, K.; Streib, J.; Springer, T. *J. Chem. Phys.* **1990**, *93*, 8383

[69] Zemel, I. S.; Roland, C. M. *Polymer* **1992**, *33*, 4522